Functional Genetic Screens of Chromosome 1q in Breast Cancer via 2D and 3D *in vitro* Models

by

Hande Özkan

A Dissertation Submitted to the

Graduate School of Health Sciences

in Partial Fulfillment of the Requirements for

the Degree of

Doctor of Philosophy

In

Cellular and Molecular Medicine

July 5th , 2024

Functional Genetic Screens of Chromosome 1q in Breast Cancer via 2D and 3D *in vitro* Models

Koç University

Graduate School of Health Sciences

This is to certify that I have examined this copy of a doctoral dissertation by

Hande Özkan

and have found that it is complete and satisfactory in all respects,

and that any and all revisions required by the final

examining committee has been made.

Committee Members:

_____

Assist. Prof. Gözde Korkmaz

_____

Prof. Tamer Önder

_____

Assist. Prof. Bahar Soğutmaz Özdemir

_____

Assist. Prof. İrem Durmaz Şahin

_____

Prof. Dilek Telci Temeltaş

Date: 05.07.2024

To my family

To my chosen family

To Oğuzhan Coşkun, always being there

&
To my four-legged creatures

ABSTRACT

Functional Genetic Screens of Chromosome 1q in Breast Cancer via 2D and 3D *in vitro* Models

Hande Özkan

Doctor of Philosophy in Cellular and Molecular Medicine
05.07.2023

Breast cancer, with an incidence rate affecting approximately 2.3 million women globally, poses significant health challenges due to high recurrence rates and resistance to therapy. The diversity of molecular subtypes further complicates targeted treatment. Genetic abnormalities, particularly chromosomal alterations, play a critical role in tumour initiation and progression. Specifically, chromosome 1q (Chr1q) copy number alterations (CNA) are linked to poor patient prognosis and survival.

This study hypotheses that Chr1q CNAs induce a genomic disorder/catastrophe, activating oncogenic drivers or causing gene expression loss. To investigate, we performed functional CRISPR screening targeting Chr1q genes in breast cancer. We utilised both 2D and 3D cultures in two breast cancer cell lines and one normal breast cell line to capture cancer-specific phenotypes influencing proliferation.

We identified cancer-specific dropout genes negatively impacting proliferation in breast cancer cells but not in non-tumorigenic controls. Among 14 shared candidates, RPRD2 and GON4L were selected for further validation due to their significant effects on breast cancer proliferation in both 2D and 3D models. RPRD2 showed cancer-specific activity, while GON4L also impacted normal breast cells.

For enriched candidates with positive phenotypes, we normalised 3D screening results by 2D (3D/2D). ARL8A and ARNT emerged as significant in at least one breast cancer cell line. Validation experiments revealed that blocking ARL8A and ARNT decreased proliferation in 2D models but increased 3D spheroid growth, indicating differential phenotypic impacts. Additionally, ARNT knockout in normal breast cells led to increased proliferation.

This study highlights the necessity of transitioning from 2D to 3D models in functional screening for more accurate phenotypic evaluations. It also underscores the importance of Chr1q in breast cancer carcinogenesis and identifies potential cancer driver genes.

ÖZETÇE

İki Boyutlu ve Üç Boyutlu *in vitro* Modeller ile Meme Kanserinde Kromozom 1q'nun Fonksiyonel Genetik Taraması

Hande Özkan
Hücresel ve Moleküler Tıp, Doktora
05.07.2023

Meme kanseri, dünya genelinde yaklaşık 2.3 milyon kadını etkileyen bir kanser türü olup yüksek nüks oranları ile ilerleyen safhalarda tedaviye direnç, meme kanserinin düşük sağkalım oranları ile ilişkilendirilmektedir. Moleküler alt tiplerin çeşitliliği, hedefe yönelik tedaviyi oldukça olumsuz yönde etkilemektedir. Genetik anormallikler, özellikle kromozomal değişiklikler, kanser oluşumunda ve ilerlemesinde kritik bir rol oynamaktadır. Özellikle kromozom 1q kopya sayısı değişiklikleri hastalığın kötü prognozu ve hasta sağkalımı ile ilişkilidir.

Bu çalışma kapsamında, kromozom 1q kopya sayısı değişikliklerinden dolayı meydana gelen genomik düzensizliklerin onkojenik genlerin aktivasyonu veya gen ekspresyonlarında kayba sebep olabileceği öngörülmektedir. Bu nedenle, aday genlerin belirlenebilmesi için meme kanseri hücre hatlarında Chr1q genlerini hedef alan fonksiyonel CRISPR taramaları gerçekleştirilmiştir. İki meme kanseri hücre hattı ve bir normal meme hücre hattında hem 2-boyutlu (2D) hem de 3-boyutlu (3D) modeller kullanılarak proliferasyonu etkileyen kansere özgü fenotiplerin belirlenebilmesi amaçlanmıştır.

Meme kanseri hücrelerinde proliferasyonu olumsuz etkileyen, ancak normal hücre kontrollerinde etkisi olmayan kansere özgü hedef genler belirlenmiştir. 14 ortak gen arasında, RPRD2 ve GON4L hem 2D hem de 3D modellerde meme kanseri proliferasyonuna önemli etkileri nedeniyle aday genler olarak belirlenmiştir. Aday genlerin susturulması ile meme kanseri hücre hatlarında proliferasyonun düştüğü gözlemlenmiştir. RPRD2 kansere özgü aktivite gösterirken, GON4L geninin hedeflendiği normal meme hücrelerinde de proliferasyonun etkilendiği gözlemlenmiştir.

Pozitif fenotiplerin belirlenebilmesi için 3D tarama sonuçları, 2D sonuçlar ile normalize edilmiş ve ARL8A ve ARNT genleri aday genler olarak belirlenmiştir. Doğrulama deneyleri sonucunda, ARL8A ve ARNT genlerinin baskılanmasının 2D modellerde proliferasyonu azalttığı; ancak 3D sferoid büyümesini artırdığı bulgulanmıştır. Normal meme hücrelerinde ARNT susturulması ile proliferasyonun arttığı gözlenmiştir.

Bu çalışma, daha doğru fenotipik değerlendirmeler için CRISPR'a dayalı fonksiyonel taramalarda 2D modellerden 3D modellere geçişin gerekliliğini vurgulamaktadır. Ayrıca, kromozom 1q'nun meme kanserindeki rolünü ve bu kromozom üzerinde bulunabilecek potansiyel kanser sürücü genleri tanımlamaktadır.

ACKNOWLEDGMENTS

First and foremost, I would like to deeply represent my gratitude to my advisor, Assist. Prof. Gözde Korkmaz. Her guidance, support, and encouragement have been always stayed with me. Her unwavering belief to me in my bad times and good times and support in every aspect have not only shaped my research but have also profoundly influenced my life. Her passion and dedication are truly inspiring, and I am honored to have the opportunity to work under her supervision.

I would also like to extend my thanks to my thesis committee members Prof. Dr. Tamer Önder and Assist. Prof. Bahar Soğutmaz Özdemir for their invaluable feedback and insightful suggestions that improve my scientific perspective. I would like to thank my thesis defence members Assist. Prof. İrem Durmaz Şahin and Prof. Dilek Telci Temeltaş for their valuable contributions.

PhD was such a long journey and works becoming funny with my invaluable lab mates. My sincere appreciation goes to Gamze Turan, Elif Kansız, Elif Güzar and Ferzan Betül Berber. Girls I can clearly say that this study would not be come to this point without you, and I am grateful for everything that you did for me. Our ultimate alumni, Elif Yapıcı, I never forget your unbelievable spirit and I am so happy to know you. The new members Aslıhan Arğun and Aleyna Kaya, our spirit have made this journey enjoyable and fulfilling.

I would also like to extend my heartfelt thanks to Barış Sergi and Naz Uzunalioğlu who makes the PhD life meaningful with their unsparing support through all my education period and for such unbelievable memories that I always remember and smile. I am also grateful to my self-sacrificing friends Burcu Candaş and Sibel Aytürk who give a great support to overcome any difficulties during in my all life. They were always with me through this project with kindly suggestions and great support. Their existence bring invaluable memories and I know they always with me. Finally, I would like to express my thanks to Uğur Çerez, Güven Ayvaz and Ergün Başoğlu for the endless support. Every time I need, they always there to help.

Finally, and most importantly, I would like to present my thanks to my family my mother Ferda ÖZKAN, my sister Idil Ilgın ÖZKAN and my father Hamdi Özkan who always trust me and encourage me with an endless love and patience. Their encouragement never ends up through all my preferences at each stage of my life. Your sacrifices and endless patience have made this achievement possible. I am the luckiest person who has their love and great support. Finally, to my significant one Oğuzhan Coşkun whose even existence is a miracle for me. He is always with me to overcome any difficulties that I faced and to make this life meaningful with great moments. The miracle of life and the beauties I could not even imagine came together with you, and Mırmır, Bulti and Mintik Hanım.

TABLE OF CONTENTS

LIST OF TABLES

LIST OF FIGURES

ABBREVIATIONS

AhR	Aryl Hydrocarbon Receptor
AHRE	Ahr-Responsive Elements
ARL8A	ADP-Ribosylation Factor-Like Protein 8A
ARNT	Aryl Hydrocarbon Receptor Nuclear Translocator
BC	Breast Cancer
bHLH-PAS	Basic Helix-Loop-Helix-Per-ARNT-Sim
CA	Chromosomal Abnormality
CDGs	Cancer Driver Genes
CE	Common Essential
CGH	Comparative Genomic Hybridization
Chr	Chromosome
CID	CTD-Interacting Domain
CNA	Copy Number Alteration
CRISPR	Clustered Regularly İnterspaced Short Palindromic Repeat
CTD	C-Terminal Domain
DMEM	Dulbecco's Modified Eagle Medium
DSB	Double Strand Break
ECM	Extracellular Matrix
EGF	Epidermal Growth Factor
ER	Estrogen Receptor
ET	Endocrine Therapy
ET-R	Endocrine Therapy Resistance
FDR	False Discovery Rates
gDNA	Genomic DNA
GFP	Green Fluorescence Protein
GOF	Gain-of-Function
GON4L	Gon-4 Like
HCC	Hepatocellular Carcinoma
HIF-1	Hypoxia Inducible Factor-1
KO	Knockout
LOF	Loss-of-Function

Log_2(FC)	Log_2 Fold Change
MCTS	Multicellular Tumour Spheroid
MM	Multiple Myeloma
NE	Non-Essential
NFW	Nuclease-Free Water
NHEJ	Non Homologous End Joining
NHR	Nuclear Hormone Receptor
NT	Non-Targeting sgRNA
OC	Oncogene
OS	Overall survival
PAM	Protospacer Adjacent Motif
PCR	Polymerase Chain Reaction
pOC	Proto Oncogene
PR	Progesterone Receptor
PTEN	Phosphatase and Tensin Homolog
Rb	Retinoblastoma Protein
RNAP II	RNA Polymerase II
RPRD2	Regulation of Nuclear Pre-mRNA Domain Containing 2
sgRNA	Single Guide RNA
ssDNA	Single Stranded DNA
TCGA	The Cancer Genome Atlas Program
TF	Transcription Factor
TNBC	Triple Negative Breast Cancer
TR	Therapy Resistance
TSG	Tumour Suppressor Gene
TTR	Tumour to Recurrence

Chapter 1

1 INTRODUCTION

1.1 Breast Cancer (BC)

BC has a high incidence rate, with approximately 2.3 million cases reported in 2020, making it the fifth leading cause of cancer-related deaths globally according to recent cancer statistics [1,2]. Even though 70% of women diagnosed at early stages can be treated successfully, BC still exhibits high recurrence rates. Unfortunately, these recurrences often develop resistance to conventional therapies such as chemotherapy and radiotherapy, rendering them less effective [2–5].

The complexity of breast anatomy significantly impacts cancer progression, contributing to the BC heterogeneity [6,7]. At the molecular level, BC is classified into four main subtypes: Luminal A, Luminal B, HER2+, and basal subtypes as indicated in **Figure 1.1** [8]. These distinctions are critical for guiding treatment decisions; however, complexities at both histopathological and molecular levels continue to affect treatment outcome [8,9].

Luminal subtypes, which are characterised by the presence of nuclear hormone receptors (NHRs) (ER+/PR+), are the most common. The HER2+ subtype is distinguished by *ERBB2* gene amplification. The basal subtype, which lacks NHRs and HER2 abnormality, represents triple-negative BC (TNBC) and is known for being highly aggressive [10–12].

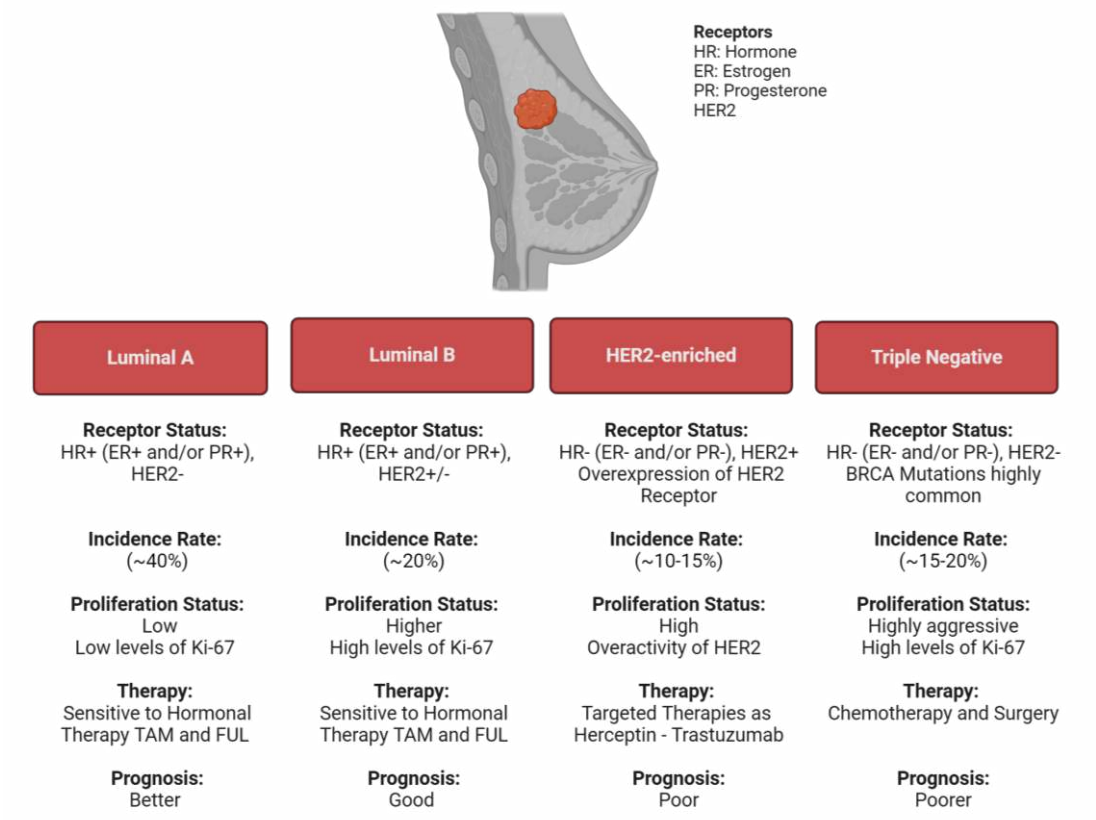

Figure 1. 1. In molecular classification of BC, four main subtypes have been reported based on specific receptor expression such as estrogen receptor (ER), progesterone receptor (PR), and HER2, as well as distinct mutational patterns. NHR positive BC is the most common subtype and endocrine therapy (ET) is the first-line treatment option, while HER2+ subtype is characterised by overactivity of mutant ERBB2 receptors. TNBC, the most aggressive subtype, lacks ER, PR and HER2 expression, and its treatment typically involves chemotherapy, mostly administered in combination regimens to improve efficacy. Adapted from [6] (Created by BioRender)

Estrogen receptors (ERs) and progesterone receptors (PRs) are steroid NHR localised in the cytoplasm. Upon activation, they translocate to the nucleus to function as transcription factors (TFs) [13]. In luminal-like BCs their activity is highly important for cancer progression. Malfunction of ER+/PR+ has a prevalent impact on proliferation, cell cycle regulation and the development of resistance to endocrine therapy (ET-R) [14–16]. In the clinic, most treatment regimens for patients with nuclear hormone receptor-positive BC are based on endocrine therapy (ET) after the diagnosis

[17]. ET could target the ER by blocking or degrading the receptor or interrupting the intrinsic pathways related to ER signalling [18]. Moreover, the production of estrogen can be directly targeted to inhibit the activation of ER [19]. Although these strategies might be highly effective in preventing the emergence of metastatic properties and local propagation in the initial stages of BC, they can potentially cause adverse chronic side effects and lead to development of ET-R [17].

1.2 Oncogenes (OCs) and Tumour Suppressor Genes (TSGs) in Cancer

During cancer evolution, mutations provide growth advantages to cancer cells, enabling them to acquire unique mutation profiles at both genetic and epigenetic levels [20,21]. Somatic mutations can drive carcinogenesis by converting a functional gene into a defective form [22]. Additionally, genetic variations such as point mutations and translocations lead to the acquisition and accumulation of further abnormalities. Large-scale mutations that alter overall chromosome composition also play a significant role in reinforcing malignancy [23,24].

In cancer progression, three types of genes - oncogenes (OCs), tumour suppressor genes (TSGs), and DNA repair genes- are defined as profound drivers [25]. Carcinogenesis is primarily induced by individual genetic variations but is exacerbated by the cumulative effects of accumulated mutations [25,26]. OCs are the mutated and activated forms of proto-oncogenes (pOC). In non-malignant conditions, several biological processes are regulated by these genes, which can act as growth factors, signal transducers, and regulatory elements [27,28]. In most cases, these genes control the cell proliferation, the cell cycle, and growth [28]. However, when they are mutated, cancer can emerge, marked by the transition from a normal stage to a malignant stage with the oncogenic functions such as uncontrolled cell division and proliferation, particularly by evading programmed cell death [29].

In BC, deregulations in pOCs have a significant impact on the progression of the disease. Activation of pOCs such as ERBB2, CCND1, MYC, and PI3KCA disrupts well-organised signalling pathways, leading to uncontrolled proliferation and cell growth, and could potentially induce metastasis [30]. PI3K, a lipid kinase, becomes activated by receptor tyrosine kinases following the binding of growth factors and hormones to their respective receptor [31]. The activation of PI3K could reinforce the several downstream

molecules such as mTOR and RAS [32]. Amplification of PI3K or point mutations acting on the catalytic subunits of the kinase are considered significant deregulations in cancer [33]. CCND1, on the other hand, serves as a regulator protein of cell cycle progression [34]. It orchestrates the transition from G1 to S phase and exerts a significant influence on cell division and proliferation [35]. Amplification of the CCND1 gene is a common occurrence in breast tumorigenesis, reported to be present in 10-35% of BC patients [36,37]. MYC is a well-known OC whose deregulation significantly enhances carcinogenesis by disrupting control mechanisms in apoptosis, cell division and DNA damage response [38]. Activation of the MYC pOC typically results from chromosomal translocation, amplification, or deregulated signalling proteins responsible for MYC stability [39,40]. Because MYC functions as a TF, its deregulation leads to the activation of several downstream target genes [41]. Another well-defined OC, ERBB2, significantly contributes to tumorigenesis by acting as a transmembrane tyrosine kinase and can activate several intracellular signalling pathways by inducing Ras or PI3K [42,43]. Deregulation of ERBB2 in BC is primarily due to the overexpression and/or gene amplification [44].

Apart from pOCs, TSGs play a diverse role in BC progression. The activation of pOCs in cancer is largely facilitated by inactivation of TSGs, with these two genetic alterations synergistically driving advanced tumorigenesis [26]. TSGs serve as common regulators of cell proliferation, tightly controlling cell proliferation and growth, repairing DNA damage, and acting in cell cycle checkpoints [21]. Loss-of-function (LOF) mutations in TSGs disrupt well-balanced regulation of normal growth and proliferation, subsequently causing unrestrained proliferation and division [30].

In BC, phosphatase and tensin homolog (PTEN) is a well-defined TSG whose inactivation is related with the overactivity of PI3K [45]. Lost or inactivation of PTEN disrupts negative regulation points in PI3K downstream signalling, leading to uncontrolled proliferation and growth capacity in cells [46].

LOF mutations in BRCA1 and BRCA2 genes predispose individuals to BC and are associated with the aggressiveness of cancer progression. Loss of these genes is linked to the acquisition of metastatic potential [47]. While earlier reports linked the BRCA1/BRCA2 loss with TNBC, later studies have shown that these mutations are

enriched in older patients with ER/PR+ [48,49]. Upon loss of BRCA1, DNA repair mechanisms are affected, rendering DNA more susceptible to gain additional mutations [50]. BRCA2 has the potential to bind both to single stranded DNA (ssDNA) and double stranded DNA and is linked with the DNA repair, particularly in homology-directed repair (HDR) [51]. The maintenance of restrained DNA repair mechanisms is highly important to protect against genomic instability and prevent the accumulation of genetic variations as seen in cases of BRCA1/BRCA2 loss [50].

TP53, often referred to as the master guardian of the genome, is responsible for the sustained monitoring of the cellular state against stress signals from both extracellular and intracellular environments [52,53]. Upon encountering any stress signal that could compromise the genomic stability, TP53 as a TF, activated checkpoints, senescence, or apoptosis by binding to several target gene promoters associated with these processes [54,55]. In BC, the most commonly shared mutation type leading to TP53 loss is reported as missense mutations. These mutations disrupt the DNA-binding capacity of TP53 and/or alter its binding pattern, which may lead to its interaction with different targets, especially contributing to genetic instability [56].

In conclusion, the progression of breast cancer is driven by the dynamic interaction between OCs, TSGs, and DNA repair genes. Oncogenes such as ERBB2, CCND1, MYC, and PI3KCA become dysregulated through mutations and amplifications, leading to uncontrolled cell division and survival. In contrast, TSGs including PTEN, BRCA1, BRCA2, and TP53, when inactivated by LOF mutations, fail to regulate cell proliferation, maintain genomic stability, and execute DNA repair, fuelling the malignancy and genetic diversity of cancer cells. These genetic alterations collectively drive the malignancy of cancer, unleashing a genetic disorder that accelerates the accumulation of further mutations.

1.3 The Importance of Chromosome Abnormalities in Cancer

Tumour formation is a multistep process that initiates with tumorigenesis. Cells acquire proliferation and survival advantages due to genomic instability which enables them to resist cell death signals, evade growth-suppressing signals, and reprogram cellular metabolism [57]. As cells begin to lose genome integrity, they acquire favoured chromosomal abnormalities (CAs) to alter their karyotypic organisation [57]. These

cells then dominate populations due to their enhanced growth and proliferation capacity [58]. Tumour-associated genomic instability has been shown to induce amplification and/or deletion of chromosomal segments (focal alterations) or entire chromosomal arms, which are considered the main phenomena disrupting genome integrity [59,60].

CAs are classified into numerical and structural types. Numerical abnormalities are associated with errors in chromosome segregation during mitosis, resulting in aneuploidy and chromosome instability [61]. Structural abnormalities on the other hand, arise from large-scale DNA damage and are the main source of copy number alterations (CNAs) at both focal levels and whole chromosome arm levels [62]. Accumulating evidence indicates that CAs are one of the essential drivers of tumour progression by modulating the expression pattern or function of RNAs [63–66]. CNAs, as a type of structural CA, have been reported in 88% of cancer samples and involve copy number gains or losses of specific subregions of chromosome/genes or entire chromosome arms [67].

Comparative genomic hybridization (CGH) stands as a well-established methodology for investigating the CNAs of genes, shedding light on the somatic mutation landscape of cancer. This technique enables the detection of specific gene losses, recurrent driver gene amplifications, or whole arm gains/losses [68]. Through CGH, significant insights are gained regarding focal and whole arm amplifications or deletions, mostly involving genes crucial for tumour progression [69]. While structural CAs may vary between cancer patients, a shared abnormality profile can be identified within certain groups of cancer patients. This shared profile offers valuable information for prognosis, diagnosis, treatment response, and importantly for development of targeted therapies [70–72]. For example, focal amplifications predominantly lead to copy number increases of oncogenic drivers [73,74]. By mapping and detecting amplified chromosomal sites, candidate OCs can be characterised, aiding in therapy response estimation, identification of therapy resistance (TR) mechanisms and the selection of potential candidates for targeted therapies [75–78].

Gene amplification directly affects gene expression, with copy number increases typically resulting in overexpression of corresponding genes, termed amplicons, as briefly explained in chapter 1.2 [70]. BC exhibits a characteristic gene amplification

signature that could include copy number increases in ERBB2, CCND1, MYCN and EGFR genes, affecting normal cellular growth and survival pathways and promoting tumour growth [72]. Alterations in gene expression profiles induced by gene copy number changes were first identified for the MYC gene, with several cancer patients harbouring MYC copy number increase exhibiting a low survival rate and poor prognosis [79]. In BC, amplification in ERBB1 (also known as HER1 or EGFR) and concomitant overexpression have a diagnostic value and potential for estimating therapy response [80,81]. Another well-known example is the EGFR gene located in Chr7p12. Its amplification is associated with tumorigenesis promotion, poor survival rate and bad prognosis. Thus, amplification status is used for prediction of the therapy response [82,83]. CCND1, a commonly amplified gene in several cancers, is also associated with poor survival and TR [84,85].

In conclusion, cancer cells have been reported to acquire oncogenic advantages through the accumulation of multiple mutations, primarily driven by genomic instability. Numerous scientific studies underscore that CNAs are frequently related with the gain of genes harbouring oncogenic functions and loss of TSGs, thus directing tumorigenesis.

1.4 Chromosome 1q Abnormalities in Cancer

CNAs are briefly defined as certain driver events that are affecting the cancer progression [71]. In various types of cancers, CNAs are reported for both chromosome arms and subregions of specific chromosomes [86–88]. Numerous reports indicate that CNA in Chr1q is prevalent in various cancers such as hepatocellular carcinoma, blood cancer, brain cancer, and BC, with well-defined numerical abnormalities [89–92]. Therefore, genes located in Chr1q are likely important for tumorigenesis.

In multiple myeloma (MM), CNAs in Chr1q have been associated with adverse prognosis, poor survival, and chemoresistance [87,93]. Studies based on patient samples indicate a strong relationship between CNA of Chr1q and aggressive disease progression [87,94]. Specifically, subregion-specific amplification of Chr1q, particularly 1q21, is a common CA occurring in 40% of MM patients [95]. The 1q21 amplicon consists of important genes such as CKS1B, PSMD4, IL6R, ADAR, and MCL1, which are crucial for uncontrolled cell proliferation and/or drug response. Therefore, amplification of this

subregion results in dysregulated gene dosage, contributing to the pathogenesis and progression of the disease [96–100].

The most recent study examining the content of Chr1q in MM integrated patient multi-omics datasets and identified PBX1 as a novel therapeutic target. PBX1 acts as a TF that regulates the critical oncogenic pathways in conjunction with FOXM1. By elucidating PBX1-regulated oncogenic circuitries, they tried to propose a novel targeted agent and revert the aggressive phenotype associated with CNA [101]. These strategies represent pioneering efforts to develop molecular targeted therapies that can mitigate distortions caused by CNAs [102].

Besides MM, CNAs are also observed in hepatocellular carcinoma (HCC). The most common copy number abnormality in HCC is also found in Chr1q, which is strongly associated with poor prognosis and short survival duration. This CNA results in the overactivation of potential OCs that prime cells to escape apoptosis, induce chemoresistance, and promote invasion and metastasis, thereby leading to a high level of tumorigenesis [89]. In 2021, a well-designed review listed genes located in Chr1q21-23 subregions, indicating genes such as JTB, SHC1, CCT3, COPA, NUF2, and TPM3 contribute to HCC progression [103].

In all cases summarised in this section, the findings are based on omics-based approaches, and there is no well-organised study investigating the Chr1q genes in a functional manner.

1.5 Insights into Chromosome 1q Copy Number Alterations in Breast Cancer

Studies aiming to clarify underlying reasons of BC complexity have shown that both small-scale and large-scale mutations, which accumulate in the genome, are major contributors to BC formation, progression, and the development of TR [22,104,105].

Chromosomal instability signatures have been linked to clinicopathologic outcomes and have diagnostic value for estimating prognosis in terms of malignancy grade and survival duration [106]. Investigations on chromosome and/or gene copy number in patient samples have correlated BC progression with specific CNAs. One of the initial studies, published in 1994, reported CNAs in both whole chromosome and chromosome

arms, as well as regional gains in BC across 5 different cell lines and 33 primary patient samples [107]. CGH showed significant copy number increases in various chromosomes, particularly in 8q, 17q and 20q. In the case of Chr1q, a certain gain was reported, but it involved a whole arm gain rather than focal increases [107].

In TNBC, CNAs are reported as highly frequent genetic changes. One study examined CNAs in TNBC using data from the TCGA database, aiming to understand the relationship between CNAs and their functional impacts on gene expression profiles. The study reported that CNAs could involve entire chromosome arm gains or losses, as well as focal amplifications or deletions, contributing to the genetic heterogeneity observed in patients. The genome-wide frequency plot of CNAs showed that entire chromosome arm gains were most commonly observed in 1q, 8q, 10p and 12p, while losses were observed in 5q, 8p and 17p, as represented in Figure 1.2 [108].

In 2020, another study also reported that subtype-independent gains commonly observed in chromosome arms 1q, 8q, and 16p, while common losses were observed in chromosome arms 16q, 17p and 8p, based on data taken from the TCGA database. Researchers in this study indicated that more than 50% of the BC samples specifically had gains in Chr1q and Chr8q, while specific losses were found in 16q and 17p [109].

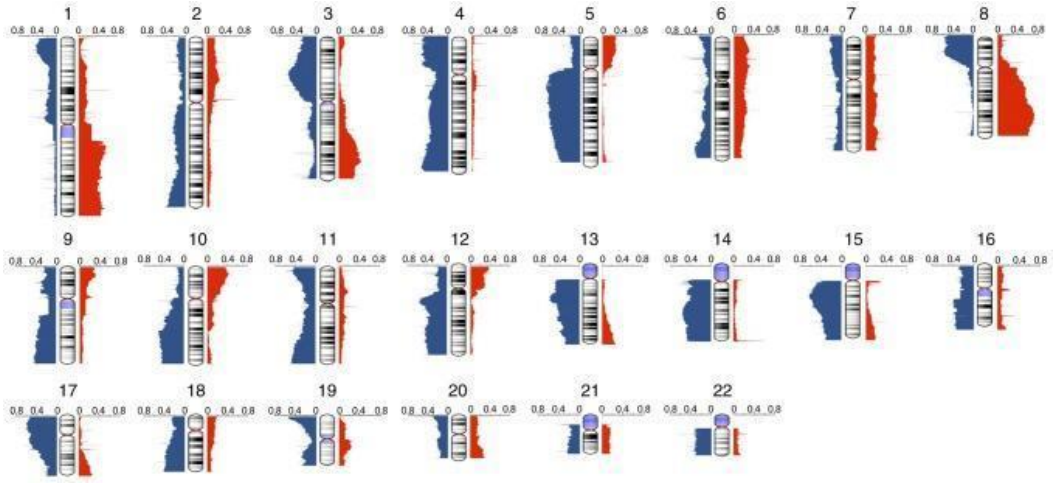

Figure 1. 2. Frequency of copy number alterations was investigated using data retrieved from the TCGA database for TNBC patient samples. In Chr1, specific somatic CNA were identified, including focal deletion in Chr1p and focal amplification in Chr1q (Red Color: Gains, Blue Color: Losses; Adapted from [108]*).

Subtype-specific examinations have revealed significant variability between four different subtypes of BC in terms of the frequency of CAs [109]. Gains in Chr1q arm were specifically observed in samples belonging to Luminal A subtype in more than 70% of cases. Luminal A cancers showed losses in 16q in more than 70% of cases [109]. In Luminal B, HER2+ and basal subtypes, the most common gains were also observed in Chr1q, with frequencies of 76.5%, 74.6%, and 74.1% respectively. Furthermore, in Luminal B and basal subtypes, gains in the Chr8q arm were also associated with Chr1q gains. This study clearly indicates that BC exhibits a unique CNA profile that specifies the progression in a subtype-specific manner [109].

In 2019, Johansson et al. conducted a groundbreaking study that, for the first time, linked CNAs with changes in expression at both mRNA and protein levels [110]. This sophisticated study utilised the knowledge about the relationship between CNAs and expression of corresponding transcripts. In this study, patient samples from four different subtypes were investigated for their genomic variabilities and consequent transcriptome and proteome landscapes [110] and showed that CNAs and altered genes showed an attenuation at the protein level. In all subgroups of BC examined, it has been shown that CNA is observed throughout the genome, affecting both protein-coding genes and regulatory regions. Notably, gains were predominantly found in Chr17 and Chr1q. While this study provides clear evidence of mRNA and protein expression changes associated with CNAs; it did not clarify the functional consequences of these CNA. The overall gain phenomena are depicted in **Figure 1.3** [110].

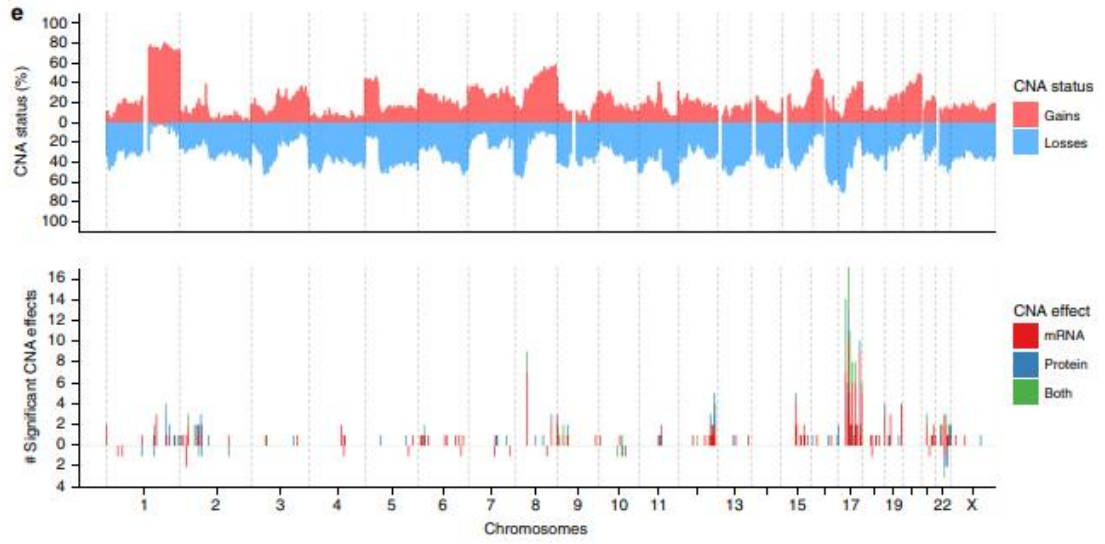

Figure 1. 3. BC patients showed a certain amplification in Chr1q arm, and this somatic alteration resulted in attenuated protein expression, as demonstrated by next generation proteome analysis (Adapted from [110]*).

Single-cell genome sequencing is a powerful tool to examine the heterogeneity of individual cells within a tumour. A study performed in 2020 clearly demonstrated that individual cells from 16 different BC patients and 200 different genomes showed an accumulation of gains in chr1q and chr8q arms - regardless of subtype [111]. In HER2+ subtype, Chr1q amplification was also observed, along with the specific amplification of Chr17q, which is directly related with ERBB2 pOC [112]. In TNBC, CNAs have been linked to lymph node metastasis, with specific amplifications and/or deletions promoting the invasive character of BC cells. A study analysing 23 invasive ductal carcinomas and 12 lymph node metastases found significant amplification in Chr1q region compared to normal adjacent tissues [113].

All these studies, based on samples from BC patients and/or cell lines demonstrated the importance of CNAs in Chr1q arm and suggest their potential role in promoting breast tumorigenesis. These CNAs likely influence expression of candidate OCs, contributing to cancer development. ***Therefore, these distinct CNAs in the Chr1q arm in BC have been investigated in terms of the corresponding genes involved in amplified regions to identify their oncogenic potential.*** In this context, researchers have started to examine subregions of Chr1q to clarify why BC cells have a high tendency for focal or whole-

arm CNAs in this region. For example, candidate OCs located on the Chr1q arm, such as *PLU-1/JARIB1,* have been reported; however, the implication in BC and the augmented expression due to CNAs have not been conclusively proven in a functional manner [114, 115].

Since the early 2000's, several reports have proven that amplified regions can modulate the expression levels of the genes located within them, potentially endowing these genes with oncogenic character that confer a proliferation and growth advantage [114,115]. For example, poor prognosis of BC patients has been linked to CNAs in Chr8q and Chr11q arm [116]. These CNAs have been correlated with array expression data, revealing that the amplified regions harbour cancer-promoting genes with oncogenic potential. Patients with these amplification profiles tend to have a poor clinical prognosis [116–118]. Most known genes with altered expression profiles and oncogenic potential include *MYC and CCNE2* on the Chr8q arm, and HER2 on the Chr17q arm [119]. In 2006, a study mapped expression level changes and CNAs to establish a well-defined pattern for CNAs on Chr1q. Based on array-CGH profiling and subsequent expression profiling in 29 cell lines and 26 primary breast tumours, it was shown that copy number increases on Chr1q were specifically enriched in some cytobands, such as 1q21.3(*PIP5K1A*), 1q22(*RAB25*), 1q41(*ESRRG*), and 1q42.13(*RAB4A*), along with an additional 16 genes located in 1q21, 1q22, 1q24, 1q32, 1q41, 1q42. ***Even though the functional consequences of CNA and the linked genes expression fluctuations of these genes in BC malignancy were not investigated, the study did show a clear relationship between CNAs and the expression levels of corresponding genes*** *[92]***.**

The frequent amplifications in subregions of the Chr1q arm suggest potential targets for BC treatment. The first report focuses on the gene expression profiles of Chr1q arm in 1635 breast tumour samples [120]. This research identified seven genes - *CENPF, KIF14, NEK2, DTL, CKS1B, ASPM and EXO1* - that were overexpressed in high-grade, aggressive breast tumours and were associated with poor clinical outcomes. Among these, as a clinical target *EXO1* was notably overexpressed and closely linked to poor prognosis, regulated by *EGFR, RAS,* and *EXO1*. Therefore, the study proposed that targeting *EXO1* could be highly effective for treating patients with *EXO1* overexpression. [120]. In addition, CNA at 1q21.3 has been associated with BC

recurrence and early relapse. While CNAs in Chr1q region occur in10-30% of primary tumours, they are found in up to 70% of recurrent tumours [121]. The relationship between 1q21.3 amplification and chemoresistance has also been investigated and authors discovered that the amplification of 1q21.3 modulates members of S100 calcium-binding protein (S100A) family specifically S100A7, S100A8, and S100A9 (S100A7/8/9), and IL-1 receptor–associated kinase 1 (IRAK1), which drive chemoresistance and relapse [121]. To counteract the IRAK1-driven resistance associated with these CNAs, pacritinib, a small-molecule kinase inhibitor, was used effectively [121].

Even though the extensive content of Chr1q, which contains approximately a thousand genes, research studies has predominantly focused on the well-known phosphoinositide signalling pathway. As an example, a study reported that 62% of the tumours exhibited CNA in the *PI4KB* gene, which is participated in PI3K/AKT pathway. In addition, the genes *PI4KB, PIP5K1A, PI3KC2B* and *AKT3*, all located on the Chr1q arm, show CNAs that are associated with elevated downstream protein expression elevation. The amplification of these genes in the PI3K/AKT pathway potentially enhances the proliferative ability of BC [122]. CNAs and corresponding gene changes have been also observed in the Basal-like subtype. Specifically, genes such as *PI4KB* (involved in the PI3K/AKT pathway), *SHC1*, and *NCSTN* (involved in the Notch pathway) have been identified as potential driver genes due to the amplification of the Chr1q21-23 subregion, making them candidates for therapeutic targeting [123]. Amplification in the 1q21.3 region has been linked to poor patient survival and increased tumour growth in TNBC patients [124]. The 1q21.3 region involves the *ENSA* gene (alpha-endosulfine), which regulates cholesterol biosynthesis by influencing sterol regulatory element-binding TF 2 (SREBP2). SREBP2 is a critical TF that directly controls cholesterol biosynthesis. Reduced SREBP2 activity is associated with increased levels of p-STAT3 (Tyr705). This finding has led to the development of a targetable therapeutic approach, suggesting that the STAT3 inhibitor Stattic could be used for TNBC patients with increased *ENSA* levels in cases of the Chr1q amplification [124].

Studies summarised so far suggest that the Chr1q arm can be amplified as a whole; however, specific subtype amplifications are more likely to occur. In addition to DNA-

level changes, epigenetic instability has been observed in the subregion 1q12 subregion, which contains the largest pericentromeric heterochromatin (PCH) structure and is associated with breakpoints. The 1q12 PCH is directly linked to 1q CNAs, and it has been proposed that the dosage of potential OCs in this region may increase with these CNAs [125].

As a result, these studies underscore the critical importance of alterations in the Chr1q arm, both as a whole and within specific subregions (focal), in driving increased gene expression of key OCs. Despite detailed elucidation of specific subregions and their contents, and recognition of Chr1q role in harbouring pivotal malignancy-related genes such as those in PI3K/AKT pathway, there remains a significant gap. The detailed functional assessment needed to evaluate the full spectrum of CNAs within Chr1q is conspicuously missing, representing a crucial area for further research and therapeutic targeting.

1.6 CRISPR-based Functional Genomic Screening

In nature, clustered regularly interspaced short palindromic repeats (CRISPRs) and CRISPR associated (Cas) genes defends bacteria and archaea against exogenic mobile genetic elements such as viruses or foreign plasmid DNAs as a protective system and acts as a genetic adaptive immunity [126,127]. In the early 2000's, CRISPR/Cas systems began to be harnessed for precise genome editing by modifying type II CRISPR/Cas9 complexes into a robust and versatile platform [127,128]. CRISPR/Cas9 can be defined as an RNA-guided nuclease-based genome editing platform that enables genetic manipulation at specific genomic locus with high precision [129,130].

Cas9 (CRISPR associated protein 9), as a nonspecific nuclease, can be programmed using guide RNA (gRNA) design to target specific genomic sequences [131,132]. Cas9 performs its nuclease activity with the guidance of sgRNA, which recognizes the target DNA sequence and directs the CRISPR/Cas9 complex to the precise genomic locus [133].

After sequence-specific binding occurs by gRNA, the enzymatic activity of Cas9 depends on the presence of protospacer adjacent motif (PAM) in the target genome, which has specific nucleotide sequence as - NGG [131,134]. Upon binding of sgRNA-

Cas9 complex to the target site and recognition of the PAM, Cas9 generates double strand breaks (DSBs) which lead to activation of DNA repair mechanisms, namely non-homologous end joining (NHEJ) and homology directed repair [135–137]. In the absence of a homologous sequence, cells primarily repair the DSBs by NHEJ which is an error-prone repair system resulting in permanent changes such as indel (insertion-deletion) mutations. In most cases, the expression of the target gene repaired by NHEJ is disrupted or abolished due to indel formation [138,139].

Since 2013s, the CRISPR/Cas9 technology has been used to manipulate mammalian cell genomes in a targeted manner, ushering in a new era for functional genomics [140–143]. After several improvements, multiple genomic regions can be targeted using pooled guide RNA libraries, enabling large-scale functional genetic screenings for both coding and regulatory regions of the human genome [14,143,144]. Genome-wide CRISPR-Cas9 dropout screening is a versatile tool for characterising oncogenic driver genes. This technique identifies candidate OCs that affect the cell viability, proliferation, and resistance to apoptosis, thereby elucidating the mechanism of malignancy during cancer initiation and progression [145]. Several studies have demonstrated the high potential of dropout screening for understanding the candidate genes and their roles in regulating downstream pathways [143,146,147]. CRISPR-based genomic screening stands as a cutting-edge method utilised for various objectives, including pinpointing candidate OCs, modulators of phenotypic traits, and potential drug targets [148,149].

Functional genomics, particularly through functional phenotypic screening, has become highly prominent in cancer-focused studies for identifying the roles of genes and regulatory elements essential to the malignant phenotype [150,151]. Over the past decade, CRISPR-based screening has emerged as a fundamental technique for genome-wide loss-of-function (LOF) analysis, offering numerous advantages over traditional methods, including decreased off-target effects and precise design capabilities [152,153]. The feasibility of genome-wide screening in mammalian cells was demonstrated in 2014, paving the way for CRISPR-based LOF assessments to elucidate cancer-specific vulnerabilities and characterise novel genes, as illustrated in the experimental work-flow shown in **Figure 1.4** [143,144].

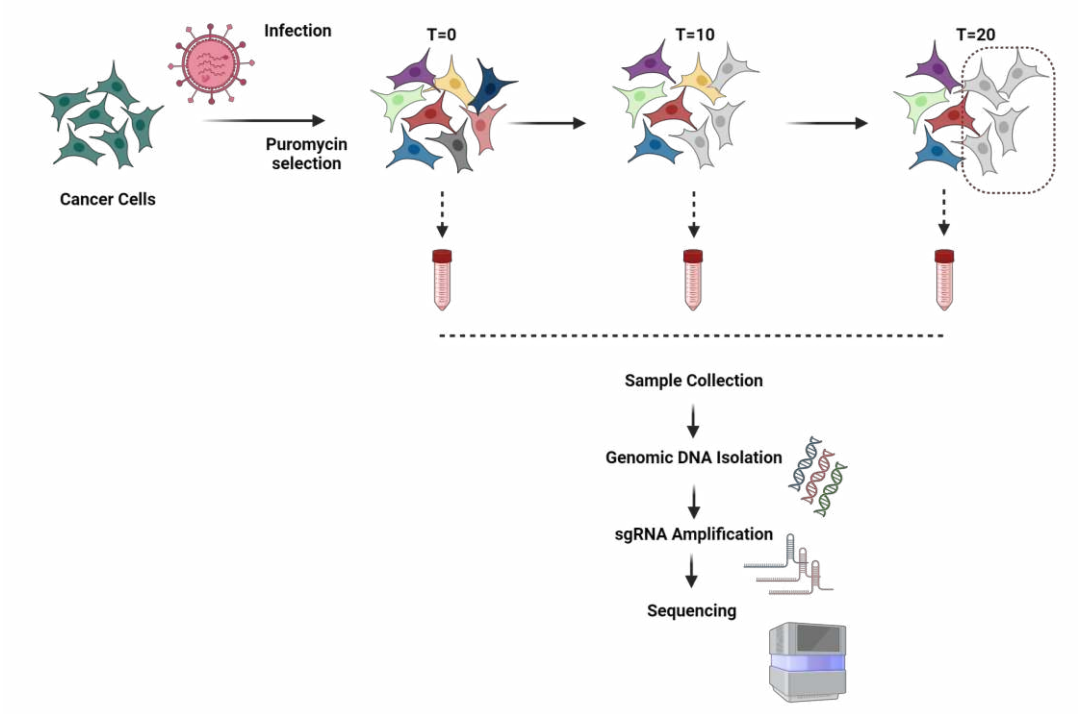

Figure 1. 4. CRISPR based functional screening workflow. In cancer cells, CRISPR-based loss-of-function (LOF) screening pinpoints essential genes crucial for cell proliferation. This technique uncovers cancer-specific vulnerabilities, shedding light on the mechanisms driving cancer initiation and progression. Adapted from [154] (Created in BioRender).

In HCC, genome wide CRISPR screening has implicated PHGDH as the driver gene responsible for Sorafenib resistance. Targeting PHGDH with a specific inhibitor NCT-503 in a combination therapy successfully overcome Sorafenib resistance [155]. Similarly, genes that are driving Lenvatinib resistance were characterised by genome wide CRISPR screening and critical genes were defined as NF1 and DUSP9 in HCC [156]. In ovarian cancer, CRISPR-based knockout screening has been instrumental in characterising key drivers of anoikis resistance and understanding the mechanisms behind metastasis. One notable candidate, PCMT1, identified through screening and linked with late-stage metastasis, controls the cell migration, adhesion, and spheroid formation. As a secreted protein, PCTM1, interacts with ECM protein LAMB3, influencing these critical processes [157]. In MM, CRISPR-Cas9 screening has been utilised to identify resistance mechanisms and resensitization factors against

Thalidomide analogues, which are commonly used treatment agents. TOP2B was identified as a new therapeutic target to overcome resistance and enhance sensitization to those agents [158]. These studies mentioned above demonstrate genome-wide CRISPR screening can effectively clarify cancer-related vulnerabilities by uncovering the mechanism behind malignant phenotypes. This approach holds great potential to identify novel targets in cancer.

Apart from genome-wide screening, smaller custom libraries that target specific subsets of genes or genomic regions can more precisely and accurately identify potential target genes [153,159]. As a targeted discovery platform, CRISPR screening with custom libraries addresses hypothesis-driven questions and identifies genes related to specific phenotypes of interest [160]. The identification of candidate OCs and TSGs, as well as the development of novel therapeutic approaches, can be performed more precisely with the arrayed libraries, which lower the complexity of the screen [161].

In BC, genome-wide CRISPR screening has been instrumental in precisely identifying genes that drive cell survival, proliferation, metastasis, and TR [162–164]. Based on analysis combined from publicly available datasets, lethal genes that are upregulated in BC have been characterised by LOF screening. Gene ontology analysis has revealed that these upregulated genes in BC overlap with lethal genes identified in DepMap database, particularly enriched in pathways related to oncogenic functions and the cell cycle [162–164].

In the luminal subtype of BC, ET targeting the ERα is the primary therapeutic approach. However, ET-R is prevalent among patients. CRISPR-based screening, has been employed to identify genes whose e loss contributes to ET-R, revealing underlying mechanisms of resistance. In addition, efforts have been focused on defining synthetic lethal targets to identify synergistic therapy options in combination with ET [165]. One identified target is CSK, a TSG driven by ERα, whose loss is directly linked with estrogen-independent growth. The mechanism is clarified in luminal subtypes, resistance to ET occurs through attenuation of the CSK expression, mediated by the activation of PAK2. PAK2 modulates estrogen-independent growth pathways, highlighting its role in ET resistance mechanisms. Synthetic lethal targets for

combinational therapy are being defined by uncovering PAK2 related mechanisms [165].

As highlighted, CRISPR screening emerges as a versatile and powerful tool adept at pinpointing vulnerabilities in cancer. Continuous improvements in this editing platform enable precise characterization of pivotal genes involved in malignant transformation through dropout screenings. Hypothesis-driven screenings using custom libraries show great potential in elucidating specific target genes.

1.7 Evolving Perspectives: From 2D Monolayered Models to 3D Spheroid Models

Cancer biology research continues to rely mostly on two-dimensional (2D) monolayered models as in vitro experimental models. While 2D models are valuable and serve research needs, accumulated experimental evidence shows their limitations in recapitulating solid tumour behaviours. This is due to their lack of highly organised cell-cell contacts and the distinct microenvironment characteristic of solid tumours [166–168].

The interactions between malignant cells and their surrounding cells and matrix have a profound impact on tumour progression. It was shown that especially solid tumours show distinct patterns in intra- and extracellular signalling during their propagation. Tumour masses also exhibit varied responses to environmental conditions, leading to remodelled cellular metabolisms [169,170]. Therefore, three-dimensional (3D) in vitro models are hypothesised as superior models for mimicking natural tumour masses due to their ability to replicate tumour heterogeneity and hierarchical reorganisation. These models also provide a more accurate representation of the effects of cell-cell contacts on cancer signalling pathways [168,171–173]. 3D in vitro models are depicted to more accurately characterise the phenotypic impacts of the cell polarisation and layered structure within tumour masses [174,175].

Multicellular tumour spheroids (MCTSs) represent a prominent 3D model in cancer research for modelling growth and division kinetics that closely mimic in vivo tumour masses [176]. The heterogeneity of cancer cells within MCTSs enables the recapitulation of malignant tumours more efficiently through gene expression profiles

[177]. These systems allow generation of 3D structures cost effectively with easy handling and prominent scalability than other systems such as patient-derived xenografts, patient-derived organoids, and genetically engineered mouse models [178]. Various methods exist for generating spheroids, including those based on chemical scaffolds like natural hydrogels and synthetic hydrogels, as well as mechanical systems such as spinner flasks. [176]. According to experimental flow and research aims, selecting the most appropriate 3D spheroid model allows researchers to conduct context-specific experiments effectively [179].

Cancer biology research predominantly utilises 2D models even this fall short in accurately replicating the complex cell-cell interactions and unique microenvironment of solid tumours. This limitation can result in mischaracterization of altered cancer metabolisms. 3D in vitro models, on the other hand, are preferable for mimicking natural tumour masses, as they better replicate tumour heterogeneity, and hierarchical organisation in cancer signalling pathways. MCTSs are prominent 3D models that closely mimic in vivo tumour growth and division kinetics through heterogeneous cancer cell gene expression profiles. MCTSs offer cost-effective, scalable solutions with easier handling; therefore, their use especially in functional studies has great promise.

1.8 Enhancing Cancer Driver Gene Identification Through Functional Screening in 3D Spheroid Models

Recent studies underscore the importance of in vitro models and highlight the necessity for more accurate models to characterise putative cancer driver genes (CDGs) that closely reflect human disease [170,180]. Functional screening in 3D cancer spheroid cultures, whether in lung, breast, prostate cancer, or human mammary epithelial cells, offers an opportunity to identify causative cancer drivers as models that better recapitulate the original tumour bulk structure [167,169,170,180,181]. Established scientific research indicates that screening in spheroids, valued for their scalability and ease of handling as in vitro models, yields distinct outcomes compared to traditional 2D models. [181]. Importantly, functional screening in 3D spheroids provides an opportunity to uncover CDG features that closely mimic in vivo tumour growth [167,169,170,180].

While CRISPR screening is highly effective for identifying OCs, conventional 2D CRISPR KO screenings are known to have limitations in identifying TSGs [181]. Pioneering studies have demonstrated that targeting the well-defined TSGs can lead to negative phenotypes in conventional 2D models, often resulting in an incomplete depiction of a gene's oncogenic activity. In contrast, 3D screening has been shown to better characterise positive phenotypes compared to 2D models; especially when results are normalised against corresponding 2D outcomes [180]. The differential behaviour of putative CDGs and their phenotypic impacts on tumorigenesis can be more accurately elucidated in 3D settings, particularly in uncovering positive phenotypes in functional screenings.

A study validating this concept underscored the imperative to enhance CRISPR screening systems for 3D models, highlighting that elucidating the functions of candidate CDGs is more effectively achieved in 3D rather than 2D settings. CRISPR screening yields distinct outcomes in 2D versus 3D, with 3D models proving more adept at representing the growth phenotype observed in actual tumour masses found in patients. This research demonstrated the more precise identification of TSGs in 3D spheroids, pinpointing a novel gene crucial in lung tumorigenesis, carboxypeptidase D, which remained undetected in 2D screening but exhibited significant effects in 3D spheroid screening alone. Following the validation of this gene, the study underscored the essential disparities between 3D and 2D models in cancer research [180].

In a study published in the same year, cancer spheroids were employed as in vitro models, leveraging their layered structure to simulate the bulk of lung tumours. This setup capitalised on the ability of inner layers to withstand oxidative stress [169]. Screening efforts identified lung cancer-specific vulnerabilities that are responsible for hyperactivation of NRF2, which is a TF regulating the OxS responses in cancer cells. The study demonstrated that the phenotypic impact of NRF2 downregulation was more pronounced in 3D spheroids compared to 2D cultures. 3D spheroids exhibited greater dependence on NRF2 hyperactivation. CRISPR screening further identified dependencies associated with hyperactivation of NRF2 that promoted spheroid growth. Simultaneous screening in both 2D and 3D models showed that the loss of TSC1 and

the gain of GPX4, which showed stronger effects in 3D screening compared to 2D screening, were related with NRF2 hyperactivation-mediated spheroid growth [169].

In BC research, CRISPR screening was performed simultaneously in 2D and 3D models to identify cancer-promoting genes involved in proliferation, DNA repair, and DNA damage response [181]. The study aimed to define the causal variants as the genes which have an ability to mediate cancer phenotypes and proposed study had concluded BC risk genes related with impaired proliferation in both 2D and 3D models. Even though this study had been performed only in normal breast cell lines, the putative OCs and TSGs were tried to be defined as causal variants that promote cancer by inducing proliferation phenotype [181].

A study published in 2022 aimed to elucidate novel regulators of PAR polymerase inhibitors (PARPi) resistance to enable new combinatorial therapeutic approaches in prostate cancer. Through the genome wide CRISPR screening in spheroids, the research identified a novel gene, TBL1XR1, which was found to regulate the sensitivity of prostate cancer to olaparib [167]. In this case, 3D spheroid screening was selected as a more reliable and relevant model to interrogate the resistance mechanisms against PAPRi in prostate cancer. A similar scientific approach was followed by another study published in 2021, which aimed to profile resistance mechanisms against CDK4/6 inhibitors. Genome-wide 3D spheroid screening enabled the identification of candidate genes responsible for drug-resistant phenotypes. This study showed that 2D monolayer models failed to discover unique driver genes, whereas 3D spheroid models showed promise for more accurately identifying novel genes [170].

Recent studies underscore the necessity of accurate in vitro models for characterising CDGs that closely reflect actual tumour biology. Functional screening in 3D models, including those of lung, breast, and prostate cancer, reveals that 3D models allow for the identification of differential LOF, and gain-of-function (GOF) phenotypes not observed in 2D models. While CRISPR screening is effective at identifying OCs in 2D models, it struggles to identify TSGs, which 3D models can reveal more accurately by providing a precise depiction of positive phenotypes. Overall, 3D models are increasingly recognized for their superior ability to recapitulate tumour behaviour and identify critical CDGs.

1.9 Aim of the study

BC imposes a significant health burden, accounting for approximately 2.3 million cases and ranking as the fifth leading cause of cancer-related deaths in 2020. CNAs in Chr1q play a significant role in the pathogenesis and progression of BC. Their presence often correlates with poor prognosis and resistance to treatment, underscoring their importance as critical targets for diagnostic and therapeutic interventions. Understanding the molecular mechanisms driving these alterations is imperative for advancing cancer treatments.

The first aim of this study is to interrogate the landscape of Chr1q in BC and identify prevalent CDGs. To achieve this, we designed and generated a CRISPR library, named LIBGENE1Q, targeting 940 genes located in Chr1q. We conducted screening using this library in two luminal BC cell lines, MCF7 and T47D, and a non-tumorigenic control cell line, MCF12A, to elucidate the functional role of Chr1q.

The second aim is to identify cancer-specific vulnerabilities that exhibit an enrichment phenotype suggestive of TSGs. We performed simultaneous screening in both 2D and 3D cell culture models, characterising positive phenotypes by normalising the screening results as 3D/2D ratios.

Chapter 2

2 MATERIALS AND METHODS

2.1 Designing and cloning of LIBGENE1Q CRISPR Library

2.1.1 Library Design and Construction

To interrogate the function of Chr1q genes, we developed a custom CRISPR library named LIBGENE1Q, specifically designed to target 940 genes annotated within Chr1q [182]. According to DepMap Public 23Q2 data version, Chr1q contains 80 common essential genes (CE), while 825 genes are annotated as non-essential genes (NEs). The library also contains sgRNAs targeting 2 genes as internal positive controls (2 genes ribosomal) and 500 non-targeting sgRNAs as negative controls (NTs). sgRNA library had been designed by combining different sgRNAs from three different publicly available libraries as Toronto, Sanjana and GecKO to maximise the knock-out efficiency [143,183,184].

2.1.2 Pooled sgRNA Library Cloning

Synthesised pools of ssDNA oligonucleotides were used to establish a LIBGENE1Q library that included 9900 different sgRNAs. Pooled oligo mix was resuspended according to manufacturer instructions and PCR based amplification was performed with the conditions as: Thermo Scientific™ Phusion™ High-Fidelity DNA Polymerase (0.5 µl) was used for 50 µl total reaction by mixing 1 ul suspended oligo mix with 2 µl of forward primer (10 µM), 2 µl of reverse primer (10 µM) (Table 2) 10 µl of 5X HF buffer (Thermo Fisher) and 0.5 µl dNTP mix (10 mM) (Thermo Fisher) and 34 µl water were prepared and amplified in thermal cycler with the conditions as 1 min at 98 °C for initial denaturation, followed by 14 or 16 cycles of (10 sec at 98 °C, 15 sec at 60 °C, 30 sec at 72 °C), 5 min at 72 °C for final extension. PCR products were loaded into agarose gel to ensure their quality and amplicon size and recovered by M/N Gel Recovery Kit

(Macherey Nagel). The product was further purified using magnetic beads (CLENNA) according to manufacturer's instructions [14,185].

Digestion of pLentiCRISPR-v2 (pLCV2 - Addgene #52961) plasmid that carries a human-codon optimised Cas9 nuclease gene was used as a backbone. Digestion reaction of that plasmid for cloning was conducted as: 5 µg plasmid was treated with 5 µl Esp3I restriction enzyme (NEB) at 37 °C for 2 hours and loaded into agarose gel. The band in 12 kb (digested and in the form of double-stranded linear strand) was recovered from agarose gel and cleaned by isopropanol precipitation to perform Gibson assembly ligation reaction [14,185].

Ligation was established by three different ligation ratios as 1:3, 1:6, and 1:10 and 120 ng vector backbone was assembled with proper oligo mix by taking consideration of ligation ratios. For 15 µl total assembly reaction, 7.5 µl 2X Gibson master mix (NEB) and water were mixed with digested backbone and oligo mix and incubated at 50 °C for 1 h followed by isopropanol precipitation. In each case different amounts of ligation products as 120 ng, 150 ng, and 200 ng were transformed to the 25 µl of electrocompetent cells (Lucigen) with Electroporator (Bio-Rad MicroPulser). After electroporation, 1 mL SOC medium added directly onto bacteria and grown for 1h at 37 °C. To calculate coverage, 100 µl bacteria spread onto ampicillin containing agar plates and 900 µl resting bacteria inoculated into 100 mL liquid LB to isolate next day. After growing overnight at 37 °C, plasmid pools from liquid growth were isolated by M/N Midi-Prep Purification Kit (Macherey Nagel) and stored at -80 °C as a library stock. To achieve proper coverage, above experiments were repeated 10 times and all assembly products combined and subcloned to generate the LIBGENE1Q plasmid library [14,185].

2.1.3 sgRNA Amplification from LIBGENE1Q plasmid library

After generation of the LIBGENE1Q plasmid library, sgRNA abundances were investigated by amplification of sgRNAs. PCR reaction was conducted to amplify each unique and ligated sgRNA as: for 25 µl total reaction, 5 µl 5X High Fidelity (HF) buffer, 0.5 µl specific Index PCR2 Primer, 0.5 µl specific Barcode PCR2 Primer, 0.5 µl Phusion High-Fidelity DNA Polymerase (NEB, USA), 0.5 µl dNTP mix (10 mM) and NFW up

to 25 µl settled for 100 ng plasmid DNA. Conditions of thermal cycler as: initial denaturation for 1 min at 98 °C, followed by (10 sec at 98 °C, 25 sec at 65 °C, 15 sec at 72 °C) for 25 cycles, final extension for 15 mins at 72 °C.

Reference volume of the PCR product was loaded into gel to ensure about the size. Remaining products were purified using magnetic beads (CLENNA) and sent to the next generation sequencing and sequencing results were analysed by MAGeCK algorithm [186].

2.2 Cell Culture

Human BC cell lines MCF7 (ATCC HTB-22™), T47D (ATCC HTB-133™), MCF10 (CRL-10317 ™), MCF12A (CRL-3598 ™), human embryonic kidney cell (HEK293T) were obtained from ATCC and were maintained at standard conditions as 37°C and 5% CO_2 incubator. MCF7 and HEK293T cells were grown in DMEM-High Glucose (Sigma), supplemented with 10% FBS and 1% Pen/Strep while T47D was maintained in RPMI-1640 (Sigma). Human breast normal cell lines MCF12A and MCF10A cell lines were cultured in DMEM/F12 (Sigma) but supplemented with 5% horse serum (Gibco), 1% Pen/Strep (Biowest), 10 ng/mL hEGF (Sigma), 10µg/ml bovine insulin (Sigma), and 500 ng/ml hydrocortisone (Sigma). All cell lines have been examined for their Mycoplasma contamination status regularly and have been passaged or medium replenished every 3-4 days depending on the confluency.

2.3 Virus Production and Virus Titration Optimization

Lentiviral virus production was performed using HEK293T cells. In total $4x10^6$ HEK293T cells were seeded per 10 cm^2 petri dishes. 10 ug library plasmid pool, 2.5 ug packaging vectors pRSV-Rev (Addgene #12253) and 5 ug pMDLg/pRRE (Addgene #12251), 3.5 ug envelope vector pCMV-VSV-G (Addgene #8454) were mixed with 63 µL PEI Reagents (Sigma) that were prepared in FBS and P/S free DMEM. After 15 mins incubation at RT, the mixture was added dropwisely onto the HEK293T cells and cells were incubated for 16 hours with the transfection mixture. Medium was collected at 36 hours post-transfection and filtered with a 45 µM filter. Virus stocks were aliquoted, snap-freezed and stored at -80 °C.

For infection of BC cells, $4x10^6$ cells were seeded in 10 cm^2 petri dishes. The virus titration was decided by applying different amounts of viruses together with 8 µg/ml polybrene (Sigma) and titration optimised for each batch as MOI<0.4. MCF7 cells were selected with 2 µg/ml puromycin for 48 h while selection of T47D cells proceeded with 4 µg/ml puromycin for 72 h.

2.4 Functional CRISPR-Based Screening

To interrogate the role of Chr1q genes in luminal subtypes of BC, CRISPR-based LOF screening was performed with a library targeting the whole genes located at the Chr1q, named LIBGENE1Q. Screening was conducted on triplicates in BC cell lines MCF7 and T47D, as well as in one human breast normal cell line, MCF12A (non-tumorigenic) in both 2D and 3D BC spheroids simultaneously to identify cancer specific vulnerabilities. For each replicate, the coverage was aimed to be more than 1000X with MOI<0.4. After puromycin selection, half of the cells were collected as T=0 (samples of initial point). Drop-out screening was performed on both 2D and 3D spheroid culture for 20 days. Cells were divided every 5 days, and the medium was refreshed each day. Samples belong to T=0 as initial point, T=10 and T=20 as the end point collected and stored in -80 °C for gDNA isolation to determine sgRNA abundances.

2.5 gDNA Isolation, Nested PCR, and Sequencing

Frozen cell pellets thawed for each sample, and gDNA was isolated with Macherey-Nagel™ NucleoSpin™ Tissue Isolation kit (M/N #740952). As a summary, after each sample pellet thawed, lysed in 360 µl Buffer T1 and incubated overnight at 56 °C with 50 µl Proteinase K. Next day, 400 µl Buffer B3 was added, and sample solution was incubated at 70 °C for 10 minutes. After addition of 420 µl 100% ethanol to adjust binding conditions of gDNA, solution divided into 3 columns. After washing steps, samples were eluted in 300 µl of water.

For each sample, nested PCR was performed to amplify unique sgRNAs, labelling them with Illumina sequencing-compatible adaptors. The nested PCR was conducted using Phusion® High-Fidelity DNA Polymerase (NEB, M0530L) in a total volume of 25 µl. The first round of PCR was performed using 40 µg of genomic DNA (gDNA) per sample

(1 µg per reaction) to achieve over 200X coverage, assuming that 10^6 cells contain 6.6 µg of DNA [14,187]. The PCR reaction mixture for each sample consisted of 1 µg gDNA template, 5 µl of 5X High Fidelity Buffer, 0.5 µl of 10 mM dNTP mix (Thermo Fisher), 0.5 µl of Forward PCR1 Primer (10 µM), 5 µl of Reverse PCR1 Primer (10 µM), 0.5 µl of Phusion Polymerase (NEB), and nuclease-free water (NFW) up to 25 µl, performed 40 times. The conditions were optimised as follows: initial denaturation at 98°C for 1 minute, followed by 15 cycles of 98°C for 10 seconds, 65°C for 25 seconds, and 72°C for 15 seconds, with a final extension at 72°C for 15 minutes.

After the first PCR step, the 40 reactions were pooled and purified using the Qiagen PCR Purification Kit to clean and concentrate the samples. For the second PCR step, 5 µl of the purified product from the first PCR was used per reaction in a total of 20 reactions (100 µl in total). The second PCR setup and conditions were the same as the first step, except that primers with specific barcodes and indexes (10 µM) provided by Illumina were used to uniquely label each time point.

Amplicons of the second step PCR were combined and reference volume was loaded into gel to ensure the size and purity. Remaining amplicons were purified using magnetic beads (CLENNA) and sent to the sequencing. Samples were sent for sequencing and sequencing results were analysed by MAGeCK algorithm [186].

2.6 CRISPR Screening Analysis

Screening analysis was performed with Model-based Analysis of Genome-wide CRISPR/Cas9 Knockout (MAGeCK) tool [186]. Initially, the presence of sgRNA sequences in sequenced reads were determined by the count function. This function took reads in fastq format and sgRNA sequences as a list as inputs. Default normalisation which is median was kept for the normalised read counts. As the sgRNA library, LIBGENE1Q was used.

To identify the depleted and enriched genes between two conditions, MAGeCK test function was used. In this step, raw sgRNA count files were used that were obtained in the counting step. For the normalisation, non-targeting sgRNAs were given to the --norm-

method parameter. Copy number correction was done using --cell-line parameters with cell line specific copy number data from Cancer Cell Line Encyclopedia [188]. Potential hit genes were determined by manual filtering according to their false discovery rates (FDR) and Log_2 fold changes (Log_2(FC)).

For generating mapping rates in bar charts, MAGeCK Flute R package was used [189]. Waterfall graphs, cumulative density plots, counts in Log_2(FC) as line graphs, and scatter plots were generated using ggplot2 [190]. Analysis and visualisations were performed by Ferzan Betül Berber in GK Lab.

2.7 sgRNA Cloning and Lentivirus Production

For validation experiments, sgRNAs were chosen according to their FDRs and Log_2(FC)s. Oligonucleotides in **Table 2.1** was purchased from Macrogen (USA) and annealed by T4 Polynucleotide Kinase (NEB) by mixing 1 µl (100 µM) forward strand, 1 µl (100 µM) reverse strand, 0.5 µl T4 PNK, 1 µl T4 Ligase Buffer containing 1 mM ATP. PCR conditions settled as 37 °C 30 min, 95 °C 5 mins and then ramps down to 25 °C at 5 °C/min. Annealed oligos were diluted as 1:200 with NFW. pLCV2 plasmid was digested with BsmBI-v2 (NEB) as 5 µg plasmid treated with 5 µl BsmBI-v2 at 55 °C for 8 h, 80 °C for 20 min and loaded into agarose gel to purify digested 12 kb fragment for ligation. Digested plasmid from gel was purified by M/N Gel and PCR Clean-up kit. From each annealed oligo mix that was diluted 1:200, 1 µl was mixed with 50 ng digested plasmid for ligation that was performed with T4 Ligase (NEB). Single colonies were sent to sanger sequencing and confirmed plasmids were used in further experiments [184].

Virus was produced for each sgRNA as it is described above.

Table 2. 1. DNA oligonucleotide sequences used for sgRNA cloning which were specifically selected for each gene from LIBGENE1Q.

Gene Name	Oligo Name	Sequence
NT	NT – g1 – FWD	CACCGATGCGCTTTAATCGCCGTTC
	NT – g1 – REV	AAACGAACGGCGATTAAAGCGCATC
	NT – g2 – FWD	CACCGTAGACAACCGCGGAGAATGC
	NT – g2 – REV	AAACGCATTCTCCGCGGTTGTCTAC
	NT – g3 – FWD	CACCGTCGGCTACAATCTTTGGCAT
	NT – g3 – REV	AAACATGCCAAAGATTGTAGCCGAC
ARL8A	ARL8A – g1 – FWD	CACCGTCTCATCCAATGCTCCCGGA
	ARL8A – g1 – REV	AAACTCCGGGAGCATTGGATGAGAC
	ARL8A – g2 – FWD	CACCGGCGCATGTTGAAACCCACGG
	ARL8A – g2 – REV	AAACCCGTGGGTTTCAACATGCGCC
	ARL8A – g3 – FWD	CACCGTCCTTCTCATCCAATGCTCC
	ARL8A – g3 – REV	AAACGGAGCATTGGATGAGAAGGAC
RPRD2	RPRD2 – g1 – FWD	CACCGTGTGACAGATAATCGTGATG
	RPRD2 – g1 – REV	AAACCATCACGATTATCTGTCACAC
	RPRD2 – g2 – FWD	CACCGAGACTCAGAACCAGTCGGGG
	RPRD2 – g2 – REV	AAACCCCCGACTGGTTCTGAGTCTC
	RPRD2 – g3 – FWD	CACCGAGGCACTGGGGTACATGAAG
	RPRD2 – g3 – REV	AAACCTTCATGTACCCCAGTGCCTC
ARNT	ARNT – g1 – FWD	CACCGTACCCTAGTCTCACCAATCG
	ARNT – g1 – REV	AAACCGATTGGTGAGACTAGGGTAC
	ARNT – g2 – FWD	CACCGACGATTGGTGAGACTAGGGT
	ARNT – g2 – REV	AAACACCCTAGTCTCACCAATCGTC
	ARNT – g3 – FWD	CACCGATCACAGTGAAATTGAACGG
	ARNT – g3 – REV	AAACCCGTTCAATTTCACTGTGATC
GON4L	GON4L – g1 – FWD	CACCGTGAGAAATTGCCTGGTACCG
	GON4L – g1 – REV	AAACCGGTACCAGGCAATTTCTCAC
	GON4L – g2 – FWD	CACCGCAAGGGCCACGACCACCTGC
	GON4L – g2 – REV	AAACGCAGGTGGTCGTGGCCCTTGC
	GON4L – g3 – FWD	CACCGGGACTCAGGAAGGAAGCAGG
	GON4L – g3 – REV	AAACCCTGCTTCCTTCCTGAGTCCC

2.8 Validation Experiments

For validation experiments, MCF7, T47D, MCF12A, and MCF10A cells were infected with indicated sgRNAs. For each cell line, a control group (CNT) was generated with an infection with non-targeting sgRNAs cloned into pLCV2. To block the expression of candidate genes indicated sgRNAs given by taking consideration of titration as kept around 0.4.

2.8.1 GFP Based Competitive proliferation assay

To observe the effect of candidate genes on proliferation, GFP based competition assay had been performed with CNT group or hit genes. Firstly, polyclonal MCF7, T47D, MCF12A cells were generated that were stably expressing GFP using pLenti-CMV-GFP-Puro (Addgene#17448) vector. GFP expressing cells were mixed in a 1:3 ratio with cells containing individual sgRNAs for the control group and each cell line containing indicated sgRNAs to block the candidate gene expression. The percentage of GFP expressing cells was assessed by Beckman Cytoflex flow cytometry at the beginning of the experiment (Day = 0) and every 72 hours onward (Day = 3, Day = 6, Day = 9 and Day = 12) [14,187]. For every condition, 10.000 events were recorded, and the data was analysed using FlowJo software. As a result, sgRNAs that have an effect on the cell proliferation compared to non-targeting sgRNA were determined.

2.8.2 Colony Formation Assay

To elucidate the colony forming ability, cells in which the target gene was blocked with control group were seeded as 4000 cells/well in triplicates in 6-well plates. For 10-14 days, each group of cells kept in culture and to finalise the experiment, cells were washed with DPBS two times and fixed with ice-cold 100% methanol for 20 min at 4 C. After discarding methanol, cells were incubated with crystal violet for 1 h at RT by shaking. To record experimental groups, crystal violet was removed, plate was washed and left to dry to scan. For quantification, colonies were resuspended in 15-20% acetic acid for until all dissolved. Then colorimetric measurement in 590 nm wavelength taken with BioTek Synergy plate reader.

2.8.3 3D Spheroid Growth Assay

Three-dimensional (3D) cell culture experiments were performed using a minimum of 750K cells on agar plates that were previously sterilised with UV [180]. In Day = 4 and Day = 6, pictures were taken by Nikon Eclipse Ts2 Light/Fluorescence microscope to assess spheroid size. For each biological replicate, at least 50 different spheroids were imaged. Spheroid sizes were compared using 20x/0.40 objective lenses, corresponding to scales of 70 µm. ImageJ software was employed to analyse spheroid areas by setting the

length of the scale bar visible in the microscope images using the 'Set Scale' option in the analysis section. Subsequently, the area of each spheroid was calculated by manually outlining its boundaries using the 'Polygon Selections' tool and the area of each spheroid recorded for each experimental group.

2.9 RT - qPCR

Total RNAs were isolated with TRIzol™ Reagent (Thermo Fisher) by following manufacturer's instructions. As a summary, 500K-1M cells resuspended in Trizol reagent and 200 µl chloroform added, mixture incubated for 2 min at RT and centrifuged in 12.000xg for 15 min at 4 ºC. The upper RNA phase was collected and mixed with ice cold isopropanol with a ratio 1:1. After incubation for 10 mins at RT, centrifugation was performed to acquire pure precipitated RNA in 12.000xg for 10 min at 4 ºC. RNA pellet was washed in ice cold 80% ethanol, then precipitated RNA dissolved in 50-60 µl NFW. For conversion of cDNA, iScript™ cDNA Synthesis Kit (BIO RAD) was used: 1 µg RNA was mixed with 1 µl iScript Reverse Transcriptase and 4 µl 5X RT reaction mix and NFW up to 20 µl. PCR conditions were adjusted as 5 min at 25 ºC, 20 min at 46 ºC, and 1 min at 95 ºC. After this reaction each cDNA stock was diluted with NFW with 1:1 ratio.

RT - qPCR was performed with 2X SYBR Green Master Mix (Qiagen) with LightCycler 480 Instrument II (Roche). 2 µL cDNA taken from dilution stock was mixed with 5 µL 2X SYBR Green, 0.8 µL forward + reverse primer mix (10 µM in final) and 2.2 µl NFW in which final volume was adjusted to 10 µl. LightCycler conditions were settled as: 5 min at 95 ºC (initial heating), for 40 rounds: 10 sec at 95 ºC, 30 sec for 60 ºC, 30 sec for 72 ºC. As the housekeeping gene for normalisation of expression data beta-actin was used and analysis to check the blockage of genes was performed with 2-DeltaCT calculation. All primers used in RT-qPCR are represented in Table 2.2.

Table 2. 2. RT - qPCR primer sequences.

Gene Name	Forward Primer	Reverse Primer
ACTB	CATGTACGTTGCTATCCAGGC	CTCCTTAATGTCACGCACGAT
ARL8A	AGTCCTGGGTAACAAGCGAGAC	GCAAGAGATGGAGTAGCAGCAG
RPRD2	CCAAAACCCAGACACAGTCAGC	GAAGTGCTCTGTGAGGCAGCTT
ARNT	CTGTCATCCTGAAGACCAGCAG	CTGGTTCTCATCCAGAGCCATTC
GON4L	CCACATCAGTGGAAGCCACCTA	CCTACCTCTCTAGCACCATCAG

2.10 Statistical Analysis

All experiments were three biological replicates if otherwise not indicated. Statistical analysis had been performed by using GraphPad Prism 10.0. Significance levels were decided by student's t-test within two groups (CNTvsHITs): * $p<0.05$, ** $p<0.01$, *** $p<0.001$.

Chapter 3

3 RESULTS

3.1 Simultaneous Screening of LIBGENE1Q in 2D and 3D Models

3.1.1 LIBGENE1Q sgRNA Distribution

To investigate the effect of Chr1q in BC, we generated a CRISPR library named LIBGENE1Q to target genes located on Chr1q. According to DepMap version 23Q2, this library includes 80 CE (with 2 located on a separate chromosome for internal control), 825 NEs and also 500 NT sgRNAs **(Figure 3.1A, B)**. To ensure the abundance of sgRNAs, sgRNA representation was examined in cells that were infected with an MOI<0.4, at 1000X coverage, and collected at T=0 after antibiotic selection. After gDNA isolation and nested PCR, samples were sent for sequencing. For each cell line, the sgRNA mapping ratio, including detected and undetected sgRNAs, is shown in **Figure 3.1C**. The complexity of LIBGENE1Q and sgRNA abundances were ensured before starting screening, as shown in **Figure 3.1D.**

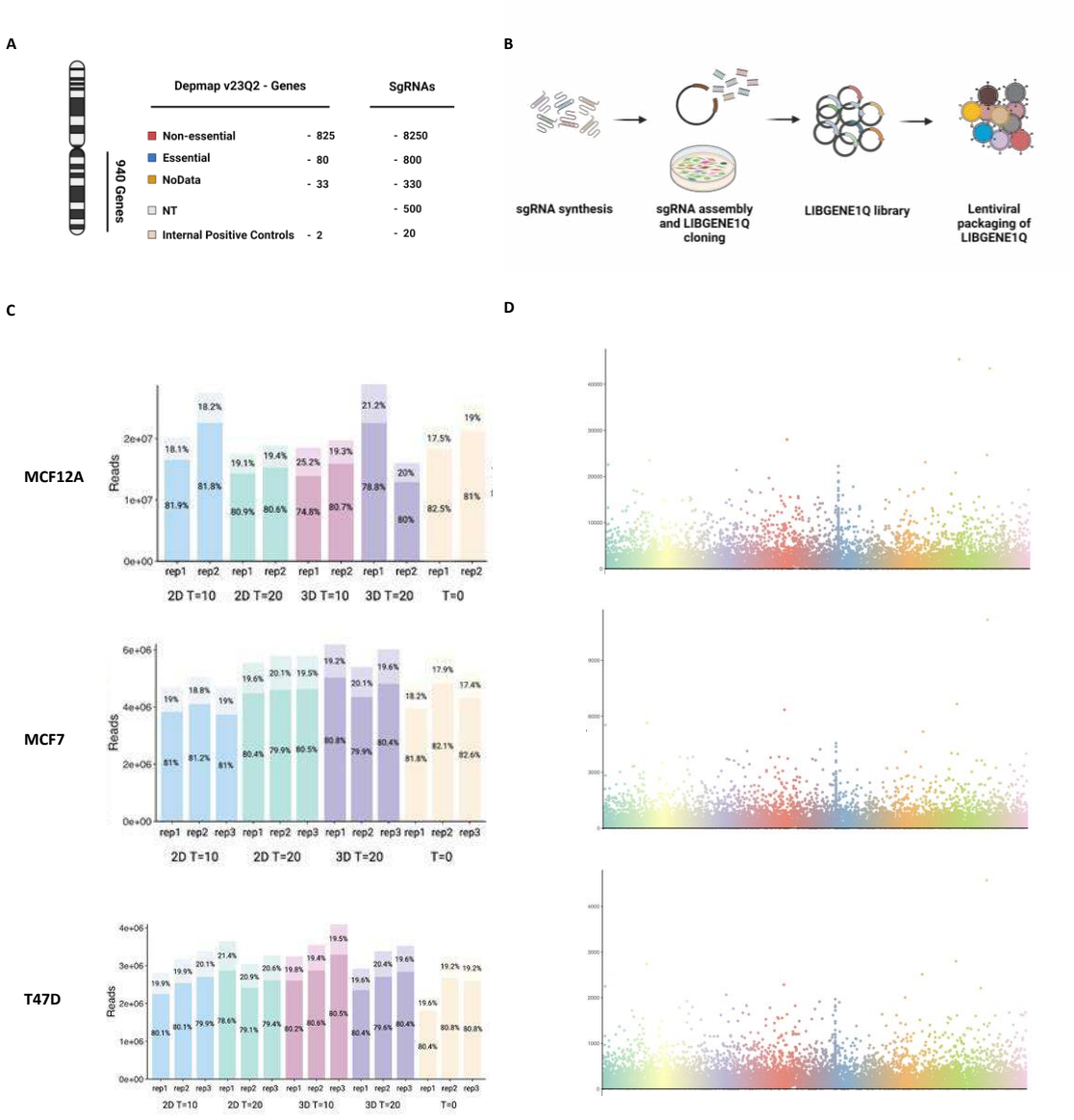

Figure 3. 1. LIBGENE1Q library and sgRNA representation. (A) Summary of Library content. (B) Cloning procedure of LIBGENE1Q. (C) Mapping of detected and undetected sgRNAs post-sequencing, ensuring screening reliability with high mapping ratios. (D) Initial data point showing sgRNA representation in each cell line.

3.1.2 Performance of the LIBGENE1Q Library in BC and Non-tumorigenic Normal Cell line

CRISPR-based LOF screening was conducted in two luminal BC cell lines, MCF7 and T47D, as well as in the normal cell line MCF12A. Cells were cultured simultaneously in

2D monolayers and 3D BC spheroids during screening. Samples were collected at three time points (T=0, T=10, and T=20) to assess sgRNA abundances, as illustrated in **Figure 3.2**.

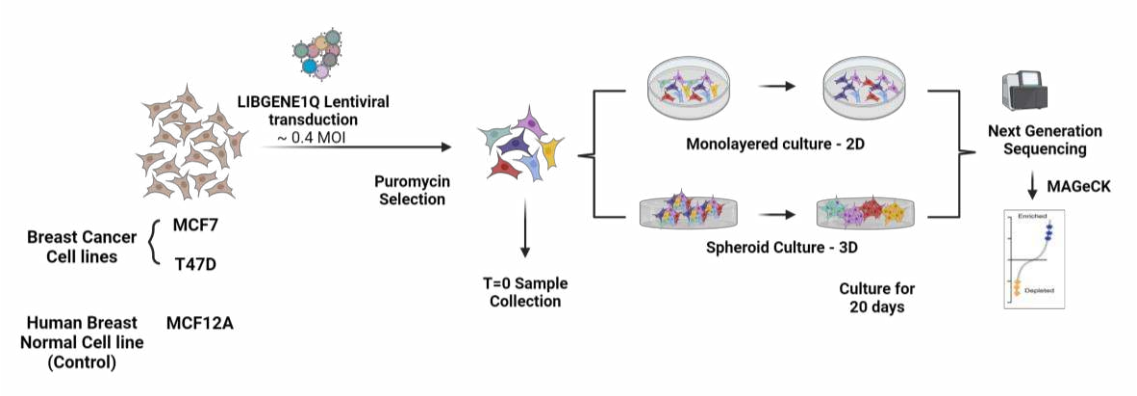

Figure 3. 2. LIBGENE1Q Screening in BC cell lines MCF7 and T47D, and breast normal cell line MCF12A. The screening utilised a viral library at a very low multiplicity of infection (MOI) of less than 0.4. Conducted over a 20-day period, the screening was executed simultaneously in both 2D and 3D culture systems. Initial samples (T=0) were collected following puromycin selection, while final samples (T=20) were obtained at the conclusion of the screening period. (Created in BioRender).

Following screening, the distribution of sgRNA was evaluated to verify the representation and quality of the screening based on initial data point (T=0). Density plots showed a normal sgRNA distribution at each time point and biological replicates exhibited high reproducibility **(Figure 3.3)**.

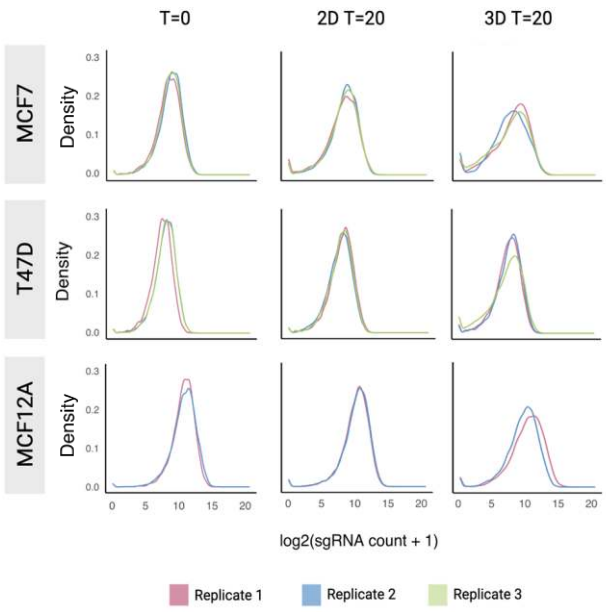

Figure 3. 3. Quality assessment of LIBGENE1Q screening. All three biological replicates in each cell line revealed high reproducibility. The distribution and abundance of sgRNA in both 2D and 3D models were consistent with each other.

The impact of LIBGENE1Q screening in BC cell lines was investigated, focusing on its effectiveness in distinguishing positive controls (CE) and negative controls (NTs) based on sgRNA abundances. At each time point, the Log_2(FC) of individual sgRNAs targeting CE genes and NTs were evaluated by transforming raw read data into Log_2 counts **(Figure 3.4)**. The distribution of individual sgRNAs reveals a pronounced depletion pattern for CE genes at the endpoint in each *in vitro* model, whereas NTs showed no significant change and maintained a regular distribution pattern.

The quality of screening in 3D models closely mirrored that of 2D models, with biological replicates demonstrating high reproducibility akin to 2D models **(Figure 3.3)**. Moreover, essential genes were detectable within the 3D population **(Figure 3.4)**.

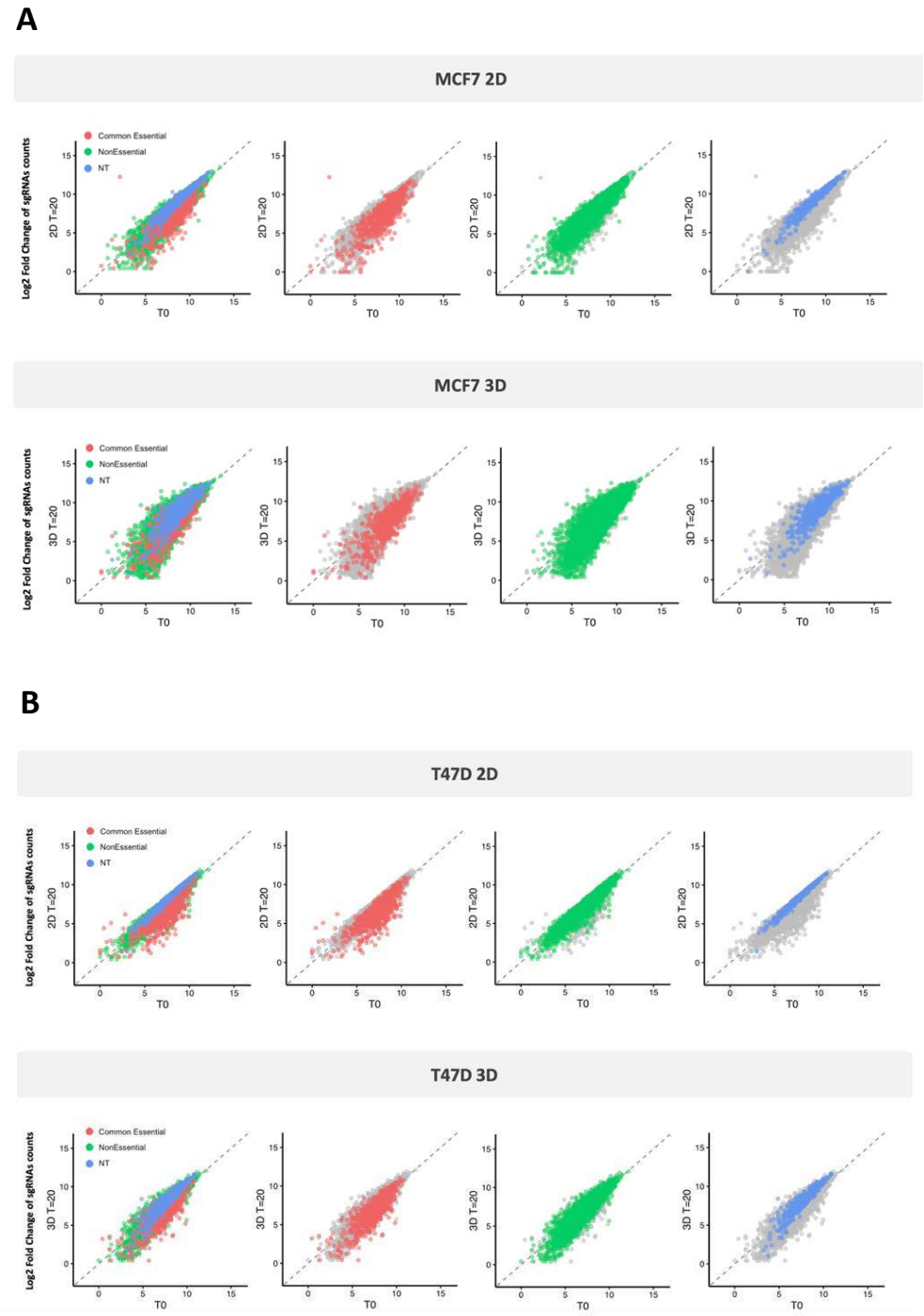

Figure 3. 4. The distribution of sgRNAs in (A) MCF7 and (B) T47D cells. Log_2(FC) of sgRNAs between the initial point (T=0) and the end point (T=20). Each dot represents the behaviour of one sgRNA over a 20-day period. The graphs include sgRNAs targeting CE genes, non-essential genes, and NTs (targeting no genes) are depicted. In both 2D and 3D models, sgRNAs targeting non-essential genes exhibited a broader distribution,

whereas those targeting CE genes clustered together and shifted to the right. NTs showed a consistent linear behaviour over time, indicating no change during screening.

In addition, cumulative densities of sgRNAs targeting CE genes and NTs were interrogated to assess depletion scores from the initial to the end point of screening. Read counts were transformed into Log_2 values, and cumulative behaviour of sgRNAs targeting non-essential genes was compared to CE genes and NTs. As shown in **Figure 3.5,** CE genes exhibited the most significant depletion scores, while NTs showed no change during screening. Screening in both 2D and 3D models effectively distinguished CE genes from non-essential genes, demonstrating the efficacy and reliability of the approach. However, the impact of essential genes differed in 3D screening, where depletion scores approached those of non-essential genes, whereas there was no change in the impact of non-essential genes in both 2D and 3D models.

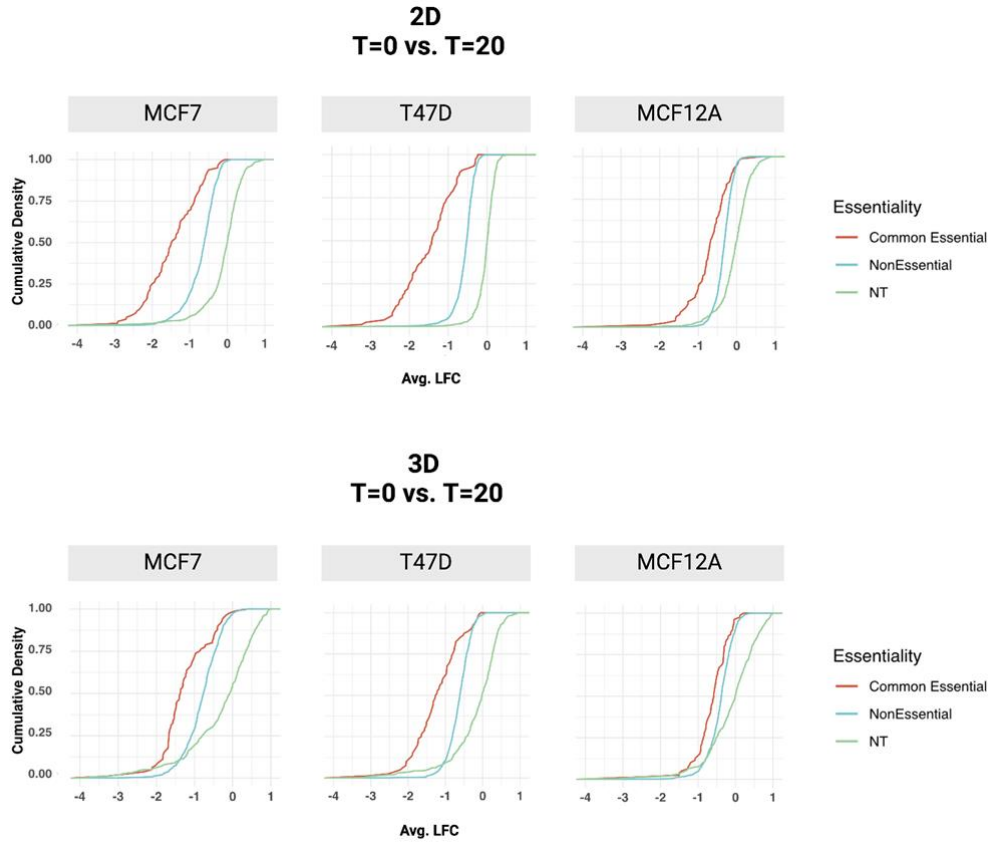

Figure 3. 5. LIBGENE1Q screening efficiently discriminated CE genes from other genes, showing the highest negative Log2(FC). Throughout the screening process, the behaviour of CE genes and NTs validated the quality and effectiveness of the screening for subsequent analysis.

3.2 Negative Selection (Drop-out) Screen of LIBGENE1Q

To interrogate the role of Chr1q genes, MAGeCK-RRA (Model-based Analysis of Genome-wide CRISPR/Cas9 Knockout) was employed to analyse depletion and enrichment scores after 20 days of culturing following LIBGENE1Q infection. For quantification, FDR value threshold of < 0.1 was applied, ensuring more than 90% reliability, while Log_2(FC) was constrained as < -1 to identify negative phenotypes in both 2D and 3D models (**Figure 3.6A**). The most prominent effect was noted in **CE genes**, which exhibited substantial downregulation in each *in vitro* model. Results were further assessed for non-essential genes shared between in 2D and 3D models. Genes

identified in both MCF7 and T47D but not in MCF12A represented cancer specific candidate hits responsible for inducing negative phenotype exclusively in cancer models.

The overlapping region (2D and 3D drop out analysis) contains 14 different genes specific to cancer that exhibited a negative phenotype in both 2D and 3D models **(Figure 3.6B).** The shared candidate genes are depicted in **Figure 3.1C**.

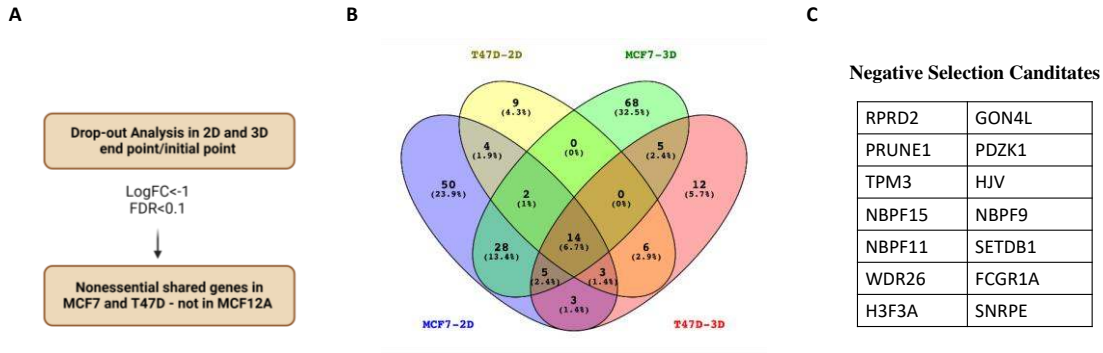

RPRD2	GON4L
PRUNE1	PDZK1
TPM3	HJV
NBPF15	NBPF9
NBPF11	SETDB1
WDR26	FCGR1A
H3F3A	SNRPE

Figure 3. 6. MAGeCK analysis identifies 14 negative selection candidates shared in both 2D and 3D models. (A) Screening results filtered with $Log_2(FC) < -1$ and FDR < 0.1 to pinpoint genes shared in MCF7 and T47D cancer cell lines, but not affecting MCF12A. (B) Classification of non-essential genes in MCF7 and T47D cell lines to identify shared genes in both 2D and 3D models. (C) The overlapping region defining 14 shared genes designated as drop-out candidates.

Across these genes, *RPRD2* (regulation of nuclear pre-mRNA domain containing 2) and *GON4L* (gon-4 like) genes were selected for further examinations due to their significant negative $Log_2(FC)$ specifically in cancer cells **(Figure 3.7A)** while their effects were minimal in MCF12A in both 2D and 3D settings **(Figure 3.7B)**. Others, such as PDZK1 [191] and PRUNE1 [192,193], have been implicated in enhancing BC malignancy. LIBGENE1Q screening effectively discriminates these genes in 2D, and 3D drop out screening in both MCF7 and T47D cell lines.

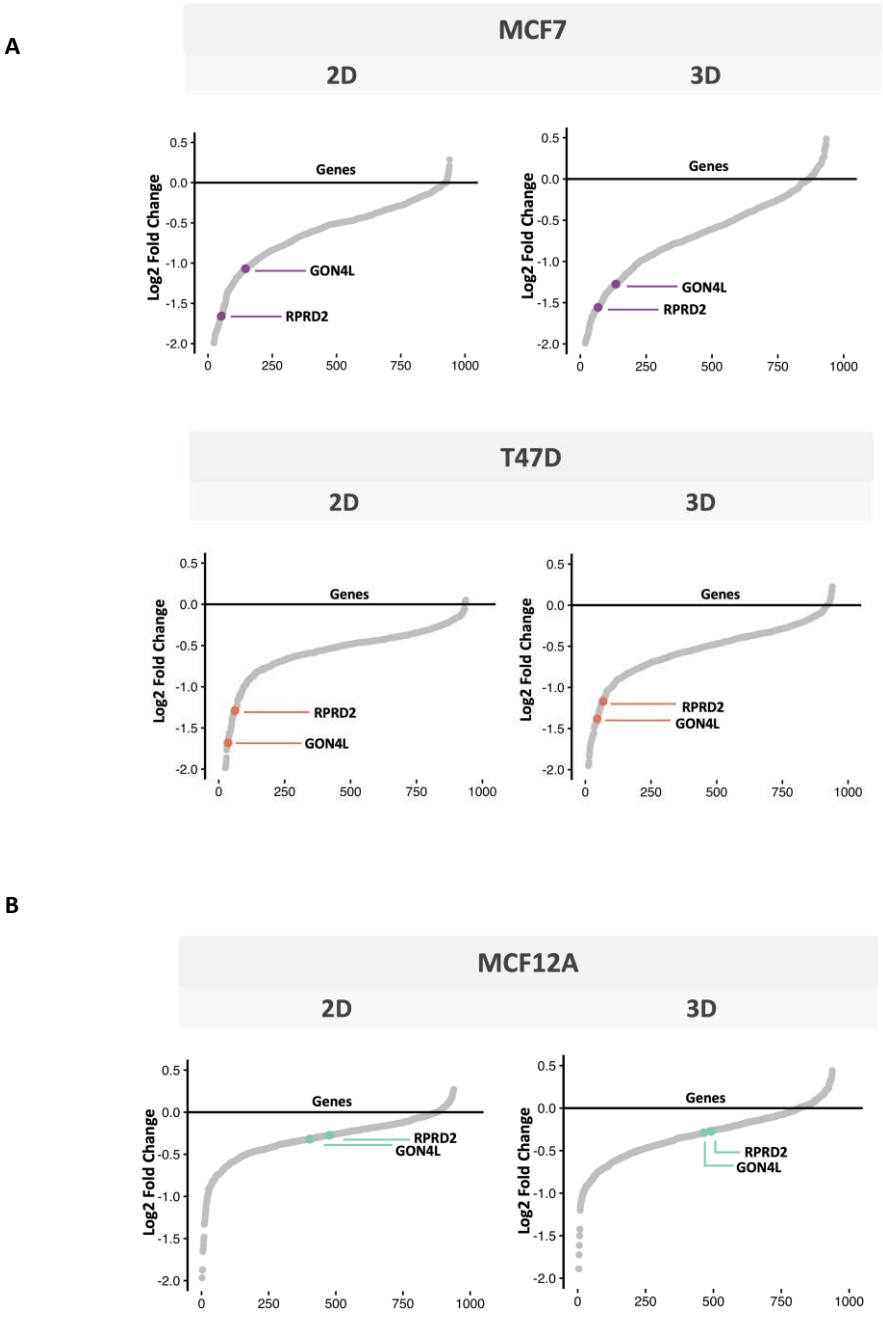

Figure 3. 7. Hit identification from dropout screen. Across these genes, RPRD2 and GON4L were selected based on their shared depletion score in MCF7 and T47D, with no effect observed in MCF12A.

3.2.1 Validation of Negative Selection Screen Findings in 2D Model

First, expression of RPRD2 and GON4L was evaluated in MCF7 and T47D cells compared to MCF12A to get insight about their gene expression levels in cancer cells relative to normal control. The expression levels were significantly higher in both MCF7 and T47D cells compared to MCF12A, indicating differential expression of RPRD2 and GON4L in cancer cells **(Figure 3.8)**.

RPRD2 plays a role in transcription initiation by facilitating the binding RNA Polymerase II (RNAP II) complex to target sites [194]. The N-terminal domain of mature RPRD2 protein can bind to the catalytic C-terminal subunit of the RNAP II, potentially modulating gene expression differentially in cancer cells [194].

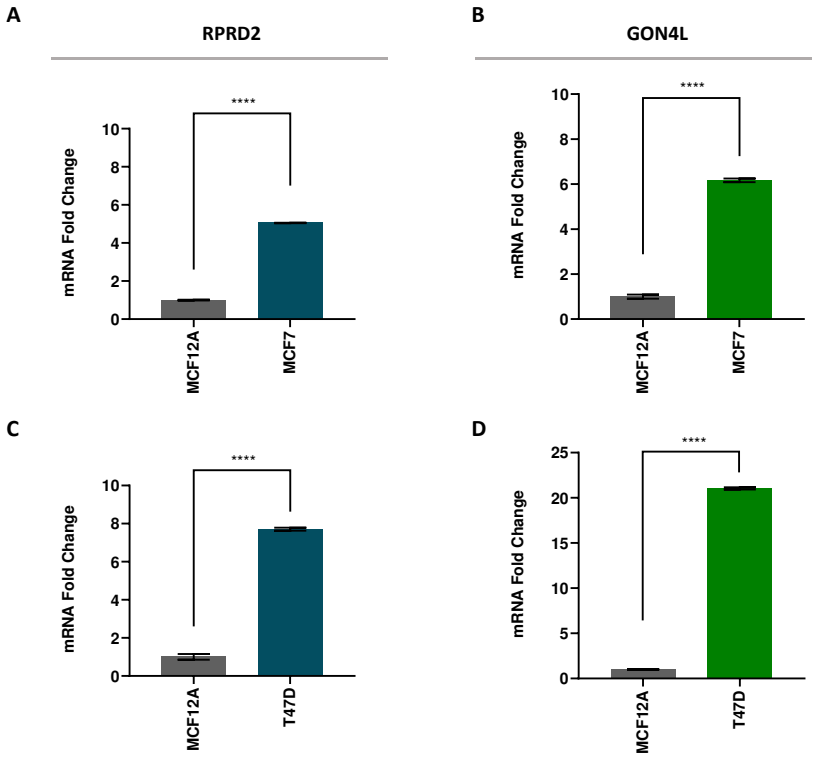

Figure 3. 8. Endogenous gene expression of candidate hits in MCF7 and T47D cells compared with MCF12A cells. RT-qPCR was performed to specify differential gene expression by analysing candidate gene expression normalised to β-Actin housekeeping gene. RPRD2 expression showed a significant increase of more than 4-fold in MCF7 (A)

and 6-fold in T47D (C). GON4L expression in BC cells were recorded as more than 10-fold in MCF7 (B) and 20-fold in T47D (D). (t-test: * $p<0.05$, ** $p<0.01$, *** $p<0.001$).

For validation experiments, gene expression was blocked using sgRNAs selected from our LIBGENE1Q (3sgRNA per gene), which were then cloned into pLCV2-Puro following the method described in the methods section. After virus production, MCF7, T47D, and MCF12A cells were infected at an MOI < 0.4 for functional assessments. GFP based competition assay was performed by mixing KO cell groups with GFP-expressing cells with a 3:1 ratio, as outlined above. In addition, a clonogenic assay was conducted simultaneously to assess the effect of the candidate hits on the colony forming ability of MCF7, T47D and MCF12A cells.

The proliferation and colony-forming ability of MCF7 and T47D cells significantly decreased when RPRD2 expression was blocked **(Figure 3.9)**. In MCF7 cells, the competition assay showed a pronounced proliferation capacity reduction by approximately 20% **(Figure 3.9A, B)**. Furthermore, the clonogenic assay demonstrate a significant repression of colony-forming ability upon RPRD2 expression was inhibited **(Figure 3.9C, D)** Although T47D cells showed less susceptible to RPRD2 blockage, a notable decrease in proliferation capacity was observed in both the competition assay and clonogenic assay (**Figure 3.9F**). Specifically, the competition assay revealed a relative proliferation capacity decrease of approximately 50% in T47D cells **(Figure 3.9F, G)**, while the clonogenic assay quantification showed a 50% reduction in long-term growth inhibitory effect **(Figure 3.9 G, H)**.

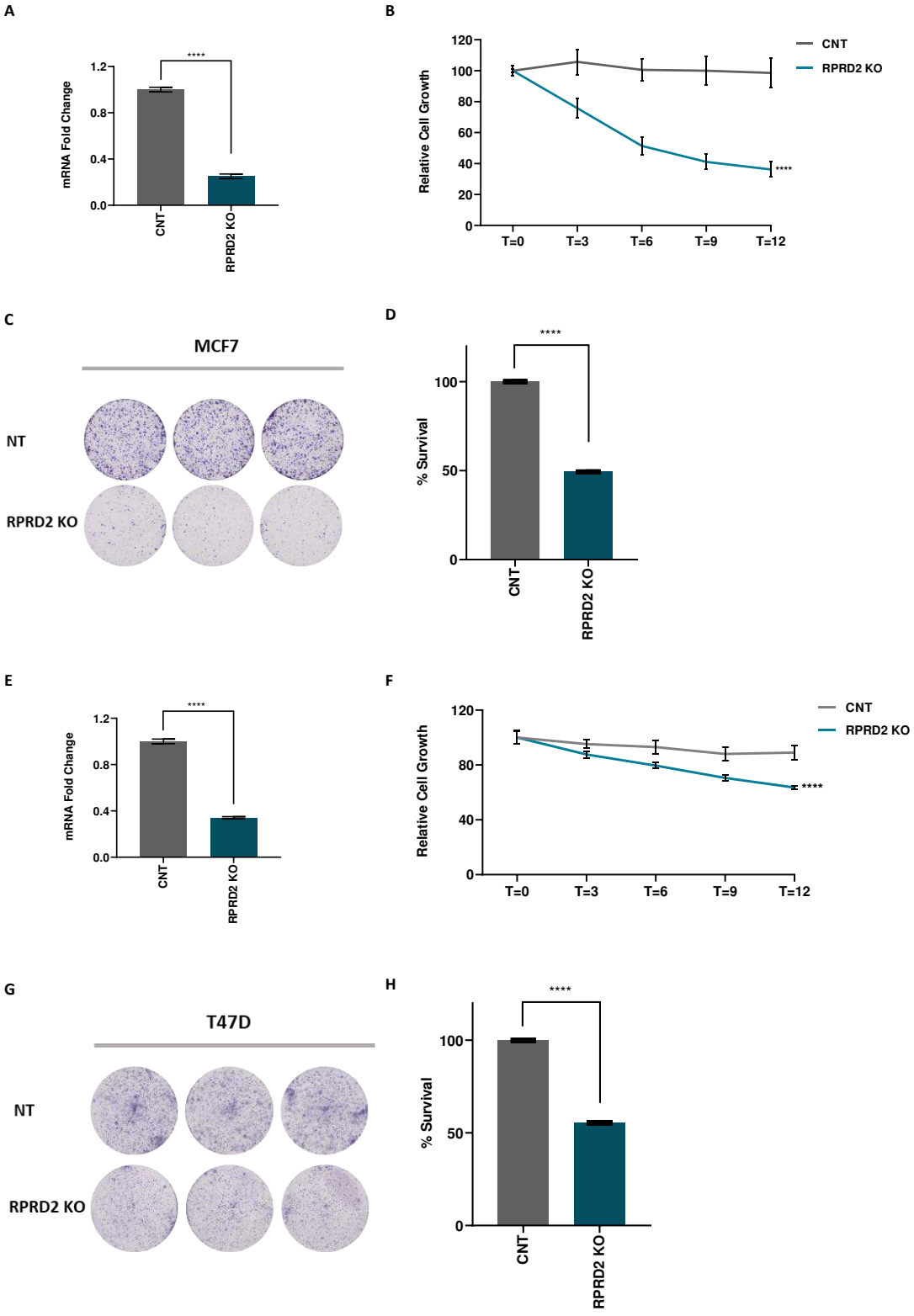
A
mRNA Fold Change
1.2
0.8
0.4
0.0
****
CNT
RPRD2 KO
B
Relative Cell Growth
120
100
80
60
40
20
0
T=0
T=3
T=6
T=9
T=12
CNT
RPRD2 KO
****
C
MCF7
NT
RPRD2 KO
D
% Survival
100
50
0
****
CNT
RPRD2 KO
E
mRNA Fold Change
1.2
0.8
0.4
0.0
****
CNT
RPRD2 KO
F
Relative Cell Growth
120
80
40
0
T=0
T=3
T=6
T=9
T=12
CNT
RPRD2 KO
****
G
T47D
NT
RPRD2 KO
H
% Survival
100
50
0
****
CNT
RPRD2 KO

Figure 3. 9. Impact of RPRD2 KO on MCF7 and T47D proliferation in 2D models (A, E) RPRD2 expression was blocked in MCF7 and T47D cells using MOI < 0.4, followed by validation experiments. RT-qPCR was performed to verify the gene expression. (B, F) GFP-based competition assay was performed to investigate proliferation capacity of RPRD2 KO cells compared with CNT one. RPRD2 blockage significantly decreased the proliferation which was assessed relatively to GFP. (C, G) Clonogenic assay showed a significant decrease in proliferation of RPRD2 KO cells in the long-term assessment. (D, H) The quantification of clonogenic assay showed a significant decrease in growth of RPRD2 KO cells. Relative survival decreased by 50% upon blockage in each cell line. (t-test: * $p<0.05$, ** $p<0.01$, *** $p<0.001$)

GON4L is a nuclear protein and a member of the coregulator family of transcription. Similar to RPRD2, it plays a role in transcription regulation, but primarily acting as a repressor through interactions with YY1, SIN3A and HDAC1 [195]. Blocking GON4L expression has a detrimental effect on the proliferation of MCF7 cells. In the competition assay, the GON4L KO group was almost completely lost in population compared to controls, which it was similarly observed in colony formation assay **(Figure 3.10)**.

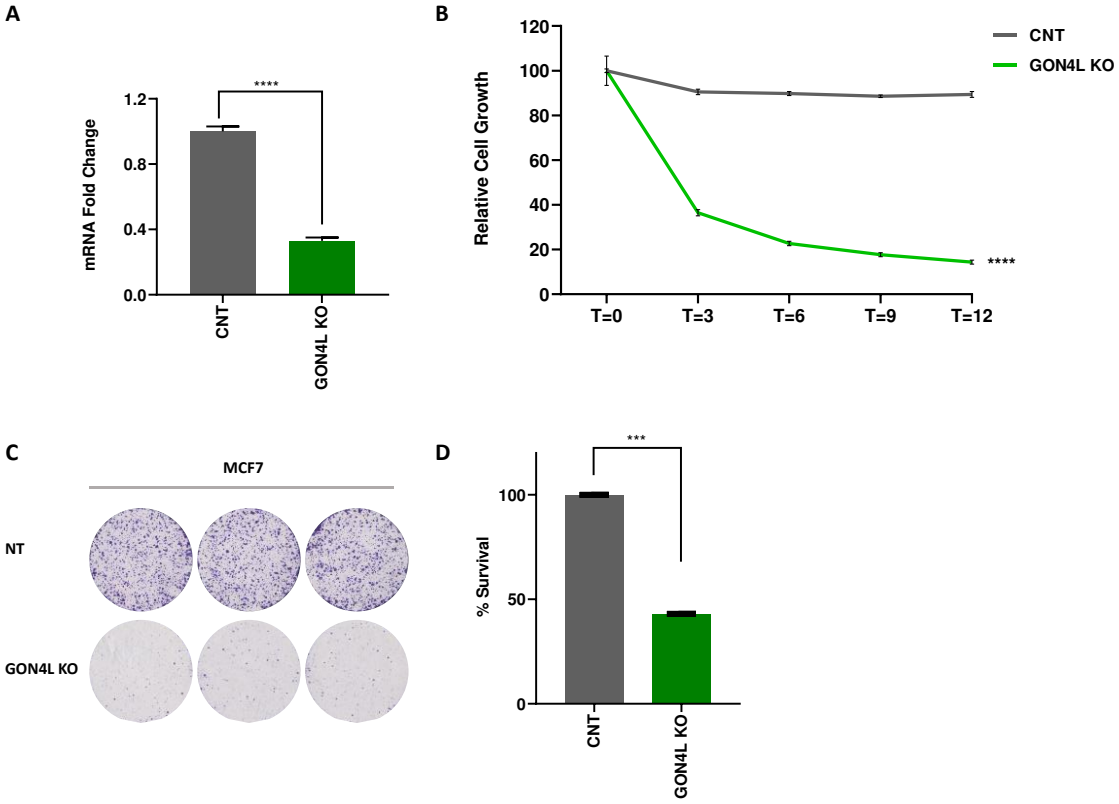

Figure 3. 10. GON4L KO significantly prevents the proliferation of MCF7 cells. In competition assay, GON4L KO MCF7 proliferation showed a significant decrease in which relative cell growth was reported by 15% at end point (A, B). Colony forming ability and proliferation capacity also significantly declined consistent with competition assay (C, D). (t-test: * $p<0.05$, ** $p<0.01$, *** $p<0.001$).

3.2.2 Validation of Negative Selection Screen Findings in 3D Spheroid Model

The effect of RPRD2 gene on spheroid growth was investigated in MCF7 and T47D cells. After puromycin selection, equal numbers of CNT and RPRD2 KO cells were seeded (750.000 cells per well) and cultured for 4 days. Spheroid area was measured using the ImageJ software as detailed in section 2.8. For each biological replicate, measurements were conducted on at least 50 individual spheroids. As indicated in **Figure 3.11**, blocking RPRD2 expression significantly impaired the ability of MCF7 and T47D cells to form spheroids. Across three biological replicates, a consistent decrease in spheroid area was

observed in both cell lines, leading to the formation of highly disorganised spheroids upon RPRD2 inhibition.

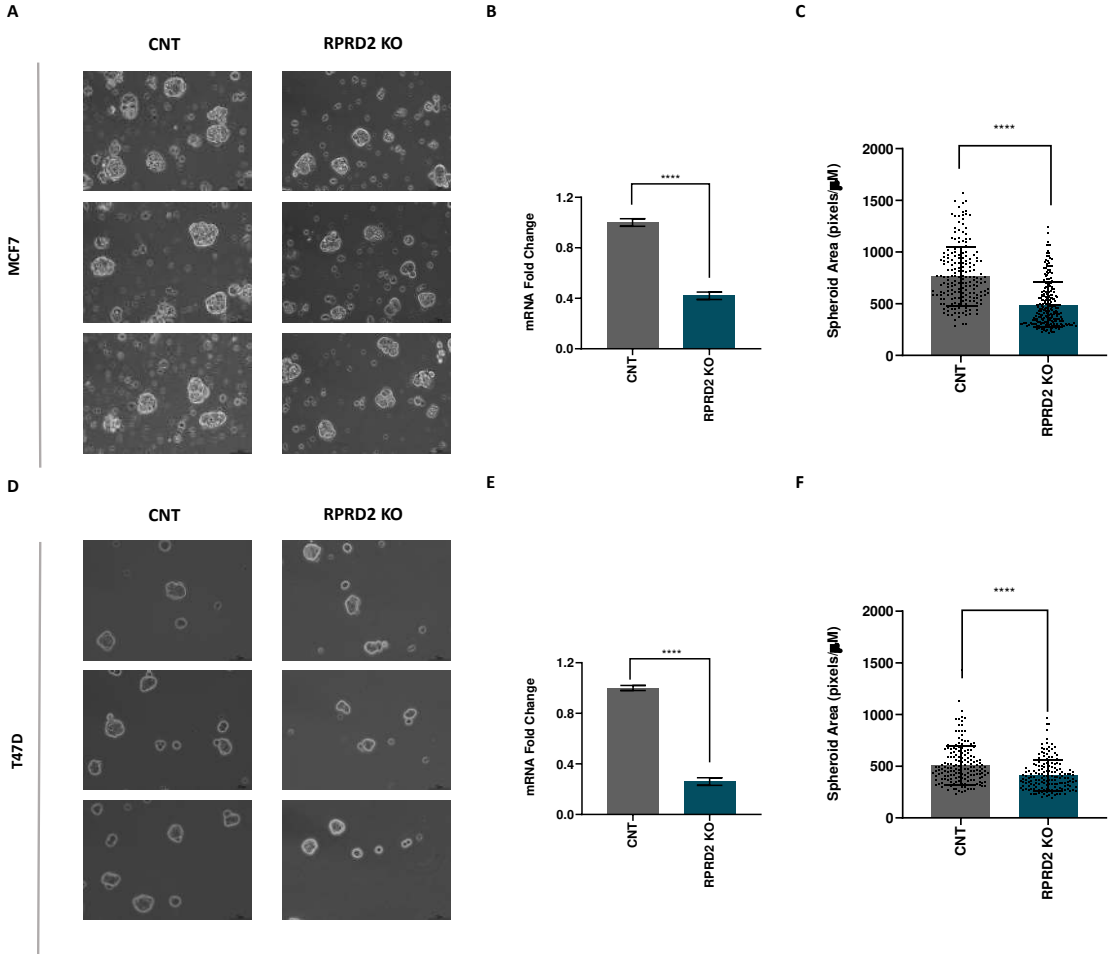

Figure 3. 11. RPRD2 KO significantly inhibited the growth of spheroids in MCF7 and T47D cells. (A) In each experiment, the area of fifty different spheroids was measured for each condition in Day = 4. (B) RT-qPCR was verifying that RPRD2 was still blocked. (C) Images taken for spheroids processed with ImageJ to measure the area and samples collected afterwards to detect blockage still proceeded in 3D. In both MCF7 and T47D, the growth inhibitory effect of blockage in 2D was also observed in 3D and cells significantly sensitive to RPRD2 blockage and could not form regular spheroids compared with CNT. Scale bar was 70 µm. (t-test: * $p<0.05$, ** $p<0.01$, *** $p<0.001$)

GON4L emerged as a potent candidate from the 3D dropout screen conducted in both MCF7 and T47D cells. Its cancer specificity was also validated in MCF12A screening. To identify its phenotypic role in 3D contexts, we blocked GON4L gene expression and evaluated its impact on the spheroid forming ability of MCF7 cells. Targeting GON4L significantly hindered the formation of spheroids and attenuated their growth in 3D settings **(Figure 3.12)**.

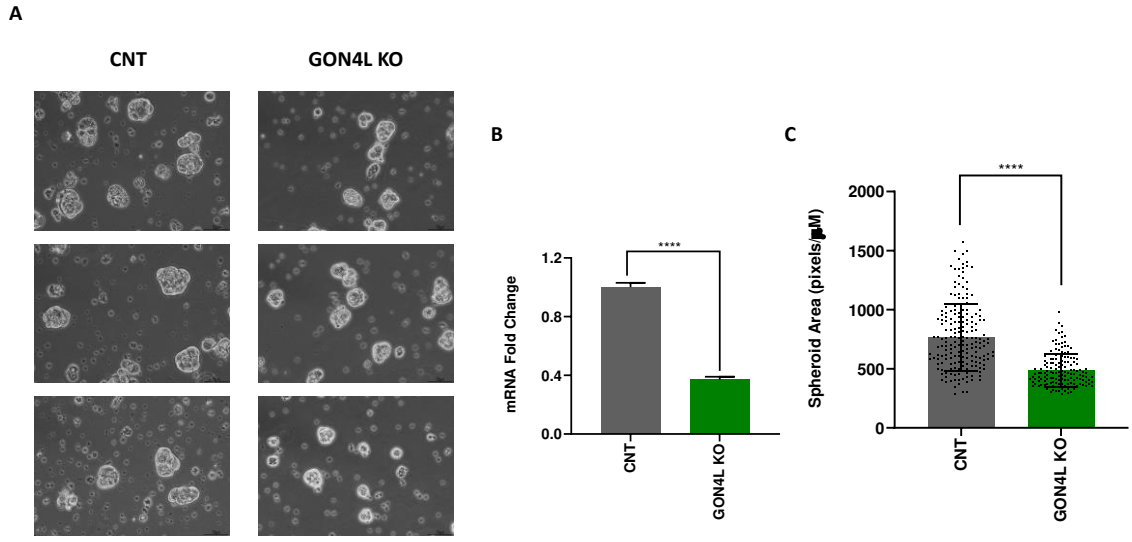

Figure 3. 12. GON4L KO shows significant impact in 3D spheroid growth capacity of MCF7 cells. (A) Spheroid growth assay performed in MCF7 cells showed that GON4L gene plays a crucial role in 3D spheroid formation. (B) RT-qPCR to verify KO status of MCF7. (C) The area was attenuated upon GON4L blockage significantly and also negative impact was observed on spheroid formation. Scale bar was 70 µm. (t-test: * $p<0.05$, ** $p<0.01$, *** $p<0.001$)

3.2.3 Validation of Negative Selection Screen Findings in MCF12A cells

RPRD2 and GON4L genes were identified through both 2D and 3D dropout screenings in MCF7 and T47D cells. In MCF12A cells, the $Log_2(FC)$ values were as - 0.18 and - 0.23 for RPRD2 in 2D and 3D cultures, respectively. These findings suggest that RPRD2's effect on proliferation is negligible in MCF12A cells, emphasising its cancer-

specific action based on screening data. To validate that, competition assay and clonogenic assay were performed in MCF12A. Targeting RPRD2 gene did not significantly affect proliferation, as evidenced by only a 95% decrease in the competition assay. In the clonogenic assay, RPRD2 KO MCF12A cells exhibited growth capacities highly similar to CNT cells as shown in **Figure 3.13.**

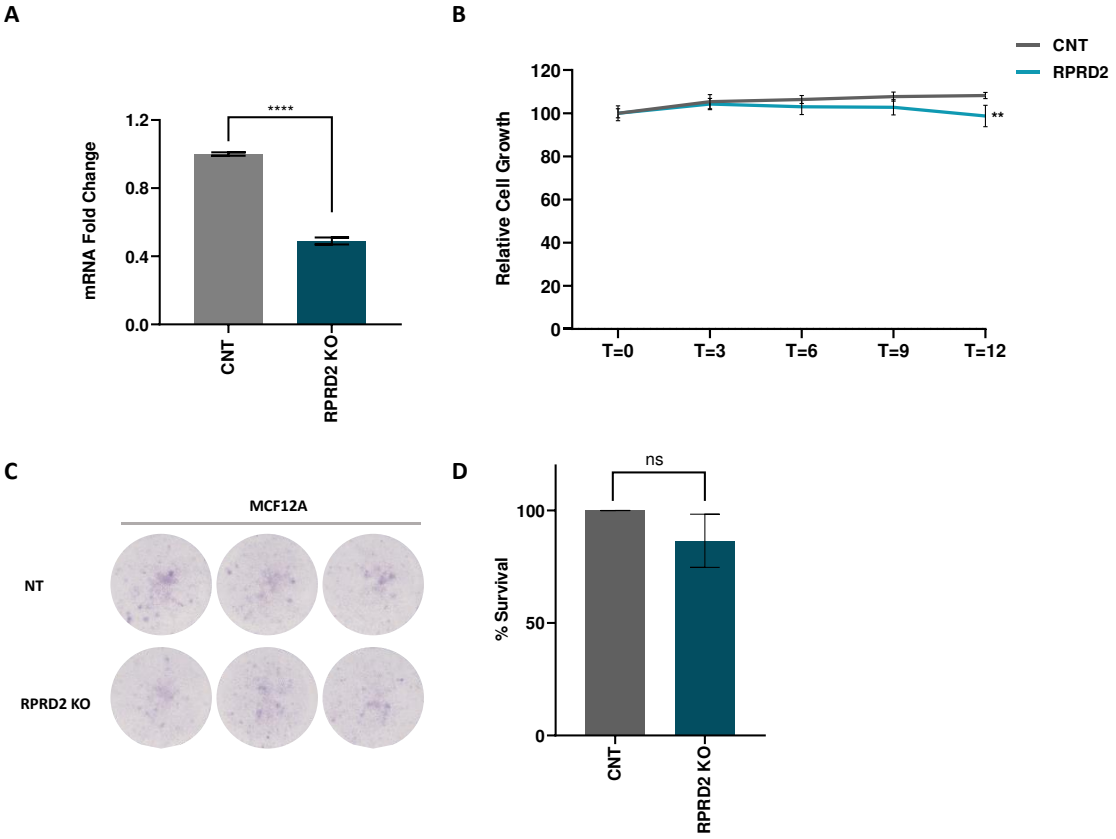

Figure 3. 13. Phenotypic impact of RPRD2 was specific to cancer cells, affecting the proliferation of MCF7 and T47D cells but not the non-tumorigenic MCF12A cells. (A) To validate cancer specific effect of RPRD2, expression was blocked in MCF12A cells for functional assessments that were verified by RT-qPCR. (B) Competition assay showed that the proliferation capacity of RPRD2 KO MCF12A cells kept constant for 12 days of measurements and decreased only by 95%. (C) Colony forming ability was also highly similar upon blockage of RPRD2. Growth pattern seems similar to the CNT group. (t-test: * $p<0.05$, ** $p<0.01$, *** $p<0.001$)

On the other hand, functional assessments of GON4L KO in MCF12A cells revealed a substantial reduction in proliferation when GON4L was absent **(Figure 3.14)**. This underscores the critical role of GON4L in regulation of the proliferation of MCF12A cells. Although initial screening did not detect a significant phenotypic impact of GON4L within the defined cutoff criteria, subsequent competition assay and clonogenic assay demonstrated that MCF12A cell proliferation is highly dependent on GON4L. This observation supports the selection of GON4L as a general depleted hit that is not specific to cancer, indicating its importance in cellular processes.

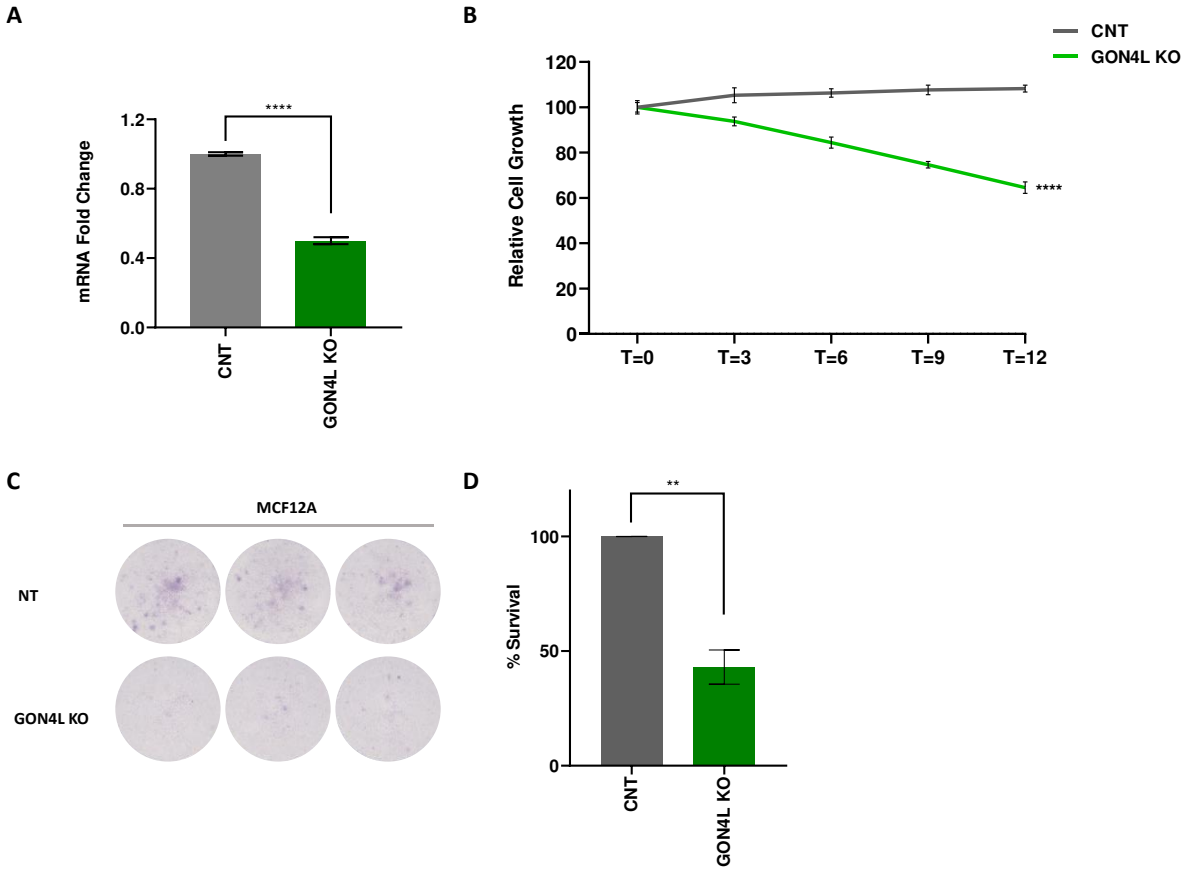

Figure 3. 14. The inhibition of GON4L expression in MCF12A cells negatively affected cell proliferation. The relative cell growth was recorded with 60% decrease in competition assay after blockage of GON4L expression (A, B) and clonogenic assay brought consistent results as survival was reported with more than 50% decrease compared with CNT group (C, D).

According to data from DepMap 23Q2, LIBGENE1Q library contains 80 CE genes. However, the latest revision in DepMap as of 24Q2 (which was released in May 2024) updated the library content as CE genes were listed as 82. GON4L is one of the newly added CE in latest version 24Q2, highlighting its inclusion due to its phenotypic impact observed in MCF12A cells. Even though GON4L was not detected in dropout screening, its impact could be captured in validation experiments. This underscores the importance of validating each candidate gene, even in normal cell lines, to fully comprehend their functional roles. This approach ensures a comprehensive understanding of the exact functions of potential candidates beyond initial screening results.

In conclusion, the RPRD2 gene has been validated to exert a significant negative phenotypic impact on BC cell lines, whereas its effect on MCF12A cells was found to be insignificant. The significant reduction in spheroid growth observed in 3D spheroid culture further solidifies RPRD2's role as a strong oncogene, specifically contributing to cancer progression. This suggests that RPRD2 may plan a critical role in malignancy and the formation of tumour masses.

3.3 Integrated 3D and 2D screening of LIBGENE1Q: Identifying positive growth phenotypes

After identification of depleted genes through dropout analysis, enrichment scores were calculated for MCF7 and T47D cells. To characterise the positive growth phenotypes, endpoint data was normalised using the reference point of 2D endpoint data, where the ratio of 3D to 2D (**3D/2D)** was used. This normalisation approach enhances the detection of differential effects between 3D and 2D cultures. Utilising 3D spheroid screening post-normalization has significant potential to discern positive phenotypes more effectively.

To identify potential genes with positive growth phenotypes, 3D/2D normalised data was processed using a cutoff of FDR < 0.15 and $\log_2(FC) > 0.8$ **(Figure 3.15)**. This analysis revealed non-essential enriched genes in MCF7 and T47D cells, but not in MCF12A cells.

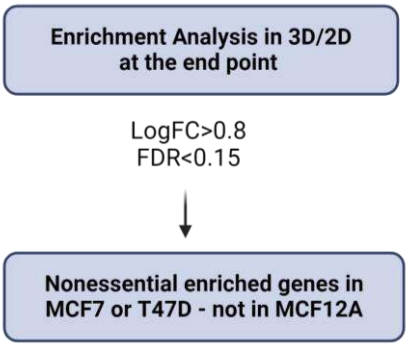

Figure 3. 15. Enrichment analysis summary. Mageck Analysis was performed to define candidates with positive phenotype as enriched genes in 3D/2D normalised data.

Among these genes, ARNT (Aryl hydrocarbon receptor nuclear translocator) and ARL8A (ADP-ribosylation factor-like protein 8A) showed a distinct phenotype: while they exhibited dropout effect in both 2D and 3D models separately, they demonstrated a positive impact on normalised 3D/2D data **(Figure 3.16)**. Based on these findings, further investigations of ARNT and ARL8A in both 2D and 3D models were deemed necessary to confirm their effects on the survival of BC cells. This approach aims to validate and understand the roles of these genes in promoting cell growth and survival in BC context.

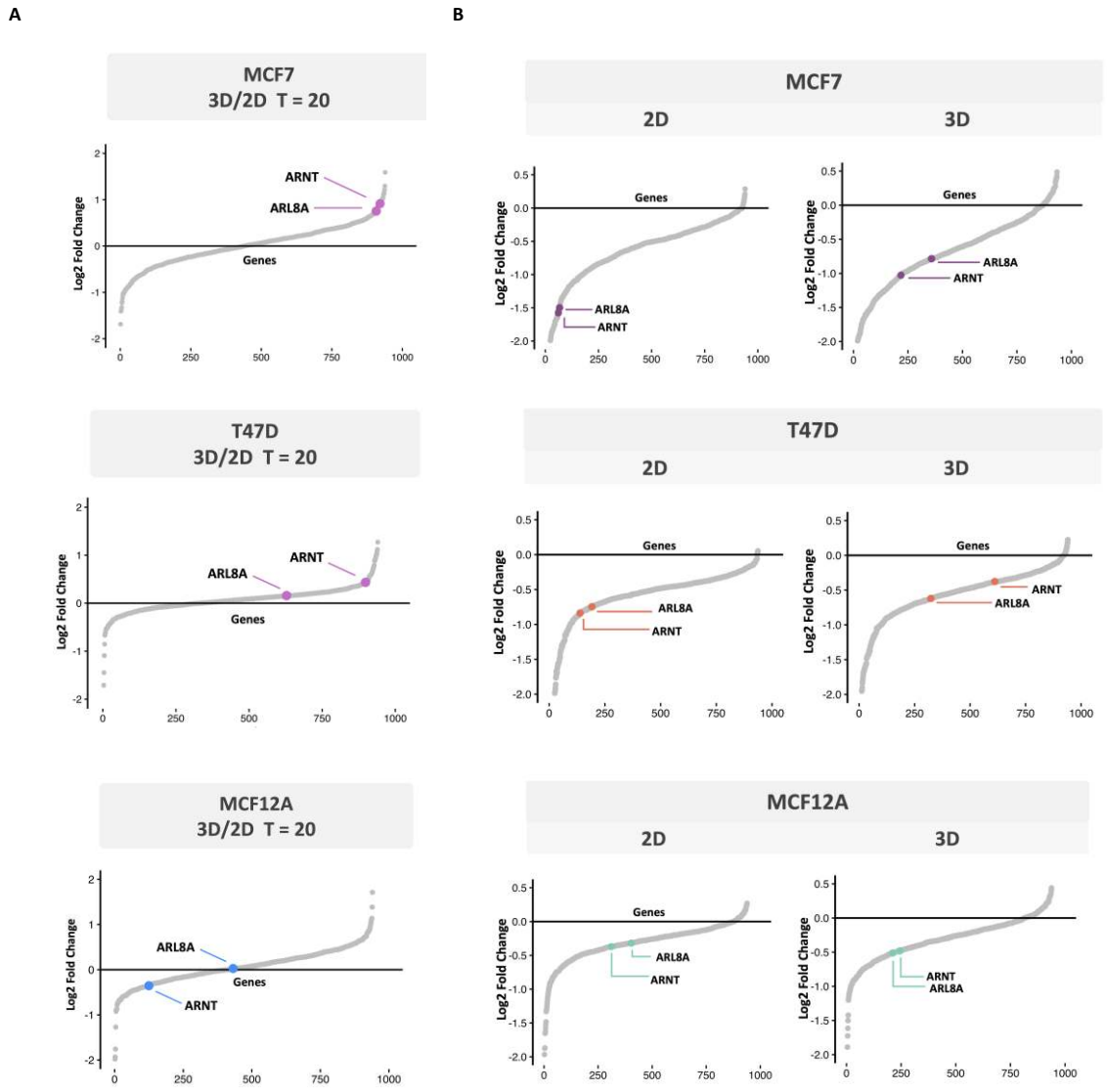

Figure 3. 16. Enrichment analysis in MCF7 and T47D identified ARNT and ARL8A had positive phenotypes while these genes depleted in drop out analysis. (A) Waterfall graphs indicated ARNT and ARL8A had positive Log_2(FC) in 3D/2D enrichment analysis. (B) In dropout analysis these genes showed a negative phenotype in all cell lines.

3.3.1 Validation of Positive Selection Screen Findings in 2D Model

The enrichment analysis of MCF7 and T47D detected 16 genes exhibiting a positive phenotypic impact. However, the focus shifted towards genes that display differential behaviour in 2D versus 3D models, aiming to understand the influence of *in vitro*

culturing conditions on screening results. This focus led to the selection of ARNT and ARL8A, which were initially identified in dropout analysis with negative phenotypes but also appeared in enrichment analysis with positive phenotype. Further investigations were initiated to explore the specific impacts of ARNT and ARL8A in both 2D and 3D settings.

First, the expression levels of ARL8A and ARNT were examined in MCF7 and T47D cells compared to the MCF12A control cell line **(Figure 3.17)**. ARL8A showed a significant upregulation, approximately 5-fold in MCF7 and up to 9-fold in T47D cells. In contrast, ARNT expression levels were highly similar across MCF12A and MCF7/T47D BC cell lines, with no significant changes observed.

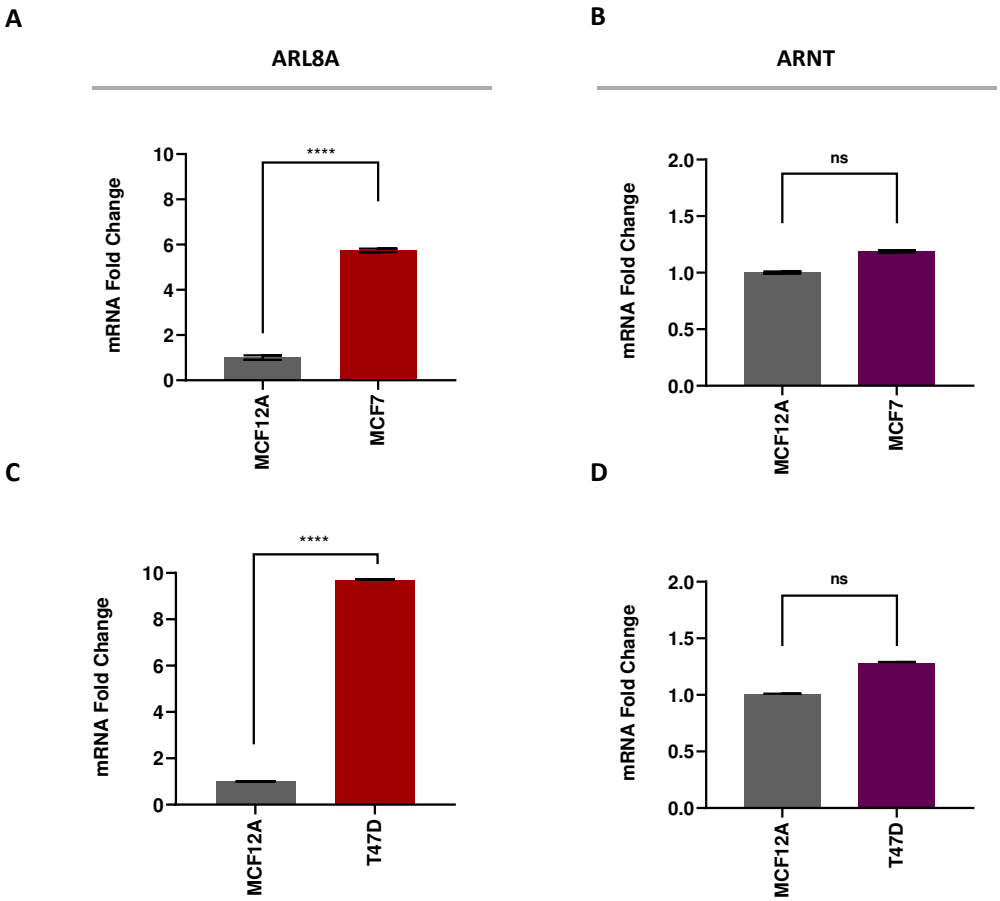

Figure 3. 17. The endogenous expression of ARL8A and ARNT in MCF7 and T47D cells compared with MCF12A cells. ARL8A expression upregulated in both cancer cell

lines significantly was verified by RT-qPCR (A, C), but ARNT expression was verified with no significant change in BC cell lines compared with MCF12A (B, D). (t-test: * $p<0.05$, ** $p<0.01$, *** $p<0.001$)

ARL8A, a member of small GTPases which has a GTP binding activity and belongs to Arf-like proteins within the Ras superfamily specifically [196], was investigated for its phenotypic impact on BC cells by blocking its expression. Validation experiments were initially conducted in 2D models due to ARL8A showing a negative phenotype in 2D screening in both MCF7 and T47D cells.

In both MCF7 and T47D cells, targeting ARL8A inhibited proliferation, consistent with the observations from dropout analysis **(Figure 3.17)**. MCF7 cells exhibited greater sensitivity upon targeting ARL8A, as evidenced by reduced proliferation in both competition and colony formation assays. Despite higher baseline expression of ARL8A in T47D cells, its inhibition resulted in less pronounced effects on proliferation compared to MCF7 cells **(Figure 3.18)**

These results underscore the role of ARL8A in promoting cell proliferation BC cells and highlight cell-type-specific differences in sensitivity to ARL8A inhibition.

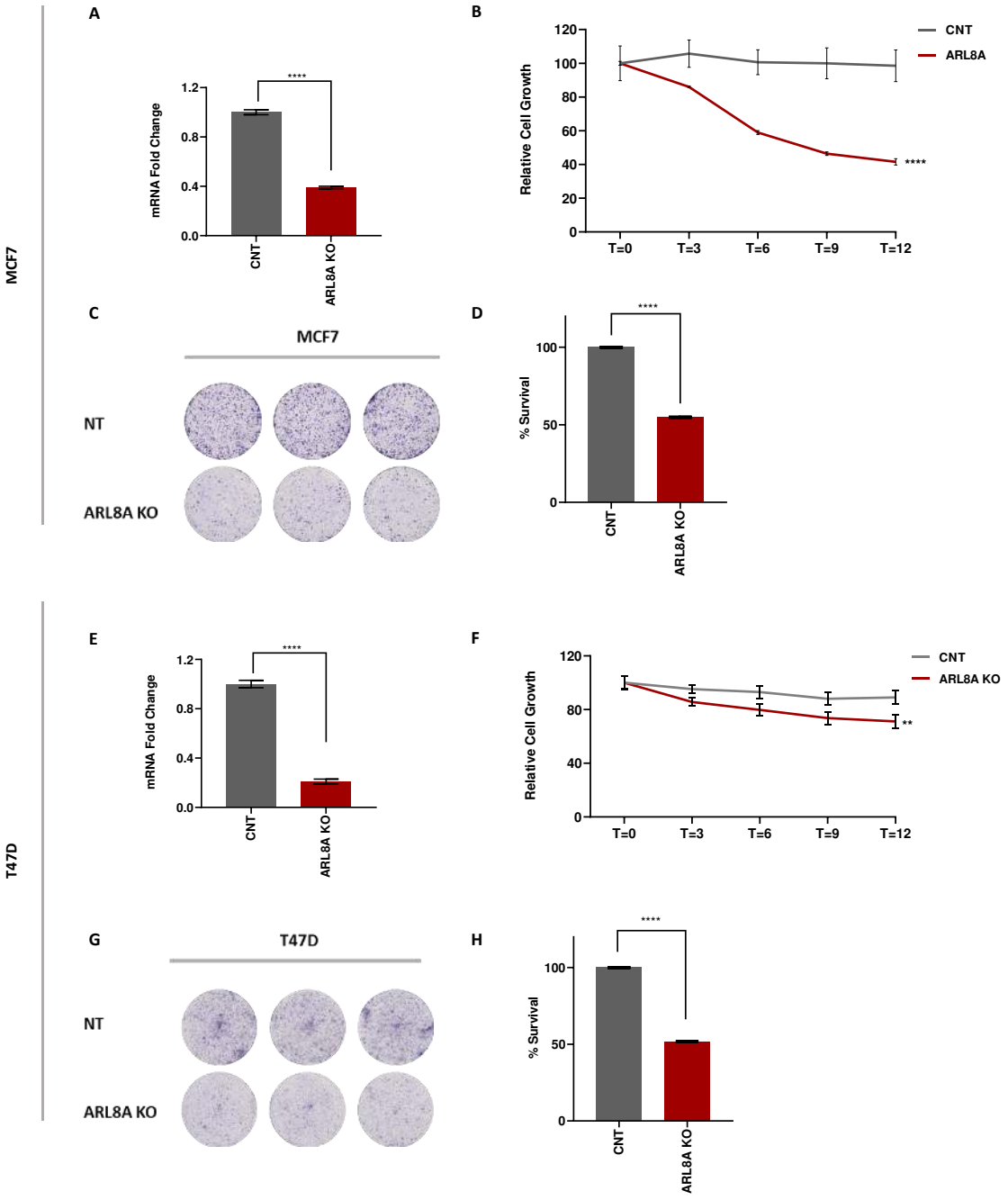

Figure 3. 18. ARL8A had been validated with negative phenotype in 2D. After the expression was blocked in MCF7 (A) and T47D (E), competition assay and clonogenic assay were performed to investigate proliferation capacity of ARL8A KO cells. Competition assay showed a significant decrease in proliferation of ARL8A KO cells in both MCF7 (B) and T47D (F). Colony forming abilities of MCF7 (C, D) and T47D (G,

H) significantly decreased upon blockage of ARL8A. (t-test: * $p<0.05$, ** $p<0.01$, *** $p<0.001$)

The second candidate gene, ARNT, functions as a translocator protein that facilitates the movement of the ligand-bound aryl hydrocarbon receptor from the cytoplasm to the nucleus. Together, they form a complex that binds to the specific enhancer sequences on DNA, thereby enhancing the transcription of target genes [197].

In 2D validation experiments, targeting ARNT resulted in a significant decrease in cell proliferation, as demonstrated in both competition assay and colony formation assay. These findings suggest that ARNT may play an oncogenic role in 2D culture **(Figure 3.19)**. Despite the observed reduction in proliferation of BC cells, the impact of ARNT inhibition was less pronounced compared to other genes investigated thus far, particularly notable in competition assays **(Figure 3.19B, F)**.

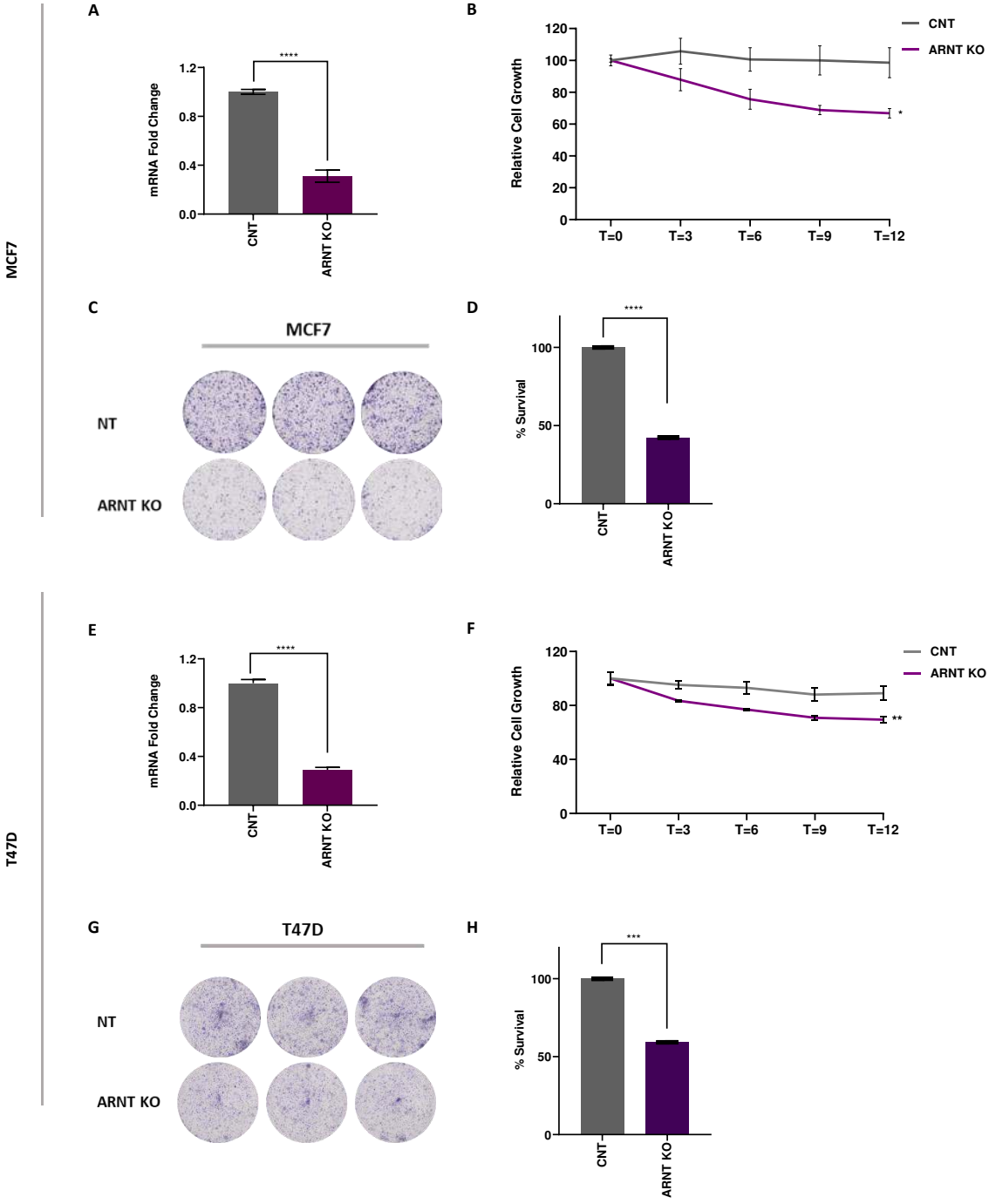

Figure 3. 19. ARNT has a certain negative phenotype in 2D monolayered culture. After the expression is blocked and verified by RT-qPCR in MCF7 (A) and T47D (E), competition assay and clonogenic assay were performed to investigate proliferation capacity of ARNT KO cells. Competition assay showed a significant decrease in proliferation of ARNT KO cells in both MCF7 (B) and T47D (F). Colony forming

abilities of MCF7 (C, D) and T47D (G, H) significantly decreased upon blockage of ARNT. (t-test: * $p<0.05$, ** $p<0.01$, *** $p<0.001$)

3.3.2 Validation of Positive Selection Screen Findings in 3D Models

In this section, the impact of ARL8A and ARNT on spheroid forming ability and growth were investigated. ARL8A and ARNT exhibited distinct behaviours in 2D dropout screening, yet they were enriched in 3D/2D positive selection analysis, prompting further investigation in 3D to clarify their phenotypic impacts.

As our first candidate, ARL8A was blocked, and its effects were evaluated using the spheroid growth assay. In both MCF7 and T47D cells, spheroid areas increased compared to the CNT, indicating enhanced spheroid growth density upon ARL8A inhibition. Interestingly, while ARL8A KO inhibited cell proliferation in 2D models of MCF7 and T47D cells, it improved spheroid formation ability in 3D spheroid models **(Figure 3.20)**.

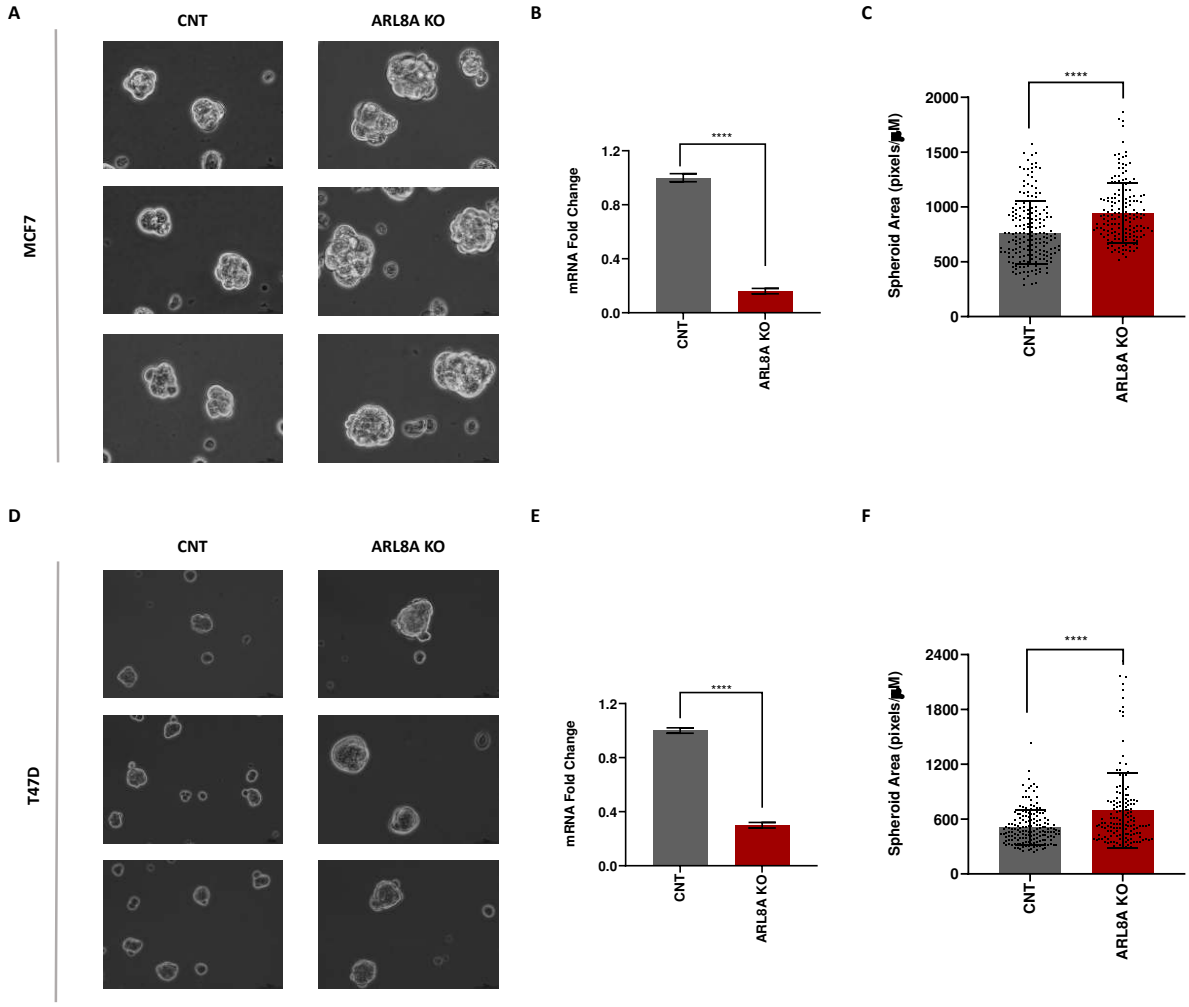

Figure 3. 20. ARL8A KO significantly improves the growth of spheroids in MCF7 (A) and T47D (B) cells. (A) After the ARL8A gene was blocked in MCF7 and T47D cells, they were seeded into 10% MC medium with CNT group and grown for 4 days. (B) In 3D culture, ARL8A expression was still kept blocked that was verified by RT-qPCR after 4 days culturing. (C) In each biological replicate, the area of at least fifty different spheroids was measured for each condition in Day=4. Images taken for spheroids processed with ImageJ to measure the area after being sure about the expression still were kept blocked. In each cell line, the growth promoting effect of the blockage in 3D which was a controversial observation with 2D allows to define this gene as a differential phenotypic gene. Scale bar was 70 µm. (t-test: * $p<0.05$, ** $p<0.01$, *** $p<0.001$)

ARNT, the second candidate identified in positive selection, was further analysed to characterise its phenotypic effect in 3D. Spheroid growth assay was conducted in two BC cell lines. Targeting ARNT significantly increased spheroid area in both MCF7 and T47D cells. Upon ARNT inhibition spheroids grew larger and appeared to enhance the formation of tumour bulks, suggesting that ARNT may function as a TSG in this context **(Figure 3.21)**.

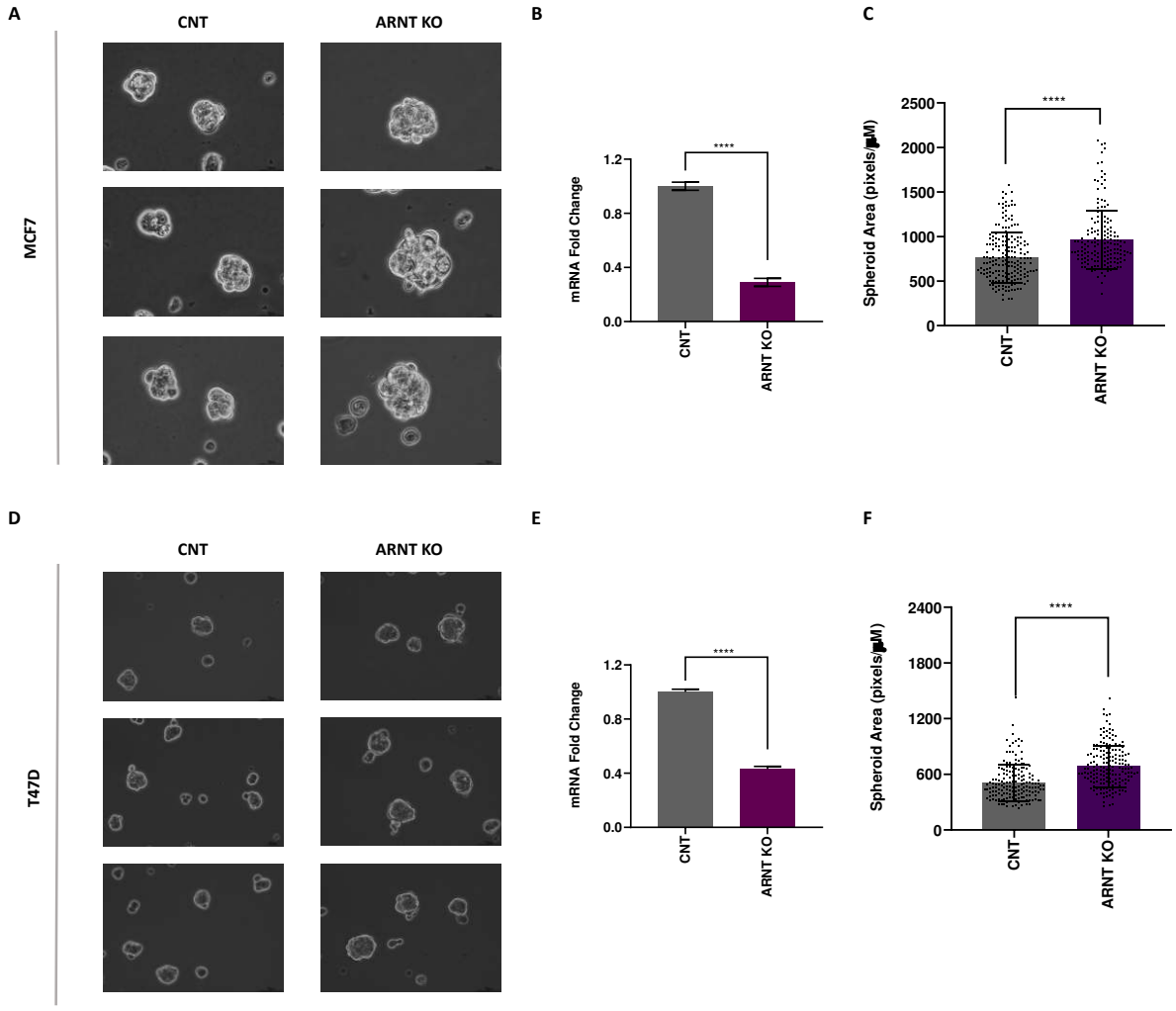

Figure 3. 21. Spheroid growth significantly enhanced upon ARNT KO in MCF7 (A) and T47D (B) cells. After the ARNT gene was blocked, cells were seeded 10% MC medium with CNT group. (A) After 4 days, spheroids were imaged in which more than fifty different spheroids were captured for each biological replicate. (B) After imaging, spheroids were collected, and ARNT gene expression level had been determined to

ensure the blockage was still proceeding by RT-qPCR. (C) Images taken for spheroids processed with ImageJ to measure the area. Scale bar was 70 µm. (t-test: * $p<0.05$, ** $p<0.01$, *** $p<0.001$)

The validation experiments for ARNT and ARL8A revealed a negative phenotype, indicating that these genes promote cancer cell growth in 2D culture. However, their effects in the 3D spheroid model presented a different phenotypic impact, where they appeared to function as TSGs. These contrasting behaviours align with the screening results from enrichment analysis, leading to the classification of **ARNT and ARL8A as differential phenotypic genes.**

3.3.3 Validation of Positive Selection Screen Findings in MCF12A cells

To investigate the phenotypic impacts of ARL8A and ARNT in MCF12A cells, functional assessments were preceded by competition assay and clonogenic assay.

When ARL8A was targeted **(Figure 3.22A)**, the proliferation of MCF12A was not affected, maintaining a similar ratio to the CNT group, with only an approximately 10% decrease observed in the competition assay **(Figure 3.22B)**. Similar observations were also recorded in the clonogenic assay, where ARL8A KO MCF12A cells retained the ability to form colonies comparable to CNT group, with colony growth slightly moderated by 10% **(Figure 3.22C, D)**. These findings indicate that ARL8A's phenotypic impact is cancer-specific, as its inhibition did not significantly affect the proliferation and growth of the MCF12A cells as it did in cancer cell lines.

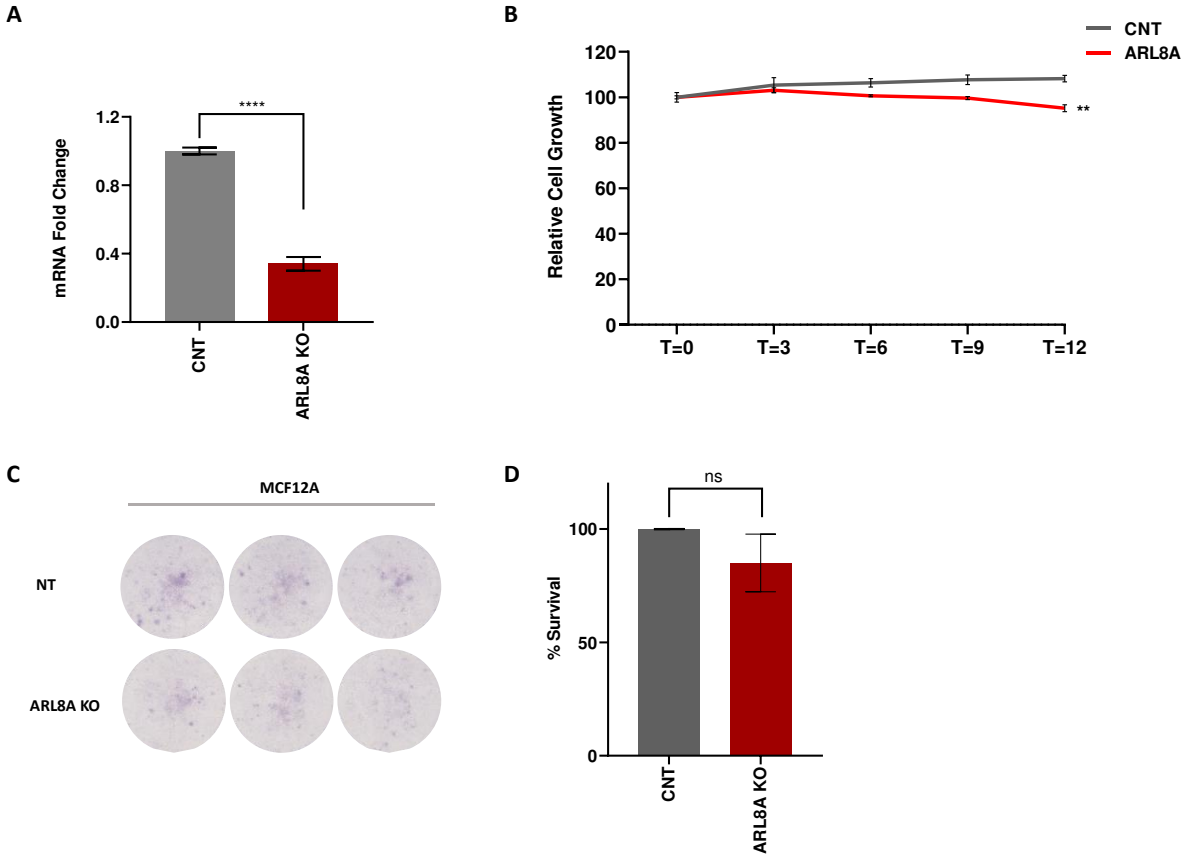

Figure 3. 22. ARL8A phenotypic impact was proved as cancer specific. RT-qPCR verified the blockage of ARL8A (A) which did not diminish the proliferation of MCF12A as recorded in competition assay (B). In the clonogenic assay (C, D), there was an insignificant change in the colony forming abilities between the CNT group and the ARL8A KO group. (t-test: * $p<0.05$, ** $p<0.01$, *** $p<0.001$)

On the other hand, targeting ARNT showed a distinct effect on the proliferation and growth of the MCF12A cells. In the competition assay, the absence of ARNT resulted in a slight improvement in proliferation. More notably, in the colony formation assay, there was a significant increase in growth, with ARNT KO MCF12A cells showing enhanced proliferation compared to CNT group **(Figure 3.23)**. These findings suggest that ARNT may play a tumour suppressive role in MCF12A cells, with its absence promoting increased proliferation.

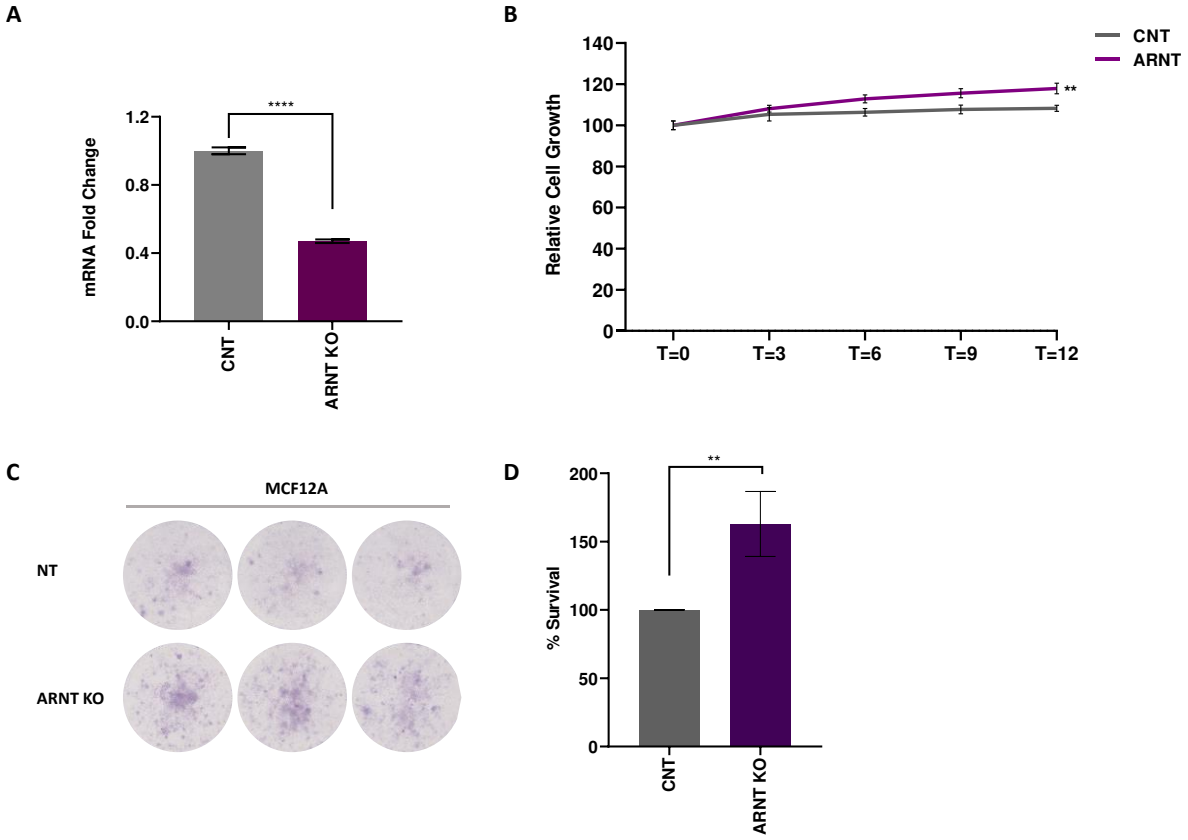

Figure 3. 23. Upon targeting ARNT expression, MCF12A proliferation showed a slight but significant increase. (A) RT-qPCR analysis to verify the expression was blocked in MCF12A cells (B) The competition assay showed the improvement in proliferation of ARNT KO MCF12A cells by 10% increase in relative cell growth. (C, D) In colony formation assay, the blockage of ARNT results in improved colony forming ability by more than 50% increase compared with CNT.

3.4 ARNT exhibits a positive phenotypic impact on MCF12A normal BC cells

The phenotypic impact of ARNT gene was also investigated in 3D models to gain insight into spheroid growth in the absence of ARNT in MCF12A cells. Given that 2D results indicated improved proliferation upon ARNT KO, the 3D spheroid growth assay was conducted to elucidate ARNT's role in tumour bulk formation. The assay showed that ARNT KO led to the formation of larger and more compact spheroids, similar to those

observed in cancer cells **(Figure 3.24)**. This positive phenotypic impact in 3D was consistent with the findings obtained from 2D models.

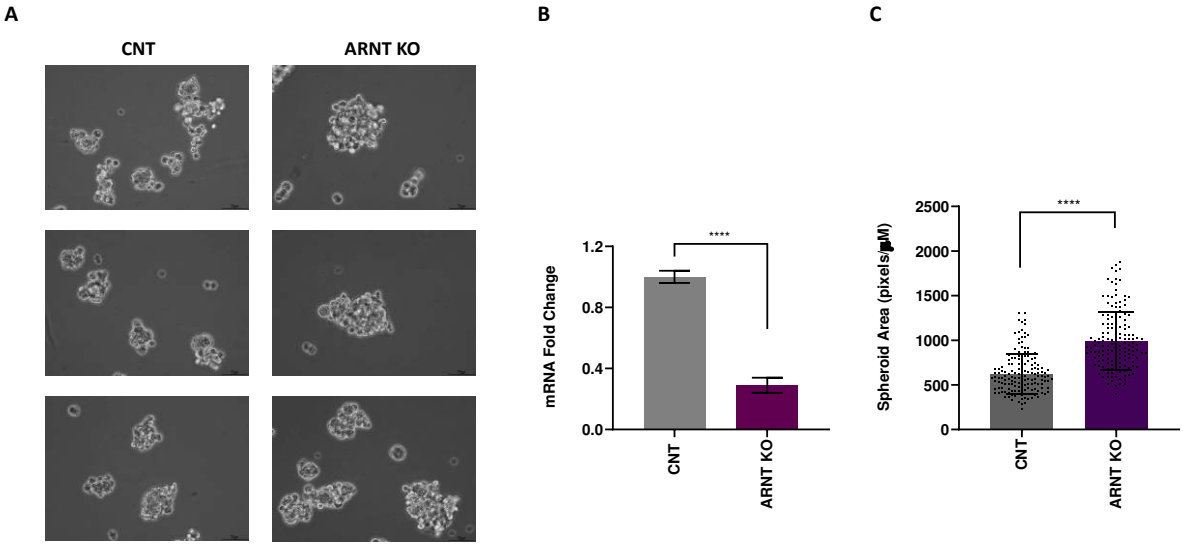

Figure 3. 24. ARNT KO MCF12A cells formed more compact spheroids with increased spheroid area compared to CNT. (A) After ARNT gene KO in MCF12A, spheroid growth assay conducted, and images belonged to Day=6. (B) RT-qPCR verified the blockage was still kept in 3D after collecting samples (C) Spheroid area was increased significantly and spheroids were observed as in more compact forms. Also, spheroid phenotypes resembled cancer spheroids while CNT group was less prominent to form condensed form of spheroids. Scale bar was 70 µm. (t-test: * $p<0.05$, ** $p<0.01$, *** $p<0.001$)

3.5 ARNT exhibits a positive phenotypic impact on MCF10A normal BC cells indicating ERα independent action

MCF10A, a breast normal cell line lacking ERα activity, was used to investigate the effect of ARNT KO and its potential association with ERα. Colony formation assay showed enhanced proliferation and growth capacity in ARNT-targeted MCF10A cells **(Figure 3.25)**. So, it might be concluded that ARNT phenotypic impact is independent from ERα in breast cell lines.

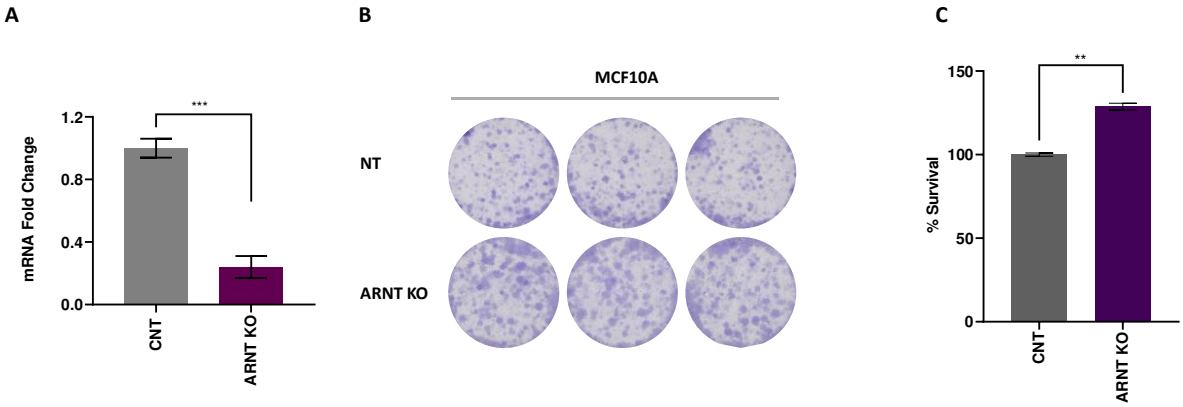

Figure 3. 25. ARNT KO showed a positive phenotypic impact in normal MCF10A cell proliferation. ARNT KO MCF10A cells exhibit improved growth in 2D culture. Because MCF10A cells lacks ERα expression, the ARNT impact may be independent from the ERα.

Chapter 4

4 DISCUSSION

The complexity of breast anatomy contributes to the heterogeneity of BC, influencing its progression [6,7]. At the molecular level, BC is classified into four main subtypes: Luminal A, Luminal B, HER2+, and TNBC, each affecting treatment strategies differently. The luminal subtypes, characterised by unrestrained activity of NHRs, are the most common subtype among patients. The HER2+ subtype involves the amplification of the *ERBB2* gene, while the basal subtype, which lacks both NHRs and HER2, is considered highly aggressive [8].

Cancer progression involves distinct mutations that provide growth advantages, enhancing proliferation at both genetic and epigenetic levels [20,21]. Somatic mutations drive carcinogenesis by converting genes into defective forms, as in the case of OCs and TSGs. The complex interplay between these genes underpins cancer progression. Therefore, the identification of unique OCs and TSGs has profound impact in advancing the understanding of genetic perturbations in BC progression [25,26]. These genetic elements are pivotal in regulating cell growth, proliferation, and apoptosis, and their dysregulation is a hallmark of cancer development and progression [28].

OCs are mutated or overexpressed forms of pOCs, which in their normal state regulate essential cellular functions such as growth and differentiation. When mutated or activated, pOCs promote uncontrolled cell proliferation and survival, contributing to tumorigenesis [27,28]. Identifying unique OCs allows researchers to unravel the molecular pathways leading to cancer, which can aid in predicting prognosis and treatment response [30,31]. In contrast, TSGs normally act to prevent uncontrolled cell growth by regulating the cell cycle, promoting apoptosis, and repairing DNA damage

[21]. The inactivation or loss of TSGs mostly dysregulates these protective mechanisms, allowing cancer cells to proliferate uncontrollably. Understanding the identification and inactivation mechanisms of TSGs is essential for comprehending genetic predispositions to cancer [30].

In summary, the detailed characterization and identification of unique OCs and TSGs are fundamental to advancing cancer research. These efforts significantly deepen our understanding of cancer biology and open new avenues for groundbreaking diagnostic, prognostic, and therapeutic approaches [198].

BC is characterised by a complex landscape of genetic alterations, encompassing both small-scale and large-scale mutations. These genetic aberrations play pivotal roles in BC initiation, progression, and the development of TR [22,104,105]. Studies investigating the mechanisms underlying BC complexity have identified diverse mutational signatures that might activate pOCs or deregulate TSGs [109]. CNAs are among the most common CAs observed in BC, such as those observed in 1q, 8q, and 17p. These CNAs are associated with aggressive tumour behaviour and poor clinical outcomes, underscoring their significant implications in BC [108].

Extensive studies emphasise that CNAs in Chr1q are associated with poor clinical outcomes, highlighting their significance in BC aggressiveness and recurrence. In all BC subtypes, CNAs in Chr1q lead to diverse chromosome configurations, potentially resulting in differential phenotypic impacts based on this complexity [109].

In this thesis, it is hypothesised that CNAs in Chr1q may drive genetic abnormalities that enhance the proliferation of BC by exploiting the genetic disorder/catastrophe. Therefore, our aim is to interrogate the content of Chr1q to uncover the underlying reasons for the prevalence of CNAs in this region in BC. Our approach involved a CRISPR-based LOF screening using a custom CRISPR library LIBGENE1Q.

To elucidate the role of Chr1q, we generated LIBGENE1Q that targets 940 genes annotated in Chr1q. After library cloning, we verified the sgRNA abundances and ensured library complexity. Next, the reproducibility of screening was assessed by

comparing the depletion scores of CE genes with NTs. As expected, CE genes exhibited the strongest depletion, while NTs showed no significant changes over the 20-days screening period. Screening was performed in two luminal cell lines and one normal cell line as control. To robustly identify CDGs with both positive and negative effects, we performed the screenings in both 2D and 3D cultures simultaneously.

The key observation is that the impact of essential genes changes significantly when cultured in 3D models, whereas NE genes do not show a significant change. This study allows, for the first time, a detailed evaluation of CE genes behaviour both cumulatively and at the single sgRNA abundance level in 3D cultures, compared to 2D cultures. Since gene essentiality has predominantly been assessed using collective data from 2D screens in cancer cells, this finding raises questions about the reliability of previous data. Annotated genes might exhibit significant depletion scores in 2D screens, which tend to preferentially detect negative phenotypes. But, 3D models, which better mimic natural tumour behaviour, might behave differently, especially for the CE genes. Our data clearly show that CE genes annotated in DepMap version 23Q2 showed differential phenotypes in 2D and 3D screens. The depletion scores of all annotated CE genes shift towards those of NE genes, indicating lower depletion scores in 3D cultures. Therefore, cumulative screening data collected from 3D culturing might necessitate revisiting annotations to accurately understand the absolute behaviour of a gene.

Moreover, for the first time, we explored the behaviour of CE genes in a normal cell line in both 2D and 3D cultures. Specifically, the annotated Chr1q CE genes in the MCF12A cell line exhibited behaviour highly similar to NE genes, especially in 3D cultures. The cancer-specific phenotypic impacts could be observed apparently by comparing the depletion pattern with cancer cells. Cancer-specific action of these genes might be related with induction of malignancy especially upon cumulative genetic abnormalities.

4.1 LOF Screen effectively distinguishes shared negative phenotypes in 2D and 3D Models.

To reveal the Chr1q genes involved in BC proliferation, dropout screening was performed in two luminal cancer cells and one normal breast cell line, each at 1000x coverage with

three biological replicates. The most potent candidates, defined as CDGs, were identified from the dropout screen based on significant depletion scores ($Log_2(FC) < -1$, FDR < 0.1). The gene lists of MCF7 and T47D included both CE and NE genes, with NE genes exhibiting a less pronounced negative effect on cell proliferation than CE genes, as indicated by FC differences. Notably, 109 NE genes in MCF7 and 40 NE genes in T47D exhibited significant depletion, with 23 NE genes shared between these two cell lines. Upon examining depletion scores for 3D spheroid screening, 122 NE genes in MCF7 and 48 NE genes in T47D were identified, with 24 depleted NE genes shared between the two cell lines and no significant changes observed in MCF12A. Across all experimental conditions, 14 NE genes were significantly depleted in both MCF7 and T47D across 2D and 3D culturing models. These genes were classified as ***strong oncogenes*** due to their consistent impact on cell proliferation in both cell culture models. Among them, RPRD2 and GON4L were selected for further validation as strong oncogene candidates.

To validate the most potent candidate genes, competition assays and colony formation assays were conducted to determine their effects on proliferation of BC cells. Targeting the RPRD2 gene resulted in a highly significant decrease in proliferation of BC cells, while there was no effect on the normal MCF12A cell line. Moreover, spheroid growth was significantly attenuated in cancer cells, consistent with the screening results.

Phosphorylation and dephosphorylation of C-terminal domain (CTD) of RNAP II by dynamic actions of kinases and phosphatases control the transcription initiation at promoters, as well as elongation and termination at downstream positions [199]. The CTD serves as a docking site for various proteins involved in transcription initiation and elongation, nascent mRNA modification, and transcription termination [200]. RPRD2, a protein containing CTD-interacting domain (CID) with repetitive serine- and proline-rich regions, is ubiquitously expressed in all human tissues [194]. It is hypothesised that RPRD2 might preferentially bind to phosphorylated forms of RNAP II, although detailed characterization is lacking [194,201,202]. An unpublished study submitted in 2021 showed that RPRD2 acts as a negative regulator of transcription; overexpression of RPRD2 downregulates the transcription, while RPRD2 repression increases RNA synthesis in HEK293T cells. Notably, depletion of RPRD2 led to a decrease in nascent

and newly synthesised RNA of MYC, a key factor in carcinogenesis. This study also linked the RPRD2 interaction with cellular growth and cell cycle progression, although the explorations were limited to non-tumorigenic HEK293T cells and did not include cancer models (Winczura et al. Unpublished).

In the context of this thesis, RPRD2 was identified and validated in dropout screens conducted in both 2D and 3D models, exhibiting a negative phenotype. RPRD2 is known as a TF with negative transcription regulation activity, but its exact function in cancer cells remains unclear. We hypothesise that in cancer cells, RPRD2 deregulates the transcription of genes important for growth and proliferation, possibly modulating apoptotic genes or even TSGs by blocking their transcription. The upregulation of RPRD2 in BC patients further underscore its importance in tumorigenesis. Further assessments will be performed to elucidate the exact role of RPRD2, guided by the findings presented in this study **(Figure 4.1).**

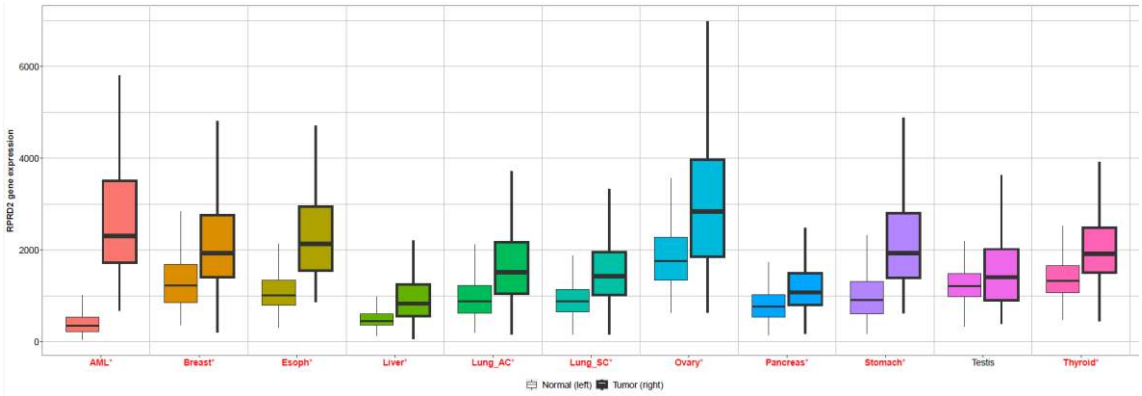

Figure 4. 1. RPRD2 Expression has been upregulated in patient samples belonging to various cancer types. Data obtained from TNMplot (https://tnmplot.com/analysis/)

GON4L was initially annotated as NE in the DepMap version 23Q2 at the start of the validation experiments. However, experimental results showed that targeting GON4L had a highly significant effect on the proliferation of MCF7 cells, leading to their apparent inability to survive. In addition, GON4L appeared to be important for the survival of MCF12A cells, as both competition and clonogenic assays showed that proliferation of

MCF12A was affected by GON4L KO. Following these observations, the latest DepMap version 24Q2, released in May 2024, reclassified GON4L as a CE gene in BC, along with the dropout candidate HJV.

The GON4L gene has been extensively studied and shown to be highly prevalent to modulate proliferation, development and differentiation acting as a transcriptional regulator across various animal models [203–206]. In the context of bladder cancer, GON4L's specific role has been elucidated: it regulates CD24 expression by interacting with the TF YY1. GON4L and YY1 form a complex that binds to the CD24 promoter. Further investigation revealed that YY1's binding to the CD24 promoter is facilitated by another TF, androgen receptor (AR). GON4L enhances this interaction by promoting the binding affinity of AR to the CD24 promoter, thereby contributing to the induction of CD24 expression. Moreover, GON4L also appears to influence proliferation through pathways independent of AR and CD24 in bladder cancer [195].

Despite the compelling evidence showing GON4L's critical role in carcinogenesis and its impact on cell proliferation, its annotation as a CE gene in DepMap suggests it may be essential for fundamental cellular processes beyond cancer-specific functions. Given that MCF12A cells also exhibit dependency on GON4L for proliferation, independent of cancer-specific mechanisms, further investigations into the role of GON4L in BC may not be prioritised at this time.

4.2 Identifying genes that promote spheroid growth in 3D culture through positive selection

The characterization of a gene whose absence increases or promotes the tumour growth becomes more prominent when screening is performed simultaneously in both 2D and 3D cultures. During analysis, the normalisation of end point data from 3D and 2D screenings enables the detection of positive phenotypes that enhance the proliferation upon loss [180].

Because we hypothesised that Chr1q CNA might trigger an event leading to either the activation of OC or the inactivation of a TSG, we analysed screening results using 3D/2D normalisation.

Enrichment scores were determined ($Log_2(FC) > 0.8$, $FDR < 0.15$) for each cell line. In MCF7, 12 genes exhibited enrichment, whereas in T47D, 4 genes showed enrichment. Among these, **ARNT** is annotated in the COSMIC database as both an OC and a TSG [207]. Supporting this, the ARNT gene is also listed in the 2D dropout list. Similarly, **ARL8A**, found also in the dropout list, shows an enrichment score in 3D/2D analysis. Thus, ARNT and ARL8A were further analysed as they are potentially exhibiting nuanced behaviour: these genes might have complex roles and effects that are not straightforward. This complexity can manifest in their ability to function as both OC and TSG, depending on the context.

4.2.1 Nuanced behaviour: ARL8A

To define phenotypic impacts of these genes, validation experiments were conducted in both 2D and 3D models. In 2D, ARL8A KO was shown to have negative effects on proliferation of cancer cells, while having no effect on MCF12A cells. But, in 3D, the knockout significantly improved the spheroid growth.

ARL8A, depicted as an Arf-like (Arl) protein, belongs to the Ras small GTPase superfamily [196]. The Arl subfamily is known to regulate several intrinsic pathways, including membrane trafficking and organisation of cytoskeleton. Besides that, these proteins are involved in carcinogenesis by regulating cell migration and spreading, thereby enhancing metastases [196,208,209].

Small GTPases are highly important molecules that function as molecular switches, mediating the actions of various effectors upon activation. Through their GTPase activity, they can phosphorylate effector proteins and initiate different cellular pathways [209].

Lysosomes are acidic organelles responsible for the degradation of cellular substrates, including proteins, lipids, and carbohydrates, using hydrolytic enzymes. In cancer, lysosomes contribute significantly to drug resistance, cell migration, tumour invasion, and metastasis [210]. ARL8, a highly conserved protein, plays a pivotal role in lysosome biology, being predominantly localised to lysosomes. It is essential for regulating lysosomal positioning, motility, and fusion with other organelles, such as multivesicular endosomes [196,210].

ARL8 is represented by two paralogs, ARL8A and ARL8B, which share 91% sequence identity and are primarily localised within lysosomes [196]. Overexpression of ARL8 proteins has been demonstrated to cause the peripheral accumulation of lysosomes along microtubules [196,210]. ARL8B interacts with various effector proteins such as SifA and SKIP, which regulate the lysosomal transport through kinesin recruitment, and with partners as HOPS and Rab7 to regulate lysosomal fusion with other organelles [211,212]. In prostate cancer, ARL8B depletion alters the lysosomal dynamics, reducing secretion and hydrolysis and subsequently inhibiting proliferation and invasion [213]. Specifically, in the case of ARL8B, the extracellular secretion of lysosomal proteases is crucial for facilitating invasion, lysosomal trafficking across cellular membranes is a critical phenomenon to remodel ECM [214]. In radiation therapy-surviving BC cells, ARL8B has been shown to mediate the peripheral distribution of lysosomes, promoting ECM degradation and thereby enhancing invasiveness, metastasis and overall tumour growth [215].

Even though they shared high sequence similarity, it remains unclear whether ARL8A and ARL8B possess compensatory capabilities. Currently, there is a lack of data regarding the regulation, mechanisms of action and role of ARL8A in cancer [210]. In this context, we plan to investigate the role of ARL8A in BC, aiming to elucidate its phenotypic impact on disease progression, in light of observations presented in this thesis.

4.2.2 Nuanced behaviour: ARNT

The ARNT validation experiments yielded significant findings. In 2D cultures, ARNT KO decreased the proliferation of cancer cells, while unexpectedly enhancing the proliferation in MCF12A and MCF10A cells. Additionally, targeting ARNT led to increased spheroid growth in both cancer cells and normal MCF12A cells. These results showed that while ARNT could act as an OC candidate in 2D cultures, its role in 3D cultures shows an opposite effect. ARNT emerges as a gene with differential phenotypic effect, promoting growth specifically in 3D spheroid models but not in 2D cultures. This duality suggests a potential role as TSG that might be lost or inactivated in the context of Chr1q CNA events.

ARNT, also known as the translocator of ligand bound aryl hydrocarbon receptor (AhR), belongs to the basic helix-loop-helix-Per-ARNT-Sim (bHLH-PAS) family of TFs [216]. It localised to the nucleus with a conserved nuclear localisation signal and has the four isoforms as ARNT (HIF-1β), ARNT2, ARNT3 (BMAL1) and ARNT4 (BMAL2). ARNT shares approximately 60% amino acid sequence similarity with ARNT2, with minor differences primarily found in their transactivation domains [216]. ARNT participates in several intracellular pathways by forming heterodimers with other bHLH-PAS family TFs, such as hypoxia inducible factor-1α (HIF-1α) and the AhR repressor (AHRR) [216]. Next chapters will further summarise this knowledge [217] **(Figure 4.2)**.

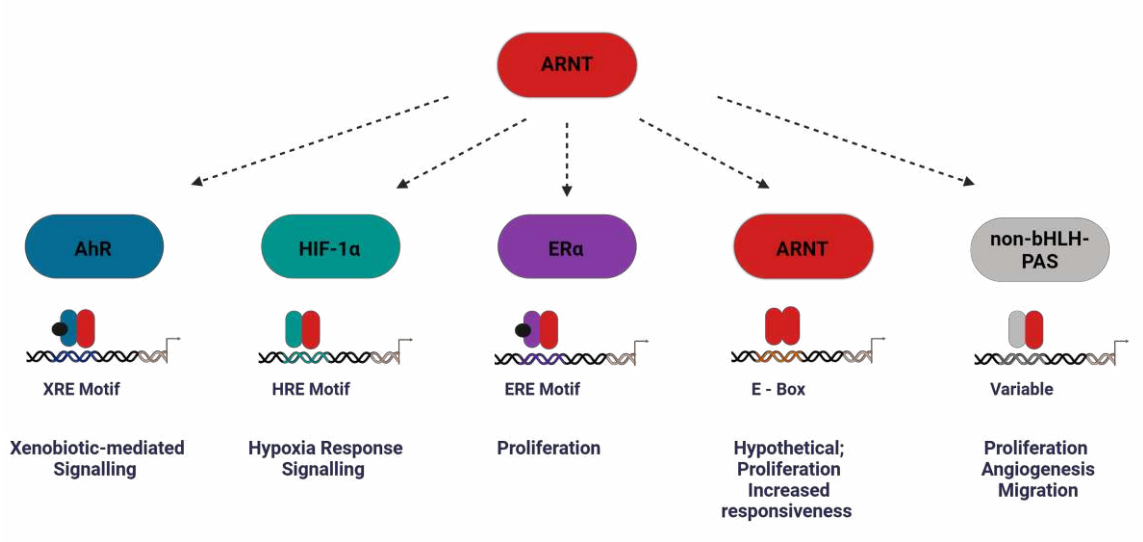

Figure 4. 2. ARNT as a bHLH-PAS TF family member. ARNT, originally identified as AhR's translocator, also participates in transcriptional regulation within the broader bHLH/PAS family of proteins. It forms heterodimers with AhR, HIF-α, or acts as a homodimer complex. These dimers bind to heterodimer specific cis-acting DNA elements to regulate gene expression. (Created by BioRender)

AhR/ARNT Complex

In the xenobiotic response, the heterodimer of AhR/ARNT plays a pivotal role in regulating metabolic enzymes to mediate toxicity in response to environmental pollutants [217]. The transcriptional activity mediated by the ARNT begins when a ligand binds to the cytosolic AhR complex, which composed of AhR, a dimer of heat shock protein 90,

p23, and X-associated protein 2 [218]. Upon ligand binding, AhR undergoes a conformational change that facilitates its translocation from the cytoplasm to the nucleus. Inside the nucleus, AhR dissociates from its associated proteins and forms a complex with ARNT [219]. The resulting AhR-ARNT-ligand complex then binds to specific DNA sequences known as AhR-responsive elements (AHREs) located in the regulatory regions of genes modulated by AhR [220,221].

Upon binding, the AhR-ligand complex recruits additional TFs and co-regulatory proteins, ultimately leading to the modulation of gene expression in the canonical AhR pathway [221,222]. The best-characterised AhR-regulated genes encode xenobiotic metabolising enzymes such as cytochrome P450 members, glutathione transferase, and aldehyde dehydrogenase, which protect cells from toxic chemicals and pollutants like dioxins [223]. It is crucial to emphasise that AhR also functions as a TF influencing various important cellular responses beyond enzyme induction, especially in physiological processes. AhR can interact with other TFs or signalling molecules (transducers) such as retinoblastoma protein (Rb), NF-κB, c-Src or ERα upon nuclear translocation [224–229]. These interactions underscore the multifaceted role of AhR in cellular regulation and response to environmental cues.

AhR could modulate the cell cycle in both ligand-dependent and independent manners, but its effects on proliferation are variable [229]. In MCF7 cells, targeting AhR with siRNAs increases the transition from G1 to S phase, decreases the proportion of cells in the G0/G1 phase, and enhances proliferation, This effect is mediated by modulation of cyclin proteins, as AhR-deficient MCF7 cells show higher proliferation rates [230]. MCF7 AHR100 cells, containing a variant with minimal AhR activity, also exhibit enhanced proliferation and invasion [231]. In contrast, human HepG2 and mouse hepatoma (Hepa 1c1c7) cells exhibit reduced proliferation upon AhR knockdown, which contrasts with the observations in MCF7 cells [230,232]. These findings highlight the cell-type-specific and context-dependent roles of AhR in regulating cell cycle progression and proliferation.

The observations regarding AhR's role in cell proliferation are contentious. AhR has been noted to facilitate the phosphorylation of the Rb by the CDK4 and cyclin D1 complex, prompting the G1 to S phase transition in BC cells and enhancing proliferation [233,234]. Conversely, when AhR is bound to ligands, it reportedly inhibits Rb phosphorylation through protein-protein interactions and may upregulate the expression of CDK4 inhibitor. This leads to reduced Rb phosphorylation, resulting in G1 arrest and inhibition of cell cycle progression [233,235]. These studies summarised here highlight the controversial nature of AhR's effects on cell proliferation, particularly in the context of its interaction with ARNT and its influence on Rb phosphorylation and cyclin interactions [229,236]. The dual roles of AhR in promoting or inhibiting proliferation depending on its binding status and cellular context underscore its complex regulatory functions in cancer biology.

Ligand-bound AhR exhibits a versatile interaction pattern, sometimes binding directly with ERα instead of ARNT upon translocation to the nucleus. This AhR/ERα complex can induce pro-estrogenic effects by inducing ERα target genes [237]. Also, AhR/ARNT complex is known to induce target genes that possess both pro- and anti-estrogenic activities [238]. The presence of estrogen and AhR-bound ligands further complicates this interaction map [219,238]. Importantly, studies have demonstrated that the relationship between AhR and ERα can occur independently of ARNT [239,240].

In cancer, the activation of AhR/ARNT complex has been found to play a dual role, capable of both promoting tumour progression and enhancing cancer cell malignancy, while also exerting tumour suppressive effects [241,242]. The functions of AhR/ARNT are highly complex, regulating distinct pathways that compete depending on the presence of specific ligands and the interaction with AhR and ARNT [243]. Elevated levels of AhR have been associated with increased malignancy, enhanced proliferation, and suppression of anti-tumour immune responses in various cancers [244–246]. Depending on the presence of ARNT, AhR can facilitate cancer cell migration, invasion, and promote cancer stemness [241,247–249]. But, there are also reports indicating that the activated form of AhR could decrease cell growth, colony-forming abilities and invasion capacity [250–252]. Here, it is important to note that the exact role of ARNT in the AhR/ARNT

complex varies significantly. Often, AhR acts through a non-genomic pathway independent of ARNT, or if bound, the specific role and contribution of ARNT are not always fully elucidated or assessed in detail.

HIF1 Family

ARNT, traditionally recognized as a translocator, plays a pivotal role in coordinating various intrinsic pathways. Recent studies have revealed that ARNT functions not only as a dimerization partner for AhR but also for other bHLH/PAS proteins [217]. ARNT is integral to multiple signalling pathways, including hypoxic response [253,254]. These pathways involve interactions with diverse bHLH/PAS partners such as hypoxia-inducible factors (HIF-1α, HIF-2α, HIF-3α) and hypoxia-like factor (HLF) [216].

In hypoxia-mediated signalling, ARNT associates with HIF proteins to form complexes that bind to hypoxia responsive elements to regulate various target genes such as erythropoietin, vascular endothelial growth factor, and glucose-transporter-1. These genes play crucial roles in adapting to hypoxic conditions and modulating normal physiological functions in response to environmental changes [255,256]. HIF proteins, including HIF-1α, are expressed specifically under hypoxic conditions, while ARNT is constitutively expressed and localised in the nucleus. ARNT serves as an O2-insensitive subunit of the HIF-1/ARNT complex, which participates in each pathway of HIF-1 as its heterodimer partner [257–260]. Notably, HIF-1α demonstrates a higher affinity for ARNT compared to AhR, which showed a preferential interaction to control tumorigenesis [261].

Cancer cells favour the hypoxia which promote uncontrolled proliferation, invasion, and metastasis by adapting and reprogramming of gene expressions through the HIF TF family [262–264]. Studies have been reported that ARNT is overexpressed in cancer cells under hypoxic conditions [260,265]. The regulator activity of HIF-1α dependents on its association with ARNT, and this overexpression provides survival advantages to cancer cells [266].

In HCC Hep3B cells, human melanoma cells, and prostate cancer cells, HIF-1α increases ARNT expression by binding to the ARNT promoter to regulate several proliferation-

promoting pathways and metastasis [267–270]. In addition, overexpressed ARNT has been linked to radiotherapy resistance when overexpressed, while its knockdown prompts the cancer cells more susceptible to radiotherapy [271]. There is one study that depicted ARNT can stabilise HIF-1α by forming the HIF-1 complex [272]. The interaction between HIF-1α and ARNT is further complicated by findings that ERβ inhibits HIF-1 activity by promoting ARNT degradation through ubiquitination, thereby reducing the formation of active HIF-1α/ARNT complexes [273].

All the reports summarised until now present conflicting points with our observations. We observed a clear increase in spheroid sizes upon ARNT KO in BC cell lines and also MCF12A cells in 3D cultures. Given that 3D spheroids closely mimic solid tumours, especially in terms of hypoxic microenvironment, spheroid size should theoretically decrease upon ARNT KO. This is because the disruption of the HIF-1/ARNT complex would impair the ability to regulate proliferation. **However, our observations suggest otherwise, indicating that ARNT may have a different role in 3D tumour models than previously understood.**

ARNT/ARNT Homodimer Complex and ARNT/non-bHLH-PAS Heterodimers

In addition to its association with AhR and HIF-1α TFs, ARNT can form a homodimer and regulate intracellular pathways by acting as a TF itself. The ARNT homodimer complex has an affinity to the canonical E-box (5'-CACGTG-3') sequence and can even compete with c-MYC/Max for binding regions [274,275]. To identify the target genes regulated by ARNT, a microarray-based analysis was performed in Hepa-1 cells. Across the 27 upregulated genes, 15 genes had an E-Box in their promoter, as NIP3, PAI1, and NDR1 [276]. Moreover, the ARNT homodimer is involved in the partial regulation of the *Cyp2a5* gene, with ARNT KO mice showing decreased expression of *Cyp2a5 [277].* However, there is limited data on the role of the ARNT homodimer complex as a TF in gene regulation, particularly in cancer cells. This remains a controversial area, and further investigation is necessary to explore the potential functions of this complex in the regulation of cancer cells [217].

There are also controversial reports underlining the growth and metastasis-promoting effects of ARNT, which depends on non-bHLH-PAS TFs such as c-Jun/Sp1 and NF-κB. ARNT can associate with c-Jun/Sp1, facilitating the binding of ARNT/c-Jun/Sp1 complex to the target gene promoters that contain SP1 binding sites. ARNT acts as a bridge between c-Jun and Sp1 to regulate EGF related pathways, enhancing angiogenesis, migration, and proliferation [278,279]. Moreover, ARNT expression has been linked to cisplatin resistance by increasing MDR1 expression by Sp1 in a complex with ARNT [280]. The anticancer activity of cisplatin is partly linked to ROS production upon ARNT deficiency [281]. In addition, ARNT, identified as a CD30 interacting protein, modulates the activity of NF-κB. In lymphoid cells lacking ARNT, there are defects in RelB recruitment to NF-κB-responsive promoters, while RelA recruitment to the same sites is enhanced, leading to deregulated expression of target genes with altered NF-κB activity [282].

These findings underscore the complex and multifaceted role of ARNT in cancer, highlighting its involvement in various pathways and interactions that can both promote and suppress tumour growth and metastasis. Further research is needed to fully elucidate the diverse mechanisms by which ARNT influences cancer progression and treatment responses.

Literature Supporting ARNT as a Tumour Suppressor Gene: Insights and Experimental Correlations

Our findings are corroborated by a study published in 2012 that performed in HCC [283]. Authors demonstrated that ARNT knockdown in three different cell lines significantly increased proliferation, reduced cell doubling time, and increased the fraction of S-phase population *in vitro*. *In vivo* experiments further validated these observations, showing that targeting ARNT led to increase the tumour size and lung metastasis with enhanced growth capacity. Conversely, ARNT overexpression resulted in attenuated proliferation *in vitro* and *in vivo*, with reduced tumour size and metastatic potential [283]. Importantly, overall survival (OS) and tumour to recurrence (TTR) of the HCC patients showed a strong dependency on the existence of ARNT. High intra-tumour ARNT levels were associated with shortened OS and TTR in HCC patients [283].

ARNT2, a homolog of ARNT, exhibits an inhibitory effect on the progression of HCC. High levels of ARNT2 are significantly correlated with longer OS and lower TTR rates. ARNT2 KO enhances cell proliferation, invasion, and migration, whereas inhibition is observed upon overexpression of ARNT2 both *in vivo* and *in vitro* [284].

In colorectal cancer, ARNT expression is attenuated in the late-stage patients, and its knock down increases the invasion by fibronectin/integrin β1/FAK signalling. Restoration of ARNT expression reverses this enhanced invasion phenotype, indicating that ARNT loss contributes to a pro-metastatic phenotype. Treatment with cisplatin, doxorubicin, and paclitaxel reduces ARNT expression in cells surviving chemotherapy, which correlates with increased migratory capacity. *In vivo* studies have shown that ARNT loss decreases tumour growth but still influences lung metastatic potential, as demonstrated by experiments involving ARNT down-regulation and subsequent rescue. Targeting ARNT promotes tumour metastasis, yet metastatic lung tumour growth is dependent on the ARNT rescue [197].

The same group extended their studies to melanoma, where ARNT deficiency was linked to PDK1 repression and excessive mitochondrial ROS production to induce metastasis. Elevated levels of ARNT and PDK1 were detected in benign stage melanoma tissues, but ARNT expression was significantly reduced in the late-stage melanoma, correlating with increased glucose uptake and decreased dependency on glucose by cancer cells [285].

In the case of ARNT, it has been demonstrated to act as a coactivator of ERs, independent of its roles as a heterodimer partner of AhR and HIF-1α. ARNT enhances ERα recruitment to the target binding sites, as evidenced in studies [239,286]. While data associating ARNT with ER remains limited, there is a hypothesis that this interaction could modulate ERα target genes, especially in NHR positive cancers [250,287].

One comprehensive study showed the differential binding patterns of AhR, ARNT, and Ahr/ARNT complex upon TCDD treatment. The study identified 2594 binding sites for AhR alone and 1352 specific binding sites for ARNT, with 882 sites showing cobound regions in MCF7 cells [288]. This study demonstrates that ARNT can bind independently

of AhR and AhR-responsive elements, although the study did not investigate binding involving HIF-1/ARNT complex [288].

ARNT expression was interrogated in patient samples across different cancer types. **Figure 4.3**. highlighted a pronounced downregulation of expression, notably in BC, ovarian cancer, and uterus cancers, **underscoring the pivotal role of hormonal regulation in cancer progression.**

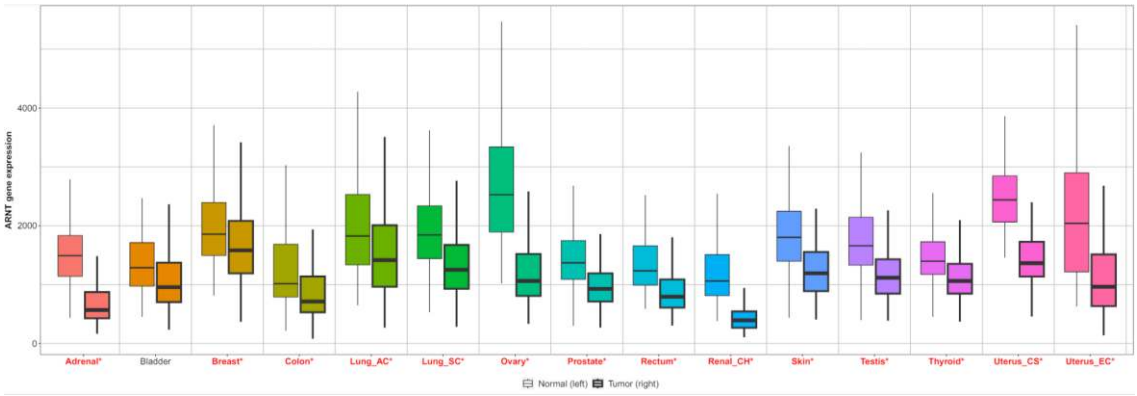

Figure 4. 3. The downregulation of ARNT gene expression in pan-cancer analysis. ARNT showed a pronounced down-regulation in different types of cancer patient samples. Data obtained from TNM plot (https://tnmplot.com/analysis/).

Due to conflicting results in the literature, we check the expression of ARNT, and two crosstalk partners AhR and HIF-1α in BC patients **(Figure 4.4A)**. HIF-1α, as expected, showed a significant upregulation in both tumour and metastatic sample. AhR expression, hypothesised to be upregulated in cancer cells, aligned with previous reports. However, ARNT showed attenuated expression in adjacent tumour samples, while its expression in metastasis did not significantly differ from normal controls. A similar pattern of expression dysregulation was observed in ovarian cancer, another malignancy dependent on NHRs **(Figure 4.4B)**.

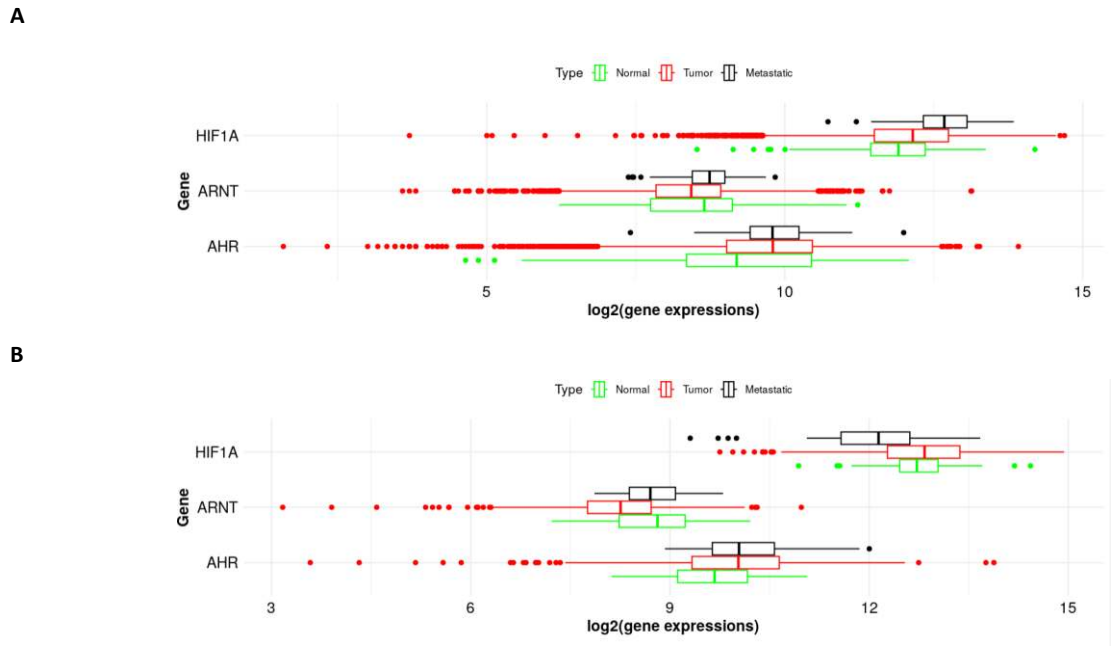

Figure 4. 4. Expression profiles of bHLH-PAS domain proteins ARNT, HIF-1α, and AhR in NHR positive patients. (A) ARNT showed a decrease, while HIF-1α and AhR were upregulated in tumorigenic samples compared with normal adjacent tissues in BC. (B) Similar expression patterns were observed in OC. Data obtained from TNMplot (https://tnmplot.com/analysis/).

Overall, all the mentioned reports reveal the controversial effects of ARNT in malignancy. This situation might have originated from the high complexity in intracellular pathways that ARNT participates in, or *in vitro* models improperly evaluate the phenotypic impact. In addition, studies mostly focused on heterodimeric partners of ARNT, but the impact still not clarified for ARNT itself and ARNT homodimer complex acting as TF. Therefore, in this thesis, ARNT is evaluated as TSG candidate in BC especially improving 3D spheroid growth in which might be related with its differential regulation pattern, relation with ERα, or modulation of unknown partners as summarised in **Figure 4.5.**

The complex and sometimes contradictory findings concerning ARNT's role in malignancy highlight its nuanced participation in intracellular pathways. This complexity likely contributes to the discrepancies observed in various studies, further compounded

by limitations in accurately assessing phenotypic impacts using *in vitro* models. Additionally, existing research has predominantly focused on ARNT's interactions as a heterodimeric partner, thereby neglecting the exploration of ARNT itself and its potential role as a transcription factor in homodimeric complexes. **In this thesis, ARNT is scrutinised as a candidate tumour suppressor gene (TSG),** with particular emphasis on its role in enhancing 3D spheroid growth. This phenomenon could be attributed to ARNT's unique regulatory mechanisms, its interactions with ERα, or its modulation by unidentified partners, as illustrated in **Figure 4.5**.

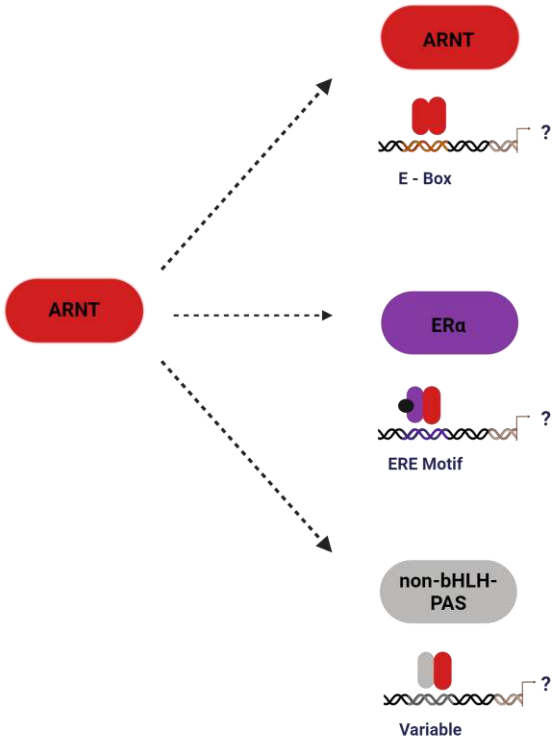

Figure 4. 5. ARNT has the potential to regulate pathways beyond those that have been previously characterised. This figure illustrates the diverse regulatory mechanisms proposed for ARNT in BC within this thesis. ARNT is shown to form a homodimeric complex that retains its DNA binding capability and functions as a transactivator. This suggests a differentiated regulatory role in BC malignancy. In addition, although data is limited, ARNT could recruit ERα on ERE binding sites or other potential activators/repressors to modulate ERα target genes. Finally, ARNT's PACA

and PACB domains (the special binding domains recognised by several factors), imply involvement of unidentified partners in regulating tumour mass proliferation. (Created by BioRender)

Our future direction aims to explore the roles of RPRD2 and ARNT, the former identified as an oncogene (OC) and the latter as a candidate tumour suppressor gene (TSG). Given their roles as transcription factors (TFs), these genes hold significant promise in regulating target genes implicated in breast cancer (BC) malignancy. Transcriptome analysis will enhance our understanding of the intracellular pathways affected by these TFs.

Additionally, we plan to validate the phenotypic impact of ARNT through *in vivo* studies, complemented by overexpression and rescue experiments in both 2D and 3D *in vitro* models. Our scope will also expand to include ovarian cancer, where ARNT expression undergoes substantial attenuation during pathogenesis.

In summary, our future investigations aim to address gaps in understanding Chr1q copy number alterations (CNA) and their role in the genomic disorder/catastrophe underlying BC progression.

5 BIBLIOGRAPHY

1. Lei S, Zheng R, Zhang S, Wang S, Chen R, Sun K, et al. Global patterns of breast cancer incidence and mortality: A population-based cancer registry data analysis from 2000 to 2020. Cancer Commun. 2021;41: 1183–1194.
2. Sung H, Ferlay J, Siegel RL, Laversanne M, Soerjomataram I, Jemal A, et al. Global Cancer Statistics 2020: GLOBOCAN Estimates of Incidence and Mortality Worldwide for 36 Cancers in 185 Countries. CA Cancer J Clin. 2021;71: 209–249.
3. Torre LA, Bray F, Siegel RL, Ferlay J, Lortet-Tieulent J, Jemal A. Global cancer statistics, 2012. CA Cancer J Clin. 2015;65: 87–108.
4. Bray F, Ferlay J, Soerjomataram I, Siegel RL, Torre LA, Jemal A. Global cancer statistics 2018: GLOBOCAN estimates of incidence and mortality worldwide for 36 cancers in 185 countries. CA Cancer J Clin. 2018;68: 394–424.
5. Pedersen RN, Esen BÖ, Mellemkjær L, Christiansen P, Ejlertsen B, Lash TL, et al. The Incidence of Breast Cancer Recurrence 10-32 Years After Primary Diagnosis. J Natl Cancer Inst. 2022;114: 391–399.
6. Harbeck N, Penault-Llorca F, Cortes J, Gnant M, Houssami N, Poortmans P, et al. Breast cancer. Nat Rev Dis Primers. 2019;5: 66.
7. Harbeck N, Gnant M. Breast cancer. Lancet. 2017;389: 1134–1150.
8. Perou CM, Sørlie T, Eisen MB, van de Rijn M, Jeffrey SS, Rees CA, et al. Molecular portraits of human breast tumours. Nature. 2000;406: 747–752.
9. Cancer Genome Atlas Research Network, Weinstein JN, Collisson EA, Mills GB, Shaw KRM, Ozenberger BA, et al. The Cancer Genome Atlas Pan-Cancer analysis project. Nat Genet. 2013;45: 1113–1120.

10. Prat A, Pineda E, Adamo B, Galván P, Fernández A, Gaba L, et al. Clinical implications of the intrinsic molecular subtypes of breast cancer. Breast. 2015;24 Suppl 2: S26–35.
11. Tan M, Yao J, Yu D. Overexpression of the c-erbB-2 gene enhanced intrinsic metastasis potential in human breast cancer cells without increasing their transformation abilities. Cancer Res. 1997;57: 1199–1205.
12. Nagini S. Breast Cancer: Current Molecular Therapeutic Targets and New Players. Anticancer Agents Med Chem. 2017;17: 152–163.
13. Yip C-H, Rhodes A. Estrogen and progesterone receptors in breast cancer. Future Oncol. 2014;10: 2293–2301.
14. Korkmaz G, Lopes R, Ugalde AP, Nevedomskaya E, Han R, Myacheva K, et al. Functional genetic screens for enhancer elements in the human genome using CRISPR-Cas9. Nat Biotechnol. 2016;34: 192–198.
15. Lopes R, Korkmaz G, Revilla SA, van Vliet R, Nagel R, Custers L, et al. CUEDC1 is a primary target of ERα essential for the growth of breast cancer cells. Cancer Lett. 2018;436: 87–95.
16. Jia S, Miedel MT, Ngo M, Hessenius R, Chen N, Wang P, et al. Clinically Observed Estrogen Receptor Alpha Mutations within the Ligand-Binding Domain Confer Distinguishable Phenotypes. Oncology. 2018;94: 176–189.
17. Burstein HJ. Systemic Therapy for Estrogen Receptor-Positive, HER2-Negative Breast Cancer. N Engl J Med. 2020;383: 2557–2570.
18. Manohar PM, Davidson NE. Updates in endocrine therapy for metastatic breast cancer. Cancer Biol Med. 2021;19: 202–212.
19. Nathan MR, Schmid P. A Review of Fulvestrant in Breast Cancer. Oncol Ther. 2017;5: 17–29.
20. Loeb KR, Loeb LA. Significance of multiple mutations in cancer. Carcinogenesis. 2000;21: 379–385.

21. Wang L-H, Wu C-F, Rajasekaran N, Shin YK. Loss of Tumor Suppressor Gene Function in Human Cancer: An Overview. Cell Physiol Biochem. 2018;51: 2647–2693.

22. Stratton MR, Campbell PJ, Futreal PA. The cancer genome. Nature. 2009;458: 719–724.

23. Thompson SL, Compton DA. Chromosomes and cancer cells. Chromosome Res. 2011;19: 433–444.

24. Weischenfeldt J, Symmons O, Spitz F, Korbel JO. Phenotypic impact of genomic structural variation: insights from and for human disease. Nat Rev Genet. 2013;14: 125–138.

25. Rieger PT. The biology of cancer genetics. Semin Oncol Nurs. 2004;20: 145–154.

26. Kontomanolis EN, Koutras A, Syllaios A, Schizas D, Mastoraki A, Garmpis N, et al. Role of Oncogenes and Tumor-suppressor Genes in Carcinogenesis: A Review. Anticancer Res. 2020;40: 6009–6015.

27. Cline MJ. The role of proto-oncogenes in human cancer: implications for diagnosis and treatment. Int J Radiat Oncol Biol Phys. 1987;13: 1297–1301.

28. Brown G. Oncogenes, Proto-Oncogenes, and Lineage Restriction of Cancer Stem Cells. Int J Mol Sci. 2021;22. doi:10.3390/ijms22189667

29. Torry DS, Cooper GM. Proto-oncogenes in development and cancer. Am J Reprod Immunol. 1991;25: 129–132.

30. Lee EYHP, Muller WJ. Oncogenes and tumor suppressor genes. Cold Spring Harb Perspect Biol. 2010;2: a003236.

31. Hemmings BA, Restuccia DF. PI3K-PKB/Akt pathway. Cold Spring Harb Perspect Biol. 2012;4: a011189.

32. Hennessy BT, Smith DL, Ram PT, Lu Y, Mills GB. Exploiting the PI3K/AKT pathway for cancer drug discovery. Nat Rev Drug Discov. 2005;4: 988–1004.

33. Samuels Y, Wang Z, Bardelli A, Silliman N, Ptak J, Szabo S, et al. High frequency of mutations of the PIK3CA gene in human cancers. Science. 2004;304: 554.

34. Jeffreys SA, Becker TM, Khan S, Soon P, Neubauer H, de Souza P, et al. Prognostic and Predictive Value of /Cyclin D1 Amplification in Breast Cancer With a Focus on Postmenopausal Patients: A Systematic Review and Meta-Analysis. Front Endocrinol . 2022;13: 895729.

35. Alao JP. The regulation of cyclin D1 degradation: roles in cancer development and the potential for therapeutic invention. Mol Cancer. 2007;6: 24.

36. Elsheikh S, Green AR, Aleskandarany MA, Grainge M, Paish CE, Lambros MBK, et al. CCND1 amplification and cyclin D1 expression in breast cancer and their relation with proteomic subgroups and patient outcome. Breast Cancer Res Treat. 2008;109: 325–335.

37. He Q, Wu J, Liu X-L, Ma Y-H, Wu X-T, Wang W-Y, et al. Clinicopathological and prognostic significance of cyclin D1 amplification in patients with breast cancer: a meta-analysis. J BUON. 2017;22: 1209–1216.

38. Gabay M, Li Y, Felsher DW. MYC activation is a hallmark of cancer initiation and maintenance. Cold Spring Harb Perspect Med. 2014;4. doi:10.1101/cshperspect.a014241

39. Boxer LM, Dang CV. Translocations involving c-myc and c-myc function. Oncogene. 2001;20: 5595–5610.

40. Dang CV. MYC on the path to cancer. Cell. 2012;149: 22–35.

41. Dang CV. MYC, metabolism, cell growth, and tumorigenesis. Cold Spring Harb Perspect Med. 2013;3. doi:10.1101/cshperspect.a014217

42. Plum PS, Gebauer F, Krämer M, Alakus H, Berlth F, Chon S-H, et al. HER2/neu (ERBB2) expression and gene amplification correlates with better survival in esophageal adenocarcinoma. BMC Cancer. 2019;19: 38.

43. Kufe DW. MUC1-C oncoprotein as a target in breast cancer: activation of signaling pathways and therapeutic approaches. Oncogene. 2013;32: 1073–1081.

44. Appert-Collin A, Hubert P, Crémel G, Bennasroune A. Role of ErbB Receptors in Cancer Cell Migration and Invasion. Front Pharmacol. 2015;6: 283.

45. Stambolic V, Suzuki A, de la Pompa JL, Brothers GM, Mirtsos C, Sasaki T, et al. Negative regulation of PKB/Akt-dependent cell survival by the tumor suppressor PTEN. Cell. 1998;95: 29–39.

46. Papa A, Wan L, Bonora M, Salmena L, Song MS, Hobbs RM, et al. Cancer-associated PTEN mutants act in a dominant-negative manner to suppress PTEN protein function. Cell. 2014;157: 595–610.

47. Lynch HT, Marcus JN, Rubinstein WS. Stemming the tide of cancer for BRCA1/2 mutation carriers. Journal of clinical oncology: official journal of the American Society of Clinical Oncology. 2008. pp. 4239–4243.

48. Atchley DP, Albarracin CT, Lopez A, Valero V, Amos CI, Gonzalez-Angulo AM, et al. Clinical and pathologic characteristics of patients with BRCA-positive and BRCA-negative breast cancer. J Clin Oncol. 2008;26: 4282–4288.

49. Tung N, Wang Y, Collins LC, Kaplan J, Li H, Gelman R, et al. Estrogen receptor positive breast cancers in BRCA1 mutation carriers: clinical risk factors and pathologic features. Breast Cancer Res. 2010;12: R12.

50. Mehrgou A, Akouchekian M. The importance of BRCA1 and BRCA2 genes mutations in breast cancer development. Med J Islam Repub Iran. 2016;30: 369.

51. Yang H, Jeffrey PD, Miller J, Kinnucan E, Sun Y, Thoma NH, et al. BRCA2 function in DNA binding and recombination from a BRCA2-DSS1-ssDNA structure. Science. 2002;297: 1837–1848.

52. Menendez D, Inga A, Resnick MA. The expanding universe of p53 targets. Nat Rev Cancer. 2009;9: 724–737.

53. Zilfou JT, Lowe SW. Tumor suppressive functions of p53. Cold Spring Harb Perspect Biol. 2009;1: a001883.

54. Reisman D, Takahashi P, Polson A, Boggs K. Transcriptional Regulation of the p53 Tumor Suppressor Gene in S-Phase of the Cell-Cycle and the Cellular Response to DNA Damage. Biochem Res Int. 2012;2012: 808934.

55. Sullivan KD, Galbraith MD, Andrysik Z, Espinosa JM. Mechanisms of transcriptional regulation by p53. Cell Death Differ. 2018;25: 133–143.

56. Xu Y. Induction of genetic instability by gain-of-function p53 cancer mutants. Oncogene. 2008;27: 3501–3507.

57. Hanahan D, Weinberg RA. Hallmarks of cancer: the next generation. Cell. 2011;144: 646–674.

58. Hanahan D, Weinberg RA. The hallmarks of cancer. Cell. 2000;100: 57–70.

59. Yao Y, Dai W. Genomic Instability and Cancer. J Carcinog Mutagen. 2014;5. doi:10.4172/2157-2518.1000165

60. Shen Z. Genomic instability and cancer: an introduction. J Mol Cell Biol. 2011;3: 1–3.

61. Kou F, Wu L, Ren X, Yang L. Chromosome Abnormalities: New Insights into Their Clinical Significance in Cancer. Mol Ther Oncolytics. 2020;17: 562–570.

62. Zhang L, Yuan Y, Lu KH, Zhang L. Identification of recurrent focal copy number variations and their putative targeted driver genes in ovarian cancer. BMC Bioinformatics. 2016;17: 222.

63. Hata T, Suenaga M, Marchionni L, Macgregor-Das A, Yu J, Shindo K, et al. Genome-Wide Somatic Copy Number Alterations and Mutations in High-Grade Pancreatic Intraepithelial Neoplasia. Am J Pathol. 2018;188: 1723–1733.

64. Li Y, Roberts ND, Wala JA, Shapira O, Schumacher SE, Kumar K, et al. Patterns of somatic structural variation in human cancer genomes. Nature. 2020;578: 112–121.

65. ICGC/TCGA Pan-Cancer Analysis of Whole Genomes Consortium. Pan-cancer analysis of whole genomes. Nature. 2020;578: 82–93.

66. Wang W-J, Li L-Y, Cui J-W. Chromosome structural variation in tumorigenesis: mechanisms of formation and carcinogenesis. Epigenetics Chromatin. 2020;13: 49.

67. Taylor AM, Shih J, Ha G, Gao GF, Zhang X, Berger AC, et al. Genomic and Functional Approaches to Understanding Cancer Aneuploidy. Cancer Cell. 2018;33: 676–689.e3.

68. Korkola J, Gray JW. Breast cancer genomes--form and function. Curr Opin Genet Dev. 2010;20: 4–14.

69. Głodzik D, Purdie C, Rye IH, Simpson PT, Staaf J, Span PN, et al. Mutational mechanisms of amplifications revealed by analysis of clustered rearrangements in breast cancers. Ann Oncol. 2018;29: 2223–2231.

70. Matsui A, Ihara T, Suda H, Mikami H, Semba K. Gene amplification: mechanisms and involvement in cancer. Biomol Concepts. 2013;4: 567–582.

71. Grade M, Difilippantonio MJ, Camps J. Patterns of Chromosomal Aberrations in Solid Tumors. Recent Results Cancer Res. 2015;200: 115–142.

72. Albertson DG. Gene amplification in cancer. Trends Genet. 2006;22: 447–455.

73. Albertson DG, Collins C, McCormick F, Gray JW. Chromosome aberrations in solid tumors. Nat Genet. 2003;34: 369–376.

74. Lockwood WW, Chari R, Coe BP, Girard L, Macaulay C, Lam S, et al. DNA amplification is a ubiquitous mechanism of oncogene activation in lung and other cancers. Oncogene. 2008;27: 4615–4624.

75. Albertson DG, Ylstra B, Segraves R, Collins C, Dairkee SH, Kowbel D, et al. Quantitative mapping of amplicon structure by array CGH identifies CYP24 as a candidate oncogene. Nat Genet. 2000;25: 144–146.

76. Collier KA, Asad S, Tallman D, Jenison J, Rajkovic A, Mardis ER, et al. Association of 17q22 Amplicon Via Cell-Free DNA With Platinum Chemotherapy Response in Metastatic Triple-Negative Breast Cancer. JCO Precis Oncol. 2021;5. doi:10.1200/PO.21.00104

77. Calcagno AM, Ambudkar SV. Molecular mechanisms of drug resistance in single-step and multi-step drug-selected cancer cells. Methods Mol Biol. 2010;596: 77–93.

78. Jiang J, Yuan J, Hu Z, Zhang Y, Zhang T, Xu M, et al. Systematic illumination of druggable genes in cancer genomes. Cell Rep. 2022;38: 110400.

79. Schieppati F, Balzarini P, Fisogni S, Re A, Pagani C, Bianchetti N, et al. An increase in copy number has a progressive negative prognostic impact in patients with diffuse large B-cell and high-grade lymphoma, who may benefit from intensified treatment regimens. Haematologica. 2020;105: 1369–1378.

80. Kauraniemi P, Kallioniemi A. Activation of multiple cancer-associated genes at the ERBB2 amplicon in breast cancer. Endocr Relat Cancer. 2006;13: 39–49.

81. Slamon DJ, Clark GM, Wong SG, Levin WJ, Ullrich A, McGuire WL. Human breast cancer: correlation of relapse and survival with amplification of the HER-2/neu oncogene. Science. 1987;235: 177–182.

82. Shinojima N, Tada K, Shiraishi S, Kamiryo T, Kochi M, Nakamura H, et al. Prognostic value of epidermal growth factor receptor in patients with glioblastoma multiforme. Cancer Res. 2003;63: 6962–6970.

83. Futreal PA, Coin L, Marshall M, Down T, Hubbard T, Wooster R, et al. A census of human cancer genes. Nat Rev Cancer. 2004;4: 177–183.

84. Schwab M. Amplification of oncogenes in human cancer cells. Bioessays. 1998;20: 473–479.

85. Brown LA, Johnson K, Leung S, Bismar TA, Benítez J, Foulkes WD, et al. Co-amplification of CCND1 and EMSY is associated with an adverse outcome in ER-positive tamoxifen-treated breast cancers. Breast Cancer Res Treat. 2010;121: 347–354.

86. Ried T, Meijer GA, Harrison DJ, Grech G, Franch-Expósito S, Briffa R, et al. The landscape of genomic copy number alterations in colorectal cancer and their consequences on gene expression levels and disease outcome. Mol Aspects Med. 2019;69: 48–61.

87. Hanamura I. Gain/Amplification of Chromosome Arm 1q21 in Multiple Myeloma. Cancers . 2021;13. doi:10.3390/cancers13020256

88. Jain AN, Chin K, Børresen-Dale AL, Erikstein BK, Eynstein Lonning P, Kaaresen R, et al. Quantitative analysis of chromosomal CGH in human breast tumors associates copy number abnormalities with p53 status and patient survival. Proc Natl Acad Sci U S A. 2001;98: 7952–7957.

89. Chen L, Chan THM, Guan X-Y. Chromosome 1q21 amplification and oncogenes in hepatocellular carcinoma. Acta Pharmacol Sin. 2010;31: 1165–1171.

90. Lamont EB, Yee AJ, Goldberg SL, Siegel DS, Norden AD. Associations Between Amplification (1q) and Prior Cancer in a Real-World De Novo Myeloma Cohort. JNCI Cancer Spectr. 2021;5. doi:10.1093/jncics/pkaa111

91. Paugh BS, Qu C, Jones C, Liu Z, Adamowicz-Brice M, Zhang J, et al. Integrated molecular genetic profiling of pediatric high-grade gliomas reveals key differences with the adult disease. J Clin Oncol. 2010;28: 3061–3068.

92. Orsetti B, Nugoli M, Cervera N, Lasorsa L, Chuchana P, Rougé C, et al. Genetic profiling of chromosome 1 in breast cancer: mapping of regions of gains and losses and identification of candidate genes on 1q. Br J Cancer. 2006;95: 1439–1447.

93. Schmidt TM, Barwick BG, Joseph N, Heffner LT, Hofmeister CC, Bernal L, et al. Gain of Chromosome 1q is associated with early progression in multiple myeloma patients treated with lenalidomide, bortezomib, and dexamethasone. Blood Cancer J. 2019;9: 94.

94. Weinhold N, Salwender HJ, Cairns DA, Raab MS, Waldron G, Blau IW, et al. Chromosome 1q21 abnormalities refine outcome prediction in patients with multiple myeloma - a meta-analysis of 2,596 trial patients. Haematologica. 2021;106: 2754–2758.

95. Schmidt TM, Fonseca R, Usmani SZ. Chromosome 1q21 abnormalities in multiple myeloma. Blood Cancer J. 2021;11: 83.

96. Fabris S, Ronchetti D, Agnelli L, Baldini L, Morabito F, Bicciato S, et al. Transcriptional features of multiple myeloma patients with chromosome 1q gain. Leukemia. 2007;21: 1113–1116.

97. Zhan F, Colla S, Wu X, Chen B, Stewart JP, Kuehl WM, et al. CKS1B, overexpressed in aggressive disease, regulates multiple myeloma growth and survival through SKP2- and p27Kip1-dependent and -independent mechanisms. Blood. 2007;109: 4995–5001.

98. Stephens OW, Zhang Q, Qu P, Zhou Y, Chavan S, Tian E, et al. An intermediate-risk multiple myeloma subgroup is defined by sIL-6r: levels synergistically increase with incidence of SNP rs2228145 and 1q21 amplification. Blood. 2012;119: 503–512.

99. Walker BA, Leone PE, Chiecchio L, Dickens NJ, Jenner MW, Boyd KD, et al. A compendium of myeloma-associated chromosomal copy number abnormalities and their prognostic value. Blood. 2010;116: e56–65.

100. Slomp A, Moesbergen LM, Gong J-N, Cuenca M, von dem Borne PA, Sonneveld P, et al. Multiple myeloma with 1q21 amplification is highly sensitive to MCL-1 targeting. Blood Adv. 2019;3: 4202–4214.

101. Trasanidis N, Katsarou A, Ponnusamy K, Shen Y-A, Kostopoulos IV, Bergonia B, et al. Systems medicine dissection of chr1q-amp reveals a novel PBX1-FOXM1 axis for targeted therapy in multiple myeloma. Blood. 2022;139: 1939–1953.

102. Bisht K, Walker B, Kumar SK, Spicka I, Moreau P, Martin T, et al. Chromosomal 1q21 abnormalities in multiple myeloma: a review of translational, clinical research, and therapeutic strategies. Expert Rev Hematol. 2021;14: 1099–1114.

103. Jacobs NR, Norton PA. Role of chromosome 1q copy number variation in hepatocellular carcinoma. World J Hepatol. 2021;13: 662–672.

104. Ellis MJ, Perou CM. The genomic landscape of breast cancer as a therapeutic roadmap. Cancer Discov. 2013;3: 27–34.

105. Ghosh M, Naik R, Lingaraju SM, Susheela SP, Patil S, Srinivasachar GK, et al. Landscape of clinically actionable mutations in breast cancer "A cohort study." Transl Oncol. 2021;14: 100877.

106. McGranahan N, Burrell RA, Endesfelder D, Novelli MR, Swanton C. Cancer chromosomal instability: therapeutic and diagnostic challenges. EMBO Rep. 2012;13: 528–538.

107. Kallioniemi A, Kallioniemi OP, Piper J, Tanner M, Stokke T, Chen L, et al. Detection and mapping of amplified DNA sequences in breast cancer by comparative genomic hybridization. Proc Natl Acad Sci U S A. 1994;91: 2156–2160.

108. Li Z, Zhang X, Hou C, Zhou Y, Chen J, Cai H, et al. Comprehensive identification and characterization of somatic copy number alterations in triple-negative breast cancer. Int J Oncol. 2020;56: 522–530.

109. Voutsadakis IA. The Landscape of Chromosome Instability in Breast Cancers and Associations with the Tumor Mutation Burden: An Analysis of Data from TCGA. Cancer Invest. 2021;39: 25–38.

110. Johansson HJ, Socciarelli F, Vacanti NM, Haugen MH, Zhu Y, Siavelis I, et al. Breast cancer quantitative proteome and proteogenomic landscape. Nat Commun. 2019;10: 1600.

111. Baslan T, Kendall J, Volyanskyy K, McNamara K, Cox H, D'Italia S, et al. Novel insights into breast cancer copy number genetic heterogeneity revealed by single-cell genome sequencing. Elife. 2020;9. doi:10.7554/eLife.51480

112. Staaf J, Jönsson G, Ringnér M, Vallon-Christersson J, Grabau D, Arason A, et al. High-resolution genomic and expression analyses of copy number alterations in HER2-amplified breast cancer. Breast Cancer Res. 2010;12: R25.

113. Pariyar M, Johns A, Thorne RF, Scott RJ, Avery-Kiejda KA. Copy number variation in triple negative breast cancer samples associated with lymph node metastasis. Neoplasia. 2021;23: 743–753.

114. Hyman E, Kauraniemi P, Hautaniemi S, Wolf M, Mousses S, Rozenblum E, et al. Impact of DNA amplification on gene expression patterns in breast cancer. Cancer Res. 2002;62: 6240–6245.

115. Lu PJ, Sundquist K, Baeckstrom D, Poulsom R, Hanby A, Meier-Ewert S, et al. A novel gene (PLU-1) containing highly conserved putative DNA/chromatin binding motifs is specifically up-regulated in breast cancer. J Biol Chem. 1999;274: 15633–15645.

116. Chin SF, Teschendorff AE, Marioni JC, Wang Y, Barbosa-Morais NL, Thorne NP, et al. High-resolution aCGH and expression profiling identifies a novel genomic subtype of ER negative breast cancer. Genome Biol. 2007;8: R215.

117. Chin K, DeVries S, Fridlyand J, Spellman PT, Roydasgupta R, Kuo W-L, et al. Genomic and transcriptional aberrations linked to breast cancer pathophysiologies. Cancer Cell. 2006;10: 529–541.

118. Chin S-F, Wang Y, Thorne NP, Teschendorff AE, Pinder SE, Vias M, et al. Using array-comparative genomic hybridization to define molecular portraits of primary breast cancers. Oncogene. 2007;26: 1959–1970.

119. Horlings HM, Lai C, Nuyten DSA, Halfwerk H, Kristel P, van Beers E, et al. Integration of DNA copy number alterations and prognostic gene expression signatures in breast cancer patients. Clin Cancer Res. 2010;16: 651–663.

120. Muthuswami M, Ramesh V, Banerjee S, Viveka Thangaraj S, Periasamy J, Bhaskar Rao D, et al. Breast tumors with elevated expression of 1q candidate genes confer poor clinical outcome and sensitivity to Ras/PI3K inhibition. PLoS One. 2013;8: e77553.

121. Goh JY, Feng M, Wang W, Oguz G, Yatim SMJM, Lee PL, et al. Chromosome 1q21.3 amplification is a trackable biomarker and actionable target for breast cancer recurrence. Nat Med. 2017;23: 1319–1330.

122. Waugh MG. Amplification of Chromosome 1q Genes Encoding the Phosphoinositide Signalling Enzymes PI4KB, AKT3, PIP5K1A and PI3KC2B in Breast Cancer. J Cancer. 2014;5: 790–796.

123. Silva GO, He X, Parker JS, Gatza ML, Carey LA, Hou JP, et al. Cross-species DNA copy number analyses identifies multiple 1q21-q23 subtype-specific driver genes for breast cancer. Breast Cancer Res Treat. 2015;152: 347–356.

124. Chen Y-Y, Ge J-Y, Zhu S-Y, Shao Z-M, Yu K-D. Copy number amplification of ENSA promotes the progression of triple-negative breast cancer via cholesterol biosynthesis. Nat Commun. 2022;13: 791.

125. Gjerstorff MF. Novel Insights Into Epigenetic Reprogramming and Destabilization of Pericentromeric Heterochromatin in Cancer. Front Oncol. 2020;10: 594163.

126. Marraffini LA, Sontheimer EJ. CRISPR interference: RNA-directed adaptive immunity in bacteria and archaea. Nat Rev Genet. 2010;11: 181–190.

127. Jinek M, Chylinski K, Fonfara I, Hauer M, Doudna JA, Charpentier E. A programmable dual-RNA-guided DNA endonuclease in adaptive bacterial immunity. Science. 2012;337: 816–821.

128. Ran FA, Hsu PD, Wright J, Agarwala V, Scott DA, Zhang F. Genome engineering using the CRISPR-Cas9 system. Nat Protoc. 2013;8: 2281–2308.

129. Trevino AE, Zhang F. Genome editing using Cas9 nickases. Methods Enzymol. 2014;546: 161–174.

130. Cong L, Ran FA, Cox D, Lin S, Barretto R, Habib N, et al. Multiplex genome engineering using CRISPR/Cas systems. Science. 2013;339: 819–823.

131. Sternberg SH, Redding S, Jinek M, Greene EC, Doudna JA. DNA interrogation by the CRISPR RNA-guided endonuclease Cas9. Nature. 2014;507: 62–67.

132. Hsu PD, Scott DA, Weinstein JA, Ran FA, Konermann S, Agarwala V, et al. DNA targeting specificity of RNA-guided Cas9 nucleases. Nat Biotechnol. 2013;31: 827–832.

133. Hille F, Charpentier E. CRISPR-Cas: biology, mechanisms and relevance. Philos Trans R Soc Lond B Biol Sci. 2016;371. doi:10.1098/rstb.2015.0496

134. Bolotin A, Quinquis B, Sorokin A, Ehrlich SD. Clustered regularly interspaced short palindrome repeats (CRISPRs) have spacers of extrachromosomal origin. Microbiology. 2005;151: 2551–2561.

135. Zhang J-H, Adikaram P, Pandey M, Genis A, Simonds WF. Optimization of genome editing through CRISPR-Cas9 engineering. Bioengineered. 2016;7: 166–174.

136. Gasiunas G, Barrangou R, Horvath P, Siksnys V. Cas9-crRNA ribonucleoprotein complex mediates specific DNA cleavage for adaptive immunity in bacteria. Proc Natl Acad Sci U S A. 2012;109: E2579–86.

137. Qi LS, Larson MH, Gilbert LA, Doudna JA, Weissman JS, Arkin AP, et al. Repurposing CRISPR as an RNA-guided platform for sequence-specific control of gene expression. Cell. 2013;152: 1173–1183.

138. Sander JD, Joung JK. CRISPR-Cas systems for editing, regulating and targeting genomes. Nat Biotechnol. 2014;32: 347–355.

139. Sánchez-Rivera FJ, Jacks T. Applications of the CRISPR-Cas9 system in cancer biology. Nat Rev Cancer. 2015;15: 387–395.

140. Cho SW, Kim S, Kim JM, Kim J-S. Targeted genome engineering in human cells with the Cas9 RNA-guided endonuclease. Nat Biotechnol. 2013;31: 230–232.

141. Jinek M, East A, Cheng A, Lin S, Ma E, Doudna J. RNA-programmed genome editing in human cells. Elife. 2013;2: e00471.

142. Mali P, Yang L, Esvelt KM, Aach J, Guell M, DiCarlo JE, et al. RNA-guided human genome engineering via Cas9. Science. 2013;339: 823–826.

143. Shalem O, Sanjana NE, Hartenian E, Shi X, Scott DA, Mikkelson T, et al. Genome-scale CRISPR-Cas9 knockout screening in human cells. Science. 2014;343: 84–87.

144. Wang T, Wei JJ, Sabatini DM, Lander ES. Genetic screens in human cells using the CRISPR-Cas9 system. Science. 2014;343: 80–84.

145. Kiessling MK, Schuierer S, Stertz S, Beibel M, Bergling S, Knehr J, et al. Identification of oncogenic driver mutations by genome-wide CRISPR-Cas9 dropout screening. BMC Genomics. 2016;17: 723.

146. Hart T, Chandrashekhar M, Aregger M, Steinhart Z, Brown KR, MacLeod G, et al. High-Resolution CRISPR Screens Reveal Fitness Genes and Genotype-Specific Cancer Liabilities. Cell. 2015;163: 1515–1526.

147. Wang T, Birsoy K, Hughes NW, Krupczak KM, Post Y, Wei JJ, et al. Identification and characterization of essential genes in the human genome. Science. 2015;350: 1096–1101.

148. Chow RD, Chen S. Cancer CRISPR Screens In Vivo. Trends Cancer Res. 2018;4: 349–358.

149. Tzelepis K, Koike-Yusa H, De Braekeleer E, Li Y, Metzakopian E, Dovey OM, et al. A CRISPR Dropout Screen Identifies Genetic Vulnerabilities and Therapeutic Targets in Acute Myeloid Leukemia. Cell Rep. 2016;17: 1193–1205.

150. Ford K, McDonald D, Mali P. Functional Genomics via CRISPR-Cas. J Mol Biol. 2019;431: 48–65.

151. Shi J, Wang E, Milazzo JP, Wang Z, Kinney JB, Vakoc CR. Discovery of cancer drug targets by CRISPR-Cas9 screening of protein domains. Nat Biotechnol. 2015;33: 661–667.

152. He C, Han S, Chang Y, Wu M, Zhao Y, Chen C, et al. CRISPR screen in cancer: status quo and future perspectives. Am J Cancer Res. 2021;11: 1031–1050.

153. Agrotis A, Ketteler R. A new age in functional genomics using CRISPR/Cas9 in arrayed library screening. Front Genet. 2015;6: 300.

154. Bowden AR, Morales-Juarez DA, Sczaniecka-Clift M, Agudo MM, Lukashchuk N, Thomas JC, et al. Parallel CRISPR-Cas9 screens clarify impacts of p53 on screen performance. Elife. 2020;9. doi:10.7554/eLife.55325

155. Wei L, Lee D, Law C-T, Zhang MS, Shen J, Chin DW-C, et al. Genome-wide CRISPR/Cas9 library screening identified PHGDH as a critical driver for Sorafenib resistance in HCC. Nat Commun. 2019;10: 4681.

156. Lu Y, Shen H, Huang W, He S, Chen J, Zhang D, et al. Correction: Genome-scale CRISPR-Cas9 knockout screening in hepatocellular carcinoma with lenvatinib resistance. Cell Death Discov. 2022;8: 74.

157. Zhang J, Li Y, Liu H, Zhang J, Wang J, Xia J, et al. Genome-wide CRISPR/Cas9 library screen identifies PCMT1 as a critical driver of ovarian cancer metastasis. J Exp Clin Cancer Res. 2022;41: 24.

158. Costacurta M, Vervoort SJ, Hogg SJ, Martin BP, Johnstone RW, Shortt J. Whole genome CRISPR screening identifies TOP2B as a potential target for IMiD sensitization in multiple myeloma. Haematologica. 2021;106: 2013–2017.

159. Zhou Y, Zhu S, Cai C, Yuan P, Li C, Huang Y, et al. High-throughput screening of a CRISPR/Cas9 library for functional genomics in human cells. Nature. 2014;509: 487–491.

160. Morgens DW, Wainberg M, Boyle EA, Ursu O, Araya CL, Tsui CK, et al. Genome-scale measurement of off-target activity using Cas9 toxicity in high-throughput screens. Nat Commun. 2017;8: 15178.

161. Iyer VS, Jiang L, Shen Y, Boddul SV, Panda SK, Kasza Z, et al. Designing custom CRISPR libraries for hypothesis-driven drug target discovery. Comput Struct Biotechnol J. 2020;18: 2237–2246.

162. Dai M, Yan G, Wang N, Daliah G, Edick AM, Poulet S, et al. In vivo genome-wide CRISPR screen reveals breast cancer vulnerabilities and synergistic mTOR/Hippo targeted combination therapy. Nat Commun. 2021;12: 3055.

163. Wang L, Zhou L, Li M, Zhao J, Liu Y, Chen Y, et al. Genome-wide CRISPR/Cas9 knockout screening uncovers ZNF319 as a novel tumor suppressor critical for breast cancer metastasis. Biochem Biophys Res Commun. 2022;589: 107–115.

164. Sun X, Wang Z, Chen X, Shen K. CRISPR-cas9 Screening Identified Lethal Genes Enriched in Cell Cycle Pathway and of Prognosis Significance in Breast Cancer. Front Cell Dev Biol. 2021;9: 646774.

165. Xiao T, Li W, Wang X, Xu H, Yang J, Wu Q, et al. Estrogen-regulated feedback loop limits the efficacy of estrogen receptor-targeted breast cancer therapy. Proc Natl Acad Sci U S A. 2018;115: 7869–7878.

166. Kostyrko K, Román M, Lee AG, Simpson DR, Dinh PT, Leung SG, et al. UHRF1 is a mediator of KRAS driven oncogenesis in lung adenocarcinoma. Nat Commun. 2023;14: 3966.

167. Zhang H, Gao H, Gu Y, John A, Wei L, Huang M, et al. 3D CRISPR screen in prostate cancer cells reveals PARP inhibitor sensitization through TBL1XR1-SMC3 interaction. Front Oncol. 2022;12: 999302.

168. Özkan H, Öztürk DG, Korkmaz G. Transcriptional Factor Repertoire of Breast Cancer in 3D Cell Culture Models. Cancers . 2022;14. doi:10.3390/cancers14041023

169. Takahashi N, Cho P, Selfors LM, Kuiken HJ, Kaul R, Fujiwara T, et al. 3D Culture Models with CRISPR Screens Reveal Hyperactive NRF2 as a Prerequisite for Spheroid Formation via Regulation of Proliferation and Ferroptosis. Mol Cell. 2020;80: 828–844.e6.

170. Grandhi TSP, To J, Romero A, Luna F, Barnes W, Walker J, et al. High-throughput CRISPR-mediated 3D enrichment platform for functional interrogation of chemotherapeutic resistance. Biotechnol Bioeng. 2021;118: 3187–3199.

171. Debnath J, Brugge JS. Modelling glandular epithelial cancers in three-dimensional cultures. Nat Rev Cancer. 2005;5: 675–688.

172. Hawk MA, Schafer ZT. RIPK1-dependent mitophagy: A novel mechanism to eliminate cells detached from the extracellular matrix. Mol Cell Oncol. 2018;5: e1465015.

173. Schafer ZT, Grassian AR, Song L, Jiang Z, Gerhart-Hines Z, Irie HY, et al. Antioxidant and oncogene rescue of metabolic defects caused by loss of matrix attachment. Nature. 2009;461: 109–113.

174. Jiang L, Shestov AA, Swain P, Yang C, Parker SJ, Wang QA, et al. Reductive carboxylation supports redox homeostasis during anchorage-independent growth. Nature. 2016;532: 255–258.

175. Takahashi N, Chen H-Y, Harris IS, Stover DG, Selfors LM, Bronson RT, et al. Cancer Cells Co-opt the Neuronal Redox-Sensing Channel TRPA1 to Promote Oxidative-Stress Tolerance. Cancer Cell. 2018;33: 985–1003.e7.

176. Nath S, Devi GR. Three-dimensional culture systems in cancer research: Focus on tumor spheroid model. Pharmacol Ther. 2016;163: 94–108.

177. Han SJ, Kwon S, Kim KS. Challenges of applying multicellular tumor spheroids in preclinical phase. Cancer Cell Int. 2021;21: 152.

178. Li S, Zhang Z, Han L. 3D Spheroids Propel Tumor Characterization. Trends Cancer Res. 2020;6: 622–624.

179. Tutty MA, Prina-Mello A. Three-Dimensional Spheroids for Cancer Research. Methods Mol Biol. 2023;2645: 65–103.

180. Han K, Pierce SE, Li A, Spees K, Anderson GR, Seoane JA, et al. CRISPR screens in cancer spheroids identify 3D growth-specific vulnerabilities. Nature. 2020;580: 136–141.

181. Tuano NK, Beesley J, Manning M, Shi W, Perlaza-Jimenez L, Malaver-Ortega LF, et al. CRISPR screens identify gene targets at breast cancer risk loci. Genome Biol. 2023;24: 59.

182. White PS, Sulman EP, Porter CJ, Matise TC. A comprehensive view of human chromosome 1. Genome Res. 1999;9: 978–988.

183. Hart T, Tong AHY, Chan K, Van Leeuwen J, Seetharaman A, Aregger M, et al. Evaluation and Design of Genome-Wide CRISPR/SpCas9 Knockout Screens. G3 . 2017;7: 2719–2727.

184. Sanjana NE, Shalem O, Zhang F. Improved vectors and genome-wide libraries for CRISPR screening. Nat Methods. 2014;11: 783–784.

185. Wang T, Lander ES, Sabatini DM. Single Guide RNA Library Design and Construction. Cold Spring Harb Protoc. 2016;2016: db.prot090803.

186. Li W, Xu H, Xiao T, Cong L, Love MI, Zhang F, et al. MAGeCK enables robust identification of essential genes from genome-scale CRISPR/Cas9 knockout screens. Genome Biol. 2014;15: 554.

187. Korkmaz G, Manber Z, Lopes R, Prekovic S, Schuurman K, Kim Y, et al. A CRISPR-Cas9 screen identifies essential CTCF anchor sites for estrogen receptor-driven breast cancer cell proliferation. Nucleic Acids Res. 2019;47: 9557–9572.

188. Ghandi M, Huang FW, Jané-Valbuena J, Kryukov GV, Lo CC, McDonald ER 3rd, et al. Next-generation characterization of the Cancer Cell Line Encyclopedia. Nature. 2019;569: 503–508.

189. Wang B, Wang M, Zhang W, Xiao T, Chen C-H, Wu A, et al. Integrative analysis of pooled CRISPR genetic screens using MAGeCKFlute. Nat Protoc. 2019;14: 756–780.

190. Wickham H. ggplot2: Elegant Graphics for Data Analysis. Springer Science & Business Media; 2009.

191. Kim H, Abd Elmageed ZY, Ju J, Naura AS, Abdel-Mageed AB, Varughese S, et al. PDZK1 is a novel factor in breast cancer that is indirectly regulated by estrogen through IGF-1R and promotes estrogen-mediated growth. Mol Med. 2013;19: 253–262.

192. Zollo M, Andrè A, Cossu A, Sini MC, D'Angelo A, Marino N, et al. Overexpression of h-prune in breast cancer is correlated with advanced disease status. Clin Cancer Res. 2005;11: 199–205.

193. Ferrucci V, Asadzadeh F, Collina F, Siciliano R, Boccia A, Marrone L, et al. Prune-1 drives polarization of tumor-associated macrophages (TAMs) within the lung metastatic niche in triple-negative breast cancer. iScience. 2021;24: 101938.

194. Ni Z, Olsen JB, Guo X, Zhong G, Ruan ED, Marcon E, et al. Control of the RNA polymerase II phosphorylation state in promoter regions by CTD interaction domain-containing proteins RPRD1A and RPRD1B. Transcription. 2011;2: 237–242.

195. Agarwal N, Dancik GM, Goodspeed A, Costello JC, Owens C, Duex JE, et al. GON4L Drives Cancer Growth through a YY1-Androgen Receptor-CD24 Axis. Cancer Res. 2016;76: 5175–5185.

196. Hofmann I, Munro S. An N-terminally acetylated Arf-like GTPase is localised to lysosomes and affects their motility. J Cell Sci. 2006;119: 1494–1503.

197. Huang C-R, Lee C-T, Chang K-Y, Chang W-C, Liu Y-W, Lee J-C, et al. Down-regulation of ARNT promotes cancer metastasis by activating the fibronectin/integrin β1/FAK axis. Oncotarget. 2015;6: 11530–11546.

198. Lyu J, Li JJ, Su J, Peng F, Chen YE, Ge X, et al. DORGE: Discovery of Oncogenes and tumoR suppressor genes using Genetic and Epigenetic features. Sci Adv. 2020;6. doi:10.1126/sciadv.aba6784

199. Egloff S, Murphy S. Cracking the RNA polymerase II CTD code. Trends Genet. 2008;24: 280–288.

200. Komarnitsky P, Cho EJ, Buratowski S. Different phosphorylated forms of RNA polymerase II and associated mRNA processing factors during transcription. Genes Dev. 2000;14: 2452–2460.

201. Ali I, Ruiz DG, Ni Z, Johnson JR, Zhang H, Li P-C, et al. Crosstalk between RNA Pol II C-Terminal Domain Acetylation and Phosphorylation via RPRD Proteins. Mol Cell. 2019;74: 1164–1174.e4.

202. Ni Z, Xu C, Guo X, Hunter GO, Kuznetsova OV, Tempel W, et al. RPRD1A and RPRD1B are human RNA polymerase II C-terminal domain scaffolds for Ser5 dephosphorylation. Nat Struct Mol Biol. 2014;21: 686–695.

203. Colgan DF, Goodfellow RX, Colgan JD. The transcriptional regulator GON4L is required for viability and hematopoiesis in mice. Exp Hematol. 2021;98: 25–35.

204. Lu P, Hankel IL, Hostager BS, Swartzendruber JA, Friedman AD, Brenton JL, et al. The developmental regulator protein Gon4l associates with protein YY1, co-repressor Sin3a, and histone deacetylase 1 and mediates transcriptional repression. J Biol Chem. 2011;286: 18311–18319.

205. Liu Y, Du L, Osato M, Teo EH, Qian F, Jin H, et al. The zebrafish udu gene encodes a novel nuclear factor and is essential for primitive erythroid cell development. Blood. 2007;110: 99–106.

206. Bulchand S, Menon SD, George SE, Chia W. Muscle wasted: a novel component of the Drosophila histone locus body required for muscle integrity. J Cell Sci. 2010;123: 2697–2707.

207. Tate JG, Bamford S, Jubb HC, Sondka Z, Beare DM, Bindal N, et al. COSMIC: the Catalogue Of Somatic Mutations In Cancer. Nucleic Acids Res. 2019;47: D941–D947.

208. Casalou C, Faustino A, Barral DC. Arf proteins in cancer cell migration. Small GTPases. 2016;7: 270–282.

209. Casalou C, Ferreira A, Barral DC. The Role of ARF Family Proteins and Their Regulators and Effectors in Cancer Progression: A Therapeutic Perspective. Front Cell Dev Biol. 2020;8: 217.

210. Khatter D, Sindhwani A, Sharma M. Arf-like GTPase Arl8: Moving from the periphery to the center of lysosomal biology. Cell Logist. 2015;5: e1086501.

211. Bagshaw RD, Callahan JW, Mahuran DJ. The Arf-family protein, Arl8b, is involved in the spatial distribution of lysosomes. Biochem Biophys Res Commun. 2006;344: 1186–1191.

212. Mrakovic A, Kay JG, Furuya W, Brumell JH, Botelho RJ. Rab7 and Arl8 GTPases are necessary for lysosome tubulation in macrophages. Traffic. 2012;13: 1667–1679.

213. Dykes SS, Gray AL, Coleman DT, Saxena M, Stephens CA, Carroll JL, et al. The Arf-like GTPase Arl8b is essential for three-dimensional invasive growth of

prostate cancer in vitro and xenograft formation and growth in vivo. Oncotarget. 2016;7: 31037–31052.

214. Koblinski JE, Ahram M, Sloane BF. Unraveling the role of proteases in cancer. Clin Chim Acta. 2000;291: 113–135.

215. Wu P-H, Onodera Y, Giaccia AJ, Le Q-T, Shimizu S, Shirato H, et al. Lysosomal trafficking mediated by Arl8b and BORC promotes invasion of cancer cells that survive radiation. Commun Biol. 2020;3: 620.

216. Kewley RJ, Whitelaw ML, Chapman-Smith A. The mammalian basic helix-loop-helix/PAS family of transcriptional regulators. Int J Biochem Cell Biol. 2004;36: 189–204.

217. Kolonko M, Greb-Markiewicz B. bHLH-PAS Proteins: Their Structure and Intrinsic Disorder. Int J Mol Sci. 2019;20. doi:10.3390/ijms20153653

218. Abel J, Haarmann-Stemmann T. An introduction to the molecular basics of aryl hydrocarbon receptor biology. Biol Chem. 2010;391: 1235–1248.

219. Furness SGB, Whelan F. The pleiotropy of dioxin toxicity--xenobiotic misappropriation of the aryl hydrocarbon receptor's alternative physiological roles. Pharmacol Ther. 2009;124: 336–353.

220. Swanson HI, Chan WK, Bradfield CA. DNA binding specificities and pairing rules of the Ah receptor, ARNT, and SIM proteins. J Biol Chem. 1995;270: 26292–26302.

221. Budinsky RA, Schrenk D, Simon T, Van den Berg M, Reichard JF, Silkworth JB, et al. Mode of action and dose-response framework analysis for receptor-mediated toxicity: The aryl hydrocarbon receptor as a case study. Crit Rev Toxicol. 2014;44: 83–119.

222. Hankinson O. Role of coactivators in transcriptional activation by the aryl hydrocarbon receptor. Arch Biochem Biophys. 2005;433: 379–386.

223. Gasiewicz TA, Singh KP, Casado FL. The aryl hydrocarbon receptor has an important role in the regulation of hematopoiesis: implications for benzene-induced hematopoietic toxicity. Chem Biol Interact. 2010;184: 246–251.

224. Gasiewicz TA, Henry EC, Collins LL. Expression and activity of aryl hydrocarbon receptors in development and cancer. Crit Rev Eukaryot Gene Expr. 2008;18: 279–321.

225. Tian Y, Rabson AB, Gallo MA. Ah receptor and NF-kappaB interactions: mechanisms and physiological implications. Chem Biol Interact. 2002;141: 97–115.

226. Elferink CJ, Ge NL, Levine A. Maximal aryl hydrocarbon receptor activity depends on an interaction with the retinoblastoma protein. Mol Pharmacol. 2001;59: 664–673.

227. Hayes JD, Dinkova-Kostova AT, McMahon M. Cross-talk between transcription factors AhR and Nrf2: lessons for cancer chemoprevention from dioxin. Toxicol Sci. 2009;111: 199–201.

228. Kim DW, Gazourian L, Quadri SA, Romieu-Mourez R, Sherr DH, Sonenshein GE. The RelA NF-kappaB subunit and the aryl hydrocarbon receptor (AhR) cooperate to transactivate the c-myc promoter in mammary cells. Oncogene. 2000;19: 5498–5506.

229. Puga A, Ma C, Marlowe JL. The aryl hydrocarbon receptor cross-talks with multiple signal transduction pathways. Biochem Pharmacol. 2009;77: 713–722.

230. Abdelrahim M, Smith R 3rd, Safe S. Aryl hydrocarbon receptor gene silencing with small inhibitory RNA differentially modulates Ah-responsiveness in MCF-7 and HepG2 cancer cells. Mol Pharmacol. 2003;63: 1373–1381.

231. Spink BC, Bennett JA, Lostritto N, Cole JR, Spink DC. Expression of the aryl hydrocarbon receptor is not required for the proliferation, migration, invasion, or estrogen-dependent tumorigenesis of MCF-7 breast cancer cells. Mol Carcinog. 2013;52: 544–554.

232. Ma Q, Whitlock JP Jr. The aromatic hydrocarbon receptor modulates the Hepa 1c1c7 cell cycle and differentiated state independently of dioxin. Mol Cell Biol. 1996;16: 2144–2150.

233. Barhoover MA, Hall JM, Greenlee WF, Thomas RS. Aryl hydrocarbon receptor regulates cell cycle progression in human breast cancer cells via a functional interaction with cyclin-dependent kinase 4. Mol Pharmacol. 2010;77: 195–201.

234. Puga A, Xia Y, Elferink C. Role of the aryl hydrocarbon receptor in cell cycle regulation. Chem Biol Interact. 2002;141: 117–130.

235. Marlowe JL, Knudsen ES, Schwemberger S, Puga A. The aryl hydrocarbon receptor displaces p300 from E2F-dependent promoters and represses S phase-specific gene expression. J Biol Chem. 2004;279: 29013–29022.

236. Matsumura F. The significance of the nongenomic pathway in mediating inflammatory signaling of the dioxin-activated Ah receptor to cause toxic effects. Biochem Pharmacol. 2009;77: 608–626.

237. Matthews J, Gustafsson J-A. Estrogen receptor and aryl hydrocarbon receptor signaling pathways. Nucl Recept Signal. 2006;4: e016.

238. Swedenborg E, Pongratz I. AhR and ARNT modulate ER signaling. Toxicology. 2010;268: 132–138.

239. Labrecque MP, Takhar MK, Hollingshead BD, Prefontaine GG, Perdew GH, Beischlag TV. Distinct roles for aryl hydrocarbon receptor nuclear translocator and ah receptor in estrogen-mediated signaling in human cancer cell lines. PLoS One. 2012;7: e29545.

240. Ohtake F, Takeyama K-I, Matsumoto T, Kitagawa H, Yamamoto Y, Nohara K, et al. Modulation of oestrogen receptor signalling by association with the activated dioxin receptor. Nature. 2003;423: 545–550.

241. Opitz CA, Holfelder P, Prentzell MT, Trump S. The complex biology of aryl hydrocarbon receptor activation in cancer and beyond. Biochem Pharmacol. 2023;216: 115798.

242. Elson DJ, Kolluri SK. Tumor-Suppressive Functions of the Aryl Hydrocarbon Receptor (AhR) and AhR as a Therapeutic Target in Cancer. Biology . 2023;12. doi:10.3390/biology12040526

243. Murray IA, Patterson AD, Perdew GH. Aryl hydrocarbon receptor ligands in cancer: friend and foe. Nat Rev Cancer. 2014;14: 801–814.

244. Wang Z, Snyder M, Kenison JE, Yang K, Lara B, Lydell E, et al. How the AHR Became Important in Cancer: The Role of Chronically Active AHR in Cancer Aggression. Int J Mol Sci. 2020;22. doi:10.3390/ijms22010387

245. Marlowe JL, Puga A. Aryl hydrocarbon receptor, cell cycle regulation, toxicity, and tumorigenesis. J Cell Biochem. 2005;96: 1174–1184.

246. Dietrich C, Kaina B. The aryl hydrocarbon receptor (AhR) in the regulation of cell-cell contact and tumor growth. Carcinogenesis. 2010;31: 1319–1328.

247. Stanford EA, Wang Z, Novikov O, Mulas F, Landesman-Bollag E, Monti S, et al. The role of the aryl hydrocarbon receptor in the development of cells with the molecular and functional characteristics of cancer stem-like cells. BMC Biol. 2016;14: 20.

248. Leclerc D, Staats Pires AC, Guillemin GJ, Gilot D. Detrimental activation of AhR pathway in cancer: an overview of therapeutic strategies. Curr Opin Immunol. 2021;70: 15–26.

249. Paris A, Tardif N, Galibert M-D, Corre S. AhR and Cancer: From Gene Profiling to Targeted Therapy. Int J Mol Sci. 2021;22. doi:10.3390/ijms22020752

250. Ahmed S, Wang A, Celius T, Matthews J. Zinc finger nuclease-mediated knockout of AHR or ARNT in human breast cancer cells abolishes basal and ligand-dependent regulation of CYP1B1 and differentially affects estrogen receptor α transactivation. Toxicol Sci. 2014;138: 89–103.

251. Hall JM, Barhoover MA, Kazmin D, McDonnell DP, Greenlee WF, Thomas RS. Activation of the aryl-hydrocarbon receptor inhibits invasive and metastatic features of human breast cancer cells and promotes breast cancer cell differentiation. Mol Endocrinol. 2010;24: 359–369.

252. Zhang S, Lei P, Liu X, Li X, Walker K, Kotha L, et al. The aryl hydrocarbon receptor as a target for estrogen receptor-negative breast cancer chemotherapy. Endocr Relat Cancer. 2009;16: 835–844.

253. Bersten DC, Sullivan AE, Peet DJ, Whitelaw ML. bHLH-PAS proteins in cancer. Nat Rev Cancer. 2013;13: 827–841.

254. Furness SGB, Lees MJ, Whitelaw ML. The dioxin (aryl hydrocarbon) receptor as a model for adaptive responses of bHLH/PAS transcription factors. FEBS Lett. 2007;581: 3616–3625.

255. Poellinger L, Johnson RS. HIF-1 and hypoxic response: the plot thickens. Curr Opin Genet Dev. 2004;14: 81–85.

256. Semenza GL. Hypoxia-inducible factor 1 (HIF-1) pathway. Sci STKE. 2007;2007: cm8.

257. Eguchi H, Ikuta T, Tachibana T, Yoneda Y, Kawajiri K. A nuclear localization signal of human aryl hydrocarbon receptor nuclear translocator/hypoxia-inducible factor 1beta is a novel bipartite type recognized by the two components of nuclear pore-targeting complex. J Biol Chem. 1997;272: 17640–17647.

258. Sharma A, Sinha S, Shrivastava N. Therapeutic Targeting Hypoxia-Inducible Factor (HIF-1) in Cancer: Cutting Gordian Knot of Cancer Cell Metabolism. Front Genet. 2022;13: 849040.

259. Prabhakar NR, Semenza GL. Adaptive and maladaptive cardiorespiratory responses to continuous and intermittent hypoxia mediated by hypoxia-inducible factors 1 and 2. Physiol Rev. 2012;92: 967–1003.

260. Mandl M, Depping R. Hypoxia-inducible aryl hydrocarbon receptor nuclear translocator (ARNT) (HIF-1β): is it a rare exception? Mol Med. 2014;20: 215–220.

261. Zhang M, Hu Y, Yang F, Zhang J, Zhang J, Yu W, et al. Interaction between AhR and HIF-1 signaling pathways mediated by ARNT/HIF-1β. BMC Pharmacol Toxicol. 2022;23: 26.

262. Tiburcio PD, Choi H, Huang LE. Complex role of HIF in cancer: the known, the unknown, and the unexpected. Hypoxia (Auckl). 2014;2: 59–70.

263. Harris AL. Hypoxia--a key regulatory factor in tumour growth. Nat Rev Cancer. 2002;2: 38–47.

264. Semenza GL. HIF-1 mediates metabolic responses to intratumoral hypoxia and oncogenic mutations. J Clin Invest. 2013;123: 3664–3671.

265. Wolff M, Jelkmann W, Dunst J, Depping R. The Aryl Hydrocarbon Receptor Nuclear Translocator (ARNT/HIF-1β) is influenced by hypoxia and hypoxia-mimetics. Cell Physiol Biochem. 2013;32: 849–858.

266. Wang GL, Jiang BH, Rue EA, Semenza GL. Hypoxia-inducible factor 1 is a basic-helix-loop-helix-PAS heterodimer regulated by cellular O2 tension. Proc Natl Acad Sci U S A. 1995;92: 5510–5514.

267. Mandl M, Depping R. is a potential direct HIF-1 target gene in human Hep3B hepatocellular carcinoma cells. Cancer Cell Int. 2017;17: 77.

268. Mandl M, Kapeller B, Lieber R, Macfelda K. Hypoxia-inducible factor-1β (HIF-1β) is upregulated in a HIF-1α-dependent manner in 518A2 human melanoma cells under hypoxic conditions. Biochem Biophys Res Commun. 2013;434: 166–172.

269. Mandl M, Lieberum M-K, Depping R. A HIF-1α-driven feed-forward loop augments HIF signalling in Hep3B cells by upregulation of ARNT. Cell Death Dis. 2016;7: e2284.

270. Zhong H, Hanrahan C, van der Poel H, Simons JW. Hypoxia-inducible factor 1alpha and 1beta proteins share common signaling pathways in human prostate cancer cells. Biochem Biophys Res Commun. 2001;284: 352–356.

271. Mandl M, Lieberum M-K, Dunst J, Depping R. The expression level of the transcription factor Aryl hydrocarbon receptor nuclear translocator (ARNT) determines cellular survival after radiation treatment. Radiat Oncol. 2015;10: 229.

272. Isaacs JS, Jung Y-J, Neckers L. Aryl hydrocarbon nuclear translocator (ARNT) promotes oxygen-independent stabilization of hypoxia-inducible factor-1alpha by modulating an Hsp90-dependent regulatory pathway. J Biol Chem. 2004;279: 16128–16135.

273. Lim W, Park Y, Cho J, Park C, Park J, Park Y-K, et al. Estrogen receptor beta inhibits transcriptional activity of hypoxia inducible factor-1 through the downregulation of arylhydrocarbon receptor nuclear translocator. Breast Cancer Res. 2011;13: R32.

274. Antonsson C, Arulampalam V, Whitelaw ML, Pettersson S, Poellinger L. Constitutive function of the basic helix-loop-helix/PAS factor Arnt. Regulation of target promoters via the E box motif. J Biol Chem. 1995;270: 13968–13972.

275. Sogawa K, Nakano R, Kobayashi A, Kikuchi Y, Ohe N, Matsushita N, et al. Possible function of Ah receptor nuclear translocator (Arnt) homodimer in transcriptional regulation. Proc Natl Acad Sci U S A. 1995;92: 1936–1940.

276. Wang F, Shi S, Zhang R, Hankinson O. Identifying target genes of the aryl hydrocarbon receptor nuclear translocator (Arnt) using DNA microarray analysis. Biol Chem. 2006;387: 1215–1218.

277. Arpiainen S, Lämsä V, Pelkonen O, Yim SH, Gonzalez FJ, Hakkola J. Aryl hydrocarbon receptor nuclear translocator and upstream stimulatory factor regulate Cytochrome P450 2a5 transcription through a common E-box site. J Mol Biol. 2007;369: 640–652.

278. Huang W-C, Chen S-T, Chang W-C, Chang K-Y, Chang W-C, Chen B-K. Involvement of aryl hydrocarbon receptor nuclear translocator in EGF-induced c-Jun/Sp1-mediated gene expression. Cell Mol Life Sci. 2010;67: 3523–3533.

279. Chang K-Y, Shen M-R, Lee M-Y, Wang W-L, Su W-C, Chang W-C, et al. Epidermal growth factor-activated aryl hydrocarbon receptor nuclear translocator/HIF-1{beta} signal pathway up-regulates cyclooxygenase-2 gene expression associated with squamous cell carcinoma. J Biol Chem. 2009;284: 9908–9916.

280. Chan Y-Y, Kalpana S, Chang W-C, Chang W-C, Chen B-K. Expression of aryl hydrocarbon receptor nuclear translocator enhances cisplatin resistance by upregulating MDR1 expression in cancer cells. Mol Pharmacol. 2013;84: 591–602.

281. Shieh J-M, Shen C-J, Chang W-C, Cheng H-C, Chan Y-Y, Huang W-C, et al. An increase in reactive oxygen species by deregulation of ARNT enhances chemotherapeutic drug-induced cancer cell death. PLoS One. 2014;9: e99242.

282. Wright CW, Duckett CS. The aryl hydrocarbon nuclear translocator alters CD30-mediated NF-kappaB-dependent transcription. Science. 2009;323: 251–255.

283. Liang Y, Li W-W, Yang B-W, Tao Z-H, Sun H-C, Wang L, et al. Aryl hydrocarbon receptor nuclear translocator is associated with tumor growth and progression of hepatocellular carcinoma. Int J Cancer. 2012;130: 1745–1754.

284. Li W, Liang Y, Yang B, Sun H, Wu W. Downregulation of ARNT2 promotes tumor growth and predicts poor prognosis in human hepatocellular carcinoma. J Gastroenterol Hepatol. 2015;30: 1085–1093.

285. Huang C-R, Chang T-W, Lee C-T, Shen C-J, Chang W-C, Chen B-K. ARNT deficiency represses pyruvate dehydrogenase kinase 1 to trigger ROS production and melanoma metastasis. Oncogenesis. 2021;10: 11.

286. Brunnberg S, Pettersson K, Rydin E, Matthews J, Hanberg A, Pongratz I. The basic helix-loop-helix-PAS protein ARNT functions as a potent coactivator of estrogen receptor-dependent transcription. Proc Natl Acad Sci U S A. 2003;100: 6517–6522.

287. Rüegg J, Swedenborg E, Wahlström D, Escande A, Balaguer P, Pettersson K, et al. The transcription factor aryl hydrocarbon receptor nuclear translocator functions as an estrogen receptor beta-selective coactivator, and its recruitment to alternative pathways mediates antiestrogenic effects of dioxin. Mol Endocrinol. 2008;22: 304–316.

288. Lo R, Matthews J. High-resolution genome-wide mapping of AHR and ARNT binding sites by ChIP-Seq. Toxicol Sci. 2012;130: 349–361.